Contents

1 Experimental details **S3**

1.1 NMR samples S3

1.2 Experimental setup S3

1.3 2D *F*1-PSYCHE-EASY-ROESY experiments of the tetrapeptide - *R,R*-cyclohexane-1,2-diol mixture S3

1.4 2D *gradient-selected F*1-PSYCHE-EASY-ROESY experiments of the cyclosporine A sample S4

1.5 2D *gradient-selected F*1-*perfect*BASH-EASY-ROESY experiments of the cyclosporine A sample S5

1.6 1D *selective* ROESY experiments of the cyclosporine A sample S6

2 Analysis of ROESY data **S8**

2.1 Extraction of cross-relaxation rates S8

2.2 Distance determination S12

3 Cyclosporine A **S13**

3.1 Proton assignment of cyclosporine A in C_6D_6 . . . . . S13

3.2 ^{1}H,^{1}H-distances extracted from 2D *gradient-selected F*1-PSYCHE-EASY-ROESY S15

3.3 ^{1}H,^{1}H-distances extracted from 2D *gradient-selected F*1-*perfect*BASH-EASY-ROESYS19

3.4 ^{1}H,^{1}H-distances extracted from 1D *selective* and *gradient-selected continuous-wave*-ROESY S22

3.5 ^{1}H,^{1}H-distances extracted from 1D *selective* and *gradient-selected*-EASY-ROESY S25

3.6 Further comparisons of extracted ^{1}H,^{1}H-distances using different methods S28

3.7 Selected ^{1}H,^{1}H-distances extracted from the *gradient-selected F*1-PSYCHE-EASY-ROESY and *gradient-selected F*1-*perfect*BASH-EASY-ROESY and comparison with a model S29

3.8 Representative PANIC plots of cyclosporine A S32

4 Monitoring chemical exchange of cyclosporine A **S33**

4.1 Extraction of exchange rates from 2D *gradient-selected F*1-PSYCHE-EASY-ROESYS33

4.2 Extracted exchange rates of cyclosporine A S38

4.3 Observing Overhauser contacts of the minor conformer of cyclosporine A with the 2D *gradient-selected F*1-*perfect*BASH-EASY-ROESY S40

5 Further comments on the pulse sequences **S41**

5.1 Analysis of the 2D *gradient-selected* $F1$-PSYCHE-EASY-ROESY pulsesequence . S41

5.2 Evaluation of diffusional intensity attenuation: Stejskal-Tanner Equation S49

5.3 Sensitivity comparisons S51

5.4 1D *gradient-selected* CW-ROESY (GS-CW-ROESY): Description S53

5.5 1D *gradient-selected* EASY-ROESY: Description S54

5.6 Dependency of the spin-lock angle in EASY-ROESY experiments S55

5.7 Evaluation of offset effects in EASY-ROESY experiments S58

5.8 2D $F1$-PSYCHE-EASY-ROESY: Spin-site dependent attenuation S60

5.9 Explanation of COSY-like artefacts in $F1$-PSYCHE-EASY-ROESY experiments S65

5.10 2D *gradient-selected* $F1$-PSYCHE-EASY-ROESY: Alternative implementations . S70

5.10.1 Implementation with gradient-encoding before t_1-evolution S70

5.10.2 Implementation without Thrippleton-Keeler-filter S71

5.11 2D *gradient-selected* $F1$-PSYCHE-NOESY S72

6 Spectra **S74**

7 References **S78**

8 Bruker pulse sequence codes **S80**

1 Experimental details

1.1 NMR samples

The experiments with the tetrapeptide - *R,R*-cyclohexane-1,2-diol mixture were done with the sample EP-07 from the previous study[1], which contains an equimolar mixture of the peptide with *R,R*-cyclohexane-1,2-diol in toluene-d_8. The experiments with cyclosporine A were done with a degassed and sealed 25 mM cyclosporine A sample in benzene-d_6 ("2D-Example" Bruker reference sample).

1.2 Experimental setup

Experiments with the tetrapeptide - *R,R*-cyclohexane-1,2-diol mixture were performed on a Bruker Avance III HD spectrometer operating at 700.17 MHz proton base frequency equipped with a QCI probe (^{1}H/^{19}F - ^{13}C/^{31}P/^{15}N - ^{2}H) with z-gradient (0.53 T·m^{-1} maximum gradient strength). The sample temperature was regulated at 300 K. The 90° proton pulse had a duration of 6.8 μs.

Experiments with the cyclosporine A sample were done on a Bruker Avance III with 600.3 MHz proton base frequency, equipped with a 5 mm triple-resonance broadband inverse probe (^{1}H/^{31}P - BB - ^{2}H) with z-gradient (0.494 T·m^{-1} maximum gradient strength). Sample temperature was regulated at 300 K. The 90° proton pulse had a duration of 9.43 μs.

All gradients had a smoothed square shape, were digitised using 100 points (SMSQ10.100) unless denoted otherwise. The gradients strengths are given as fractions of the maximum amplitude and were followed by a recovery delay (D16) of 200 μs.

All bandwidths given for the pulse shapes used for frequency selective refocusing were calculated with the Bruker Shape Tool of TopSpin 3.5 using the *"Calculate Bandwidth for Refocusing -My"* option. The numbers given are calculated by default for 70 % of the maximum refocusing profile. Note that in the case of homonuclear decoupling using the *perfect*BASH scheme at least 95 % of the maximum refocusing profile is required to obtain clean homonuclear decoupling. The pulses used herein were adjusted to fulfill this criterion.

1.3 2D *F*1-PSYCHE-EASY-ROESY experiments of the tetrapeptide - *R,R*-cyclo-hexane-1,2-diol mixture

The 2D *F*1-PSYCHE-EASY-ROESY spectra were acquired using the pulse sequence in chapter 9.1. A mixing time series of 5 independent time points with 150 ms, 200 ms, 300 ms, 375 ms and 400 ms was collected. In the experiments with mixing-times 150 ms, 200 ms and 300 ms both dimensions had a spectral width of 7.71 ppm (5400 Hz), the carrier frequency offset was set to 4.5 ppm. The indirect dimension *F*1 was acquired with 2048 increments (190 ms acquisition time) and States-TPPI selection. The direct dimension *F*2 was acquired with 4096 complex points (378.5 ms acquisition time). The experiments with mixing-times 375 ms and 400 ms both dimensions had a spectral width of 2.7 ppm (1890 Hz), the carrier frequency offset was set to 2.15 ppm. The indirect dimension *F*1 was acquired with 512 increments (135 ms acquisition

time) and States-TPPI selection. The direct dimension $F2$ was acquired with 2048 complex points (541.8 ms acquisition time). In all experiments the EASY-ROESY mixing was performed using two spinlocks with a spinlock angle of 45° (CNST28) and an RF field of 6400 Hz (CNST26). The frequency offsets for spinlocking were shifted by +6400 Hz (*high frequency*) and -6400 Hz (*low frequency*) relative to the offset in $F1$ (4.5 ppm or 2.15 ppm). Each ramp (half-Gaussian shape) had a duration of 1 ms. Power calibration and the offset calculation for symmetrical shifting are hard coded in the pulse program. Purge gradients (GPZ5 and GPZ6) before and after the spinlock had 1 ms duration and strengths of 31 % and 11 %, respectively.

PSYCHE homonuclear decoupling in the indirect dimension was done with a 30 ms (P40) long element (*Crp_psyche.20*) consisting of two low power chirp pulses with 20° flip angle (CNST20), 10 kHz sweep width (CNST21) and 15 ms durations each. Power calibration is hard coded in the pulse program. The gradient during the PSYCHE element (GPZ10) was rectangular (RECT.1), had a duration of 30 ms and a strength of 2 %. Gradients for coherence selection (GPZ1 and GPZ2) had durations of 1 ms each, and 77 % and 49 % gradient strength, respectively. The relaxation delay (D1) was set to 14 s ($\geq 5\,T_1$)[1]. The acquired FIDs were zero filled to the next power of two in both dimensions. Both dimensions were multiplied with a 90° shifted squared sine bell. Phase correction was done manually in both dimensions, followed by an automatic baseline correction.

1.4 2D *gradient-selected F*1-PSYCHE-EASY-ROESY experiments of the cyclosporine A sample

The 2D *gradient-selected* $F1$-PSYCHE-EASY-ROESY spectra were acquired using the pulse sequence in chapter 9.2. Both dimensions had spectral widths of 8.5 ppm (5102.6 Hz) and the carrier frequency offset was set to 4.45 ppm. The indirect dimension $F1$ was acquired with 2048 increments (200.7 ms acquisition time) and States-TPPI selection. The direct dimension $F2$ was acquired with 8192 complex points (1.245 s acquisition time). The EASY-ROESY mixing was performed using two spinlocks with a spinlock angle of 50° (CNST28) and an RF field of 5500 Hz (CNST26). The frequency offsets for spinlocking were shifted by +4615 Hz (*high frequency*) and -4615 Hz (*low frequency*) relative to the offset in $F1$ (4.45 ppm). Each ramp (half-Gaussian shape) had a duration of 1 ms. Power calibration and the offset calculation for symmetrical shifting are hard coded in the pulse program. Purge gradients before and after the spinlock (GPZ5 and GPZ6) had 1 ms duration and strengths of 31 % and 11 %, respectively. A mixing time series of 6 independent time points with 50 ms, 100 ms, 200 ms, 300 ms, 400 ms and 500 ms was collected. PSYCHE homonuclear decoupling in the indirect dimension was applied with a 30 ms (P40) long element (*Crp_psyche.20*) consisting of two low power chirp pulses with 22° flip angle (CNST20), 10 kHz sweep width (CNST21) and 15 ms durations each. Power calibration is hard coded in the pulse program. The gradient during the PSYCHE element (GPZ10) was rectangular (RECT.1), had a duration of 30 ms and a strength of 2.45 %. Gradients for coherence selection (GPZ1 and GPZ2) had durations of 900 μs each, and 77 % and 49 % gradient strength, respectively. Gradient en- and decoding (GPZ4) was done with two gradients of 5.18 % strength and 900 μs duration. The purge gradient in the final z-filter (GPZ7) had a duration of 2 ms and a strength of 61 %. The Thrippleton-Keeler element consisted of a 10 ms long adiabatic

180° pulse (20 % smoothed chirp, 25 kHz sweep-width, γB_1 = 1410 Hz) and a gradient of equal duration, with a strength (GPZ11) of 5.25 %. The number of scans (NS) per increment was set to 8 and the relaxation delay (D1) to 8 s ($\geq 5\,T_1$), giving a total duration of 43 h for one experiment with one mixing-time. The acquired FIDs were zero filled to the next power of two in both dimensions. Both dimensions were subjected to Lorentz-to-Gauss transformation for resolution enhancement ($F1$: LB = -2.5 Hz, GB = 0.333 ; $F2$: LB = -1 Hz, GB = 0.352). Phase correction was done manually in both dimensions, followed by an automatic baseline correction.

1.5 2D *gradient-selected* $F1$-*perfect*BASH-EASY-ROESY experiments of the cyclosporine A sample

The 2D *gradient-selected* $F1$-PSYCHE-EASY-ROESY spectra were acquired using the pulse sequence in chapter 9.3. The indirect dimension ($F1$) was acquired with a spectral width of 5.664 ppm (3400 Hz), using 1536 increments (226 ms acquisition time) and States-TPPI selection. The carrier frequency offset was set to 5.984 ppm. The direct dimension ($F2$) was acquired with 16.658 ppm spectral width and 8192 complex points (410 ms acquisition time). The EASY-ROESY mixing was performed using two spinlocks with a spinlock angle of 45° (CNST28) and a RF field of 5000 Hz (CNST26). The frequency offsets for spinlocking were shifted by +4109 Hz (*high frequency*) and -5891 Hz (*low frequency*) relative to the carrier frequency offset in F1, to ensure a symmetrical spinlocking with respect to center of the ^{1}H spectrum of cyclosporine A (4.5 ppm). In the pulse sequence implementation, the midpoint for the symmetrical offset shifting is defined via CNST0. Each ramp (half-Gaussian shape) had a duration of 1 ms. Power calibration and the offset calculation for symmetrical shifting are hard coded in the pulse program. Purge gradients before and after the spinlock (GPZ5 and GPZ6) had 1 ms duration and strengths of 31 % and 11 %, respectively. A mixing time series of 6 independent time points (P15) with 50 ms, 100 ms, 125 ms, 150 ms, 200 ms and 250 ms was collected. *Perfect*BASH homonuclear decoupling in the indirect dimension ($F1$) was achieved with two 1.45 ms ReBurp refocusing pulses (P40, 4000 Hz bandwidth), whose offsets (CNST1) were set to 6.125 ppm - between the amide-proton and α-proton regions. Gradients for coherence selection in the decoupling element (GPZ1, GPZ2 and GPZ3) had strengths of $G_1 = 37\%$, $G_2 = 23\%$, and $G_3 = 55\%$. Gradient en- and decoding (GPZ4) was done with two gradients of 5.18 % strength and 800 μs duration (P18). The purge gradient in the final z-filter (GPZ7) had a duration of 1.5 ms (P19) and a strength of 61 % (GPZ8). The Thrippleton-Keeler element consisted of a 10 ms long adiabatic 180° pulse (P43, 20 % smoothed chirp, 25 kHz sweep-width, γB_1 = 1410 Hz) and a gradient of equal duration, with a strength (GPZ11) of 5%. The number of scans (NS) per increment was set to 8 and the relaxation delay (D1) to 7s ($\geq 5\,T_1$), giving a total duration of 28 h for one experiment with one mixing-time. The acquired FIDs were zero filled to the next power of two in both dimensions. The direct dimension $F2$ was multiplied with an exponential apodization function (1.5 Hz line broadening) and the indirect dimension $F1$ was multiplied with a 90° shifted squared sine bell. Phase correction was done manually in both dimensions, followed by an automatic baseline correction.

1.6 1D *selective* ROESY experiments of the cyclosporine A sample

1D *selective* and *gradient-selected continuous-wave*-ROESY experiments The 1D *selective* and *gradient-selected continuous-wave*-ROESY spectra were acquired using the pulse sequence in chapter 9.4. All spectra were acquired with a spectral width of 9 ppm and 32768 complex points (3.03 s acquisition time). The carrier frequency offset was set to 4.5 ppm. A mixing time series of 6 independent time points with 50 ms, 100 ms, 200 ms, 300 ms, 400 ms and 500 ms was collected. The ROESY mixing was performed using a single CW-spinlock (P15) with an RF field of 2500 Hz. The selection of the protons was done with a *pulsed-field-gradient selected selective* spin-echo before the spin-lock using a selective refocusing pulse with RSnob shape. The offset (CNST1), the duration of the selective pulse (P12) and its bandwidth are listed in table 1.6 for each selected proton. Power calibration is hard coded in the pulse program. Defocusing gradients before and after the selective refocusing pulse had 1 ms duration (P16) and strengths of 7.5 % (GPZ1). The refocusing gradient had a strength of -15 % (GPZ2) and 1 ms duration. A recovery delay (D1) of 10 s ($\geq 5\,T_1$) was used. The number of scans (NS) per mixing-time point is listed in table 1.6 for each selected proton. The acquired FIDs were zero filled to the next power of two and multiplied with an exponential apodization function (1 Hz line broadening) before Fourier transformation. Before integration, the spectra were subjected to manual phase correction and an automatic baseline correction.

1D *selective* and *gradient-selected*-EASY-ROESY experiments The 1D *selective* and *gradient-selected* EASY-ROESY spectra were acquired using the pulse sequence in chapter 9.5. All spectra were acquired with a spectral width of 9 ppm and 32768 complex points (3.03 s acquisition time). The carrier frequency offset was set to 4.5 ppm. A mixing time series of 6 independent time points with 50 ms, 100 ms, 200 ms, 300 ms, 400 ms and 500 ms was collected. The EASY-ROESY mixing was performed using two spinlocks with a spinlock angle of 45° (CNST28) and a RF field of 5000 Hz (CNST26). The frequency offsets for spinlocking were shifted to +5000 Hz (*high frequency*) and -5000 Hz (*low frequency*) symmetrically to the offset 4.5 ppm. Each ramp (half-Gaussian shape) had a duration of 1 ms. Power calibration and the offset calculation for symmetrical shifting is hard coded in the pulse program. Purge gradients before and after the spinlock had 1.1 ms duration and strengths of 31 % (GPZ1) and 11 % (GPZ2), respectively. The selection of the protons was done with a *pulsed-field-gradient selected selective* spin-echo before the spin-lock using a selective refocusing pulse with RSnob shape. The offset (CNST1), the duration of the selective pulse (P12) and its bandwidth are listed in table 1.6 for each selected proton. Power calibration is hard coded in the pulse program. Defocusing gradients before and after the selective refocusing pulse had 1 ms duration (P16) and strengths of 7.45 % (GPZ3). The refocusing gradient had a gradient strength of 14.9 % (GPZ4) and 1 ms duration. A recovery delay (D1) of 8 s ($\geq 5\,T_1$) was used. The number of scans (NS) per mixing-time point is listed in table 1.6 for each selected proton. The acquired FIDs were zero filled to the next power of two and multiplied with an exponential apodization function (1 Hz line broadening) before Fourier transformation. Before integration, the spectra were subjected to manual phase correction and automatic baseline correction.

Table 1.1: Selected proton frequencies for the 1D *gradient-selected* CW-ROESY and the 1D *gradient-selected* EASY-ROESY experiments, including the chemical shift, the pulse duration and its bandwidth (for RSnob pulse shape[2]) and the number of scans.

sel. protons	chem. shift / ppm	pulse duration / ms	bandwidth / Hz	NS
2-NH	8.2444	15	155	32
7-NH	7.9556	15	155	32
8-NH	7.6033	30	78	32
5-NH	7.445	30	78	32
9-α	5.8638	35	67	32
1-α	5.7214	48	49	64
6-α	5.3768	120	19	64
10-α	5.3279	120	19	64
11-α	5.2543	80	29	64
2-α	5.1146	35	67	32
1-β	4.1907	28	83	32
3-α_1	4.0058	26	90	32
1-NMe	3.7166	18	130	32
6-NMe	3.2185	30	78	32
3-NMe	3.0668	45	52	32
11-NMe	2.9667	120	19	64
9-NMe	2.9225	120	19	64
10-NMe	2.8415	55	42	64
4-NMe	2.585	120	19	64
10-β_1	2.4155	40	58	32
7-β	1.6693	80	29	64
6-β_2	1.4484	120	19	64
4-γ	1.3904	120	19	64
8-β, 6-δ_2	1.0403	90	26	64
11-γ_2	0.6427	25	93	32

2 Analysis of ROESY data

2.1 Extraction of cross-relaxation rates

Herein we outline how the extraction of cross-relaxation rates from the 2D *gradient-selected* $F1$-PSYCHE-EASY-ROESY experiment is performed here. This contains in particular the impact of the factors introduced to account for diffusion and the homonuclear decoupling on the choosen procedures to analyse the EASY-ROESY spectra in this work. The ROESY spectra are analysed using the *isolated spin pair approximation* (ISPA), which assumes that the whole network of dipolarly coupled protons can be broken down into an ensemble of independent dipolarly coupled proton pairs. Such an approximation is valid only for sufficiently short mixing periods. Cross-relaxation rates are extracted from the 2D $F1$-PSYCHE-EASY-ROESY spectra, the 2D *gradient-selected* $F1$-PSYCHE-EASY-ROESY spectra and all 1D-ROESY spectra using the procedure described by Hu and Krishnamurthy[14] Herein we chose the quantification procedure via integration of 1D spectra, which we obtain by extracting traces along the direct dimension $F2$ at the peak maximum of one proton in the $F1$ dimension. The following analysis will be performed only with the 2D *gradient-selected* $F1$-PSYCHE-EASY-ROESY experiment, nevertheless the whole discussion can be directly transferred to the $F1$-PSYCHE-EASY-ROESY experiment without gradient selection. The main difference in the theoretical discussions is the absence of the diffusional factor D and the factor $\frac{1}{2}$.

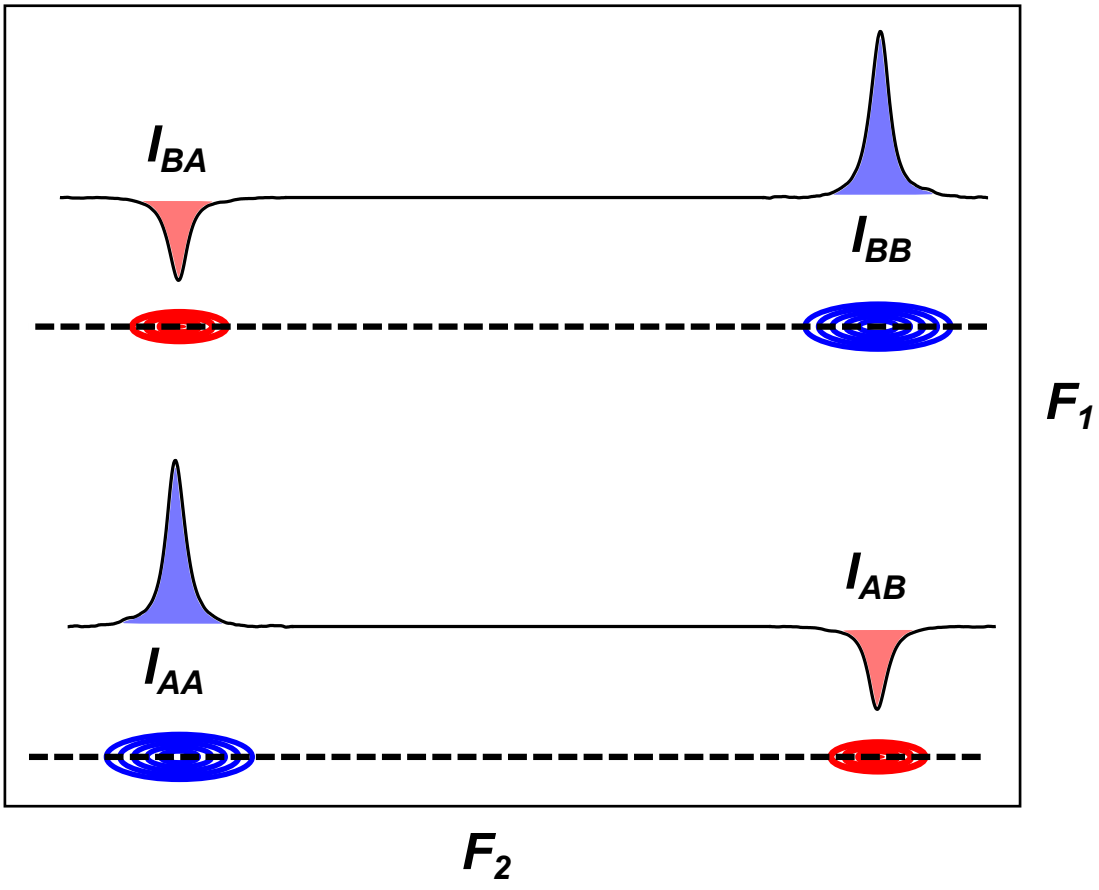

Figure 2.1: Quantification of the ROESY peaks from the 2D $F1$-*pure-shift*-EASY-ROESY spectra by cutting out and integrating $F2$-traces at the peak maximum in $F1$ to extract cross-relaxation rates σ_{ij}.

The analysis starts with the expression for the acquired signal S_+ of the 2D *gradient-selected* $F1$-PSYCHE-EASY-ROESY experiment after double Fourier transformation and phase correction. The expression in 2.1 is derived in the analysis of the 2D *gradient-selected* $F1$-PSYCHE-EASY-ROESY experiment in chapter 5.1. To reduce the complexity of the mathematical expressions we limit our theoretical description to the transversal relaxation processes. The longitudinal cross-relaxation part can be analysed in the same way.

$$\begin{aligned} S_+(\omega_{F1},\omega_{F2},\tau_m) \;=\; & \sum_k \sum_l \\ & \frac{1}{2}\cdot w_L M_0 \boldsymbol{\beta} D \,\frac{R_{2,k}}{R_{2,k}^2 \,+\, (\omega_{F1}-\Omega_k)^2}\cdot \vec{e}_l \cdot \exp(\mathbf{L}\tau_m)\cdot \vec{e}_k \cdot \frac{R_{2,l}}{R_{2,l}^2 \,+\, (\omega_{F2}-\Omega_l)^2} \\ +\; & \frac{1}{2}\cdot w_T M_0 \boldsymbol{\beta} D \,\frac{R_{2,k}}{R_{2,k}^2 \,+\, (\omega_{F1}-\Omega_k)^2}\cdot \vec{e}_l \cdot \exp(\mathbf{T}\tau_m)\cdot \vec{e}_k \cdot \frac{R_{2,l}}{R_{2,l}^2 \,+\, (\omega_{F2}-\Omega_l)^2} \end{aligned} \tag{2.1}$$

Therefore we define for our system the transversal cross-relaxation matrix $\mathbf{T}$:

$$\mathbf{T} \;=\; \begin{pmatrix} -R_{AA} & -R_{AB} \\ -R_{BA} & -R_{BB} \end{pmatrix} \tag{2.2}$$

For R_{AA}, R_{BB}, R_{AB} and R_{BA} we use the definitions by Jeener *et al.* [3]. Herein δ_A and δ_B are auto-relaxation rates, σ_{AB} is the transversal cross-relaxation rate and n_A and n_B are the number of protons. We assume to have only relaxation processes and no chemical exchange ($k = 0$).

$$\begin{aligned} R_{AA} &= \delta_A \,+\, 2n_B\sigma_{AB} \\ R_{BB} &= \delta_B \,+\, 2n_A\sigma_{AB} \\ R_{AB} &= n_A\sigma_{AB} \\ R_{BA} &= n_B\sigma_{AB} \end{aligned} \tag{2.3}$$

Inserting the relaxation matrix in equation 2.1 and then writing out the matrix exponential as described in literature[3,10] gives the four expressions for the integrated intensities I_{kl} of the diagonal- and cross-peaks:

$$\begin{aligned} I_{AA}(\Omega_{1,A},\,\Omega_{2,A},\,\tau_m) &= \frac{1}{2} w_T M_0 \beta_A D\, a_{AA}(\tau_m) \\ I_{BB}(\Omega_{1,B},\,\Omega_{2,B},\,\tau_m) &= \frac{1}{2} w_T M_0 \beta_B D\, a_{BB}(\tau_m) \\ I_{AB}(\Omega_{1,A},\,\Omega_{2,B},\,\tau_m) &= \frac{1}{2} w_T M_0 \beta_A D\, a_{AB}(\tau_m) \\ I_{BA}(\Omega_{1,B},\,\Omega_{2,A},\,\tau_m) &= \frac{1}{2} w_T M_0 \beta_B D\, a_{BA}(\tau_m) \end{aligned} \tag{2.4}$$

In analogy to literature[3,10] we use the mixing coefficients $a_{kl}(\tau_m)$, which describe the intensity of the integrated diagonal- and cross-peaks for a given mixing time τ_m in the absence of spin diffusion,

$$\begin{aligned}
a_{AA}(\tau_m) &= \frac{1}{2}\frac{n_A}{n_A+n_B}\exp(-R_L\tau_m)\cdot \\
&\quad \left[\left(1 - \frac{R_{AA}-R_{BB}}{R_C}\right) + \left(1 + \frac{R_{AA}-R_{BB}}{R_C}\right)\exp(-R_C\tau_m)\right] \\
a_{BB}(\tau_m) &= \frac{1}{2}\frac{n_B}{n_A+n_B}\exp(-R_L\tau_m)\cdot \\
&\quad \left[\left(1 - \frac{R_{BB}-R_{AA}}{R_C}\right) + \left(1 + \frac{R_{BB}-R_{AA}}{R_C}\right)\exp(-R_C\tau_m)\right] \\
a_{AB}(\tau_m) &= a_{BA}(\tau_m) = -\frac{n_A n_B}{n_A+n_B}\frac{\sigma_{AB}}{R_C}\exp(-R_L\tau_m)\cdot[1 - \exp(-R_C\tau_m)]
\end{aligned} \tag{2.5}$$

where R_C and R_L are the cross-relaxation and the leakage-relaxation rate constants as defined by[10]:

$$\begin{aligned}
R_C &= \sqrt{(R_{AA} - R_{BB})^2 + 4\sigma_{AB}\sigma_{BA}} \\
R_L &= \frac{1}{2}(R_{AA} + R_{BB}) - \frac{1}{2}R_C
\end{aligned} \tag{2.6}$$

We quantify the $F1$-homonuclear decoupled EASY-ROESY spectra by extracting and integrating traces along the direct dimension $F2$. If we take the $F2$-trace at the peak maximum of proton A ($\omega_{F1} = \Omega_A$) in the $F1$ dimension (assuming perfect homodecoupling performance),the expression in equation 2.1 simplifies to:

$$\begin{aligned}
&S_{+,A}(\omega_{F2},\, \tau_m) = \sum_l \\
&\frac{1}{2}\frac{1}{R_{2,A}} w_T M_0 \beta_A D \exp(-\mathbf{T}\tau_m)\cdot\vec{e}_l\cdot\frac{R_{2,l}}{R_{2,l}^2 + (\omega_{F2}-\Omega_l)^2}
\end{aligned} \tag{2.7}$$

Then we use the mixing coefficients $a(\tau_m)$, which we obtain from the evaluation of the matrix exponential. As we have extracted the $F2$-trace, only the two expressions for the *target*-proton A I_{AA} and I_{AB} are relevant for further examination:

$$\begin{aligned}
I_{AA}(\Omega_{2,A},\, \tau_m) &= \frac{1}{2} w_T M_0 \beta_A D \frac{1}{R_{2,A}}\cdot a_{AA}(\tau_m) \\
I_{AB}(\Omega_{2,B},\, \tau_m) &= -\frac{1}{2} w_T M_0 \beta_A D \frac{1}{R_{2,A}}\cdot a_{AB}(\tau_m)
\end{aligned} \tag{2.8}$$

The peak integration is performed in a 1D spectrum analogous to a selective 1D-ROESY experiment. Hence we can take advantage from the PANIC approach described by Hu and Krishnamurthy[14], which is the 1D equivalent to the procedure described by Macura *et al.* [15]

for 2D-NOESY experiments and normalise the NOE cross-peak integral by the corresponding diagonal-peak integral:

$$\begin{aligned}\widetilde{\zeta}\left(\tau_m\right) &= \frac{-I_{AB}\left(\tau_m\right)}{n_B I_{AA}\left(\tau_m\right)} \\ &= \frac{\frac{1}{2} w_T M_0 \beta_A D \frac{1}{R_{2,A}} \cdot a_{AB}\left(\tau_m\right)}{\frac{1}{2} n_B w_T M_0 \beta_A D \frac{1}{R_{2,A}} \cdot a_{AA}\left(\tau_m\right)}\end{aligned} \tag{2.9}$$

In equation 2.9 all constants including the factors for accounting diffusion D and the homonuclear decoupling using the PSYCHE method β_k vanish and only the mixing coefficients and n_B remain. The PSYCHE parameter β_k vanishes only, however, if we normalise the NOE cross-peak integral by the corresponding diagonal-peak integral with the same chemical shift in $F1$ (integrated in the same row, as is proposed to do here). Inserting then the expression for the mixing coefficients a_{AA} and a_{AB} and tidying up, we get:

$$\widetilde{\zeta}\left(\tau_m\right) \;=\; \frac{2\sigma_{AB}}{R_C} \cdot \frac{1 \;-\; \exp\left(-R_C\tau_m\right)}{1 \;+\; \exp\left(-R_C\tau_m\right) \;+\; \frac{R_{AA}-R_{BB}}{R_C}\left(1 \;-\; \exp\left(-R_C\tau_m\right)\right)} \tag{2.10}$$

Evaluation of this expression in a Taylor series as described by Hu and Krishnamurthy[14] and discarding all terms with higher order than three we get:

$$\begin{aligned}\widetilde{\zeta}\left(\tau_m\right) \;\approx\; & \sigma_{AB}\tau_m \;+\; \frac{1}{2}\sigma_{AB}(R_{BB}-R_{AA})\,\tau_m^2 \;-\; \frac{1}{12}\sigma_{AB}\left(R_C^2 - 3R_{BB}^2 + 6R_{AA}\,R_{BB} - 3R_{AA}^2\right)\tau_m^3 \\ & +\; \cdots\end{aligned} \tag{2.11}$$

If $R_{AA} \;\approx\; R_{BB}$ we can neglect the second-order term in the series and extract the cross-relaxation rate σ_{AB} from the slope of an linear-fit between the normalised peak-integrals and the mixing-time τ_m. If the difference in the self-relaxation rates are not negligible, the second order term should be included in the fitting procedure. However the majority of our PANIC plots derived from a mixing-time series of the 2D $F1$-PSYCHE-EASY-ROESY, the 2D *gradient-selected* $F1$-PSYCHE-EASY-ROESY and all 1D-ROESY experiments show a good linear behaviour, rendering a quadratic fit of the data usually unnecessarily. The quadratic fit was applied only in some cases, when the data points in the PANIC plots clearly differ from the linear trend. Herein the parameter $(R_{BB} - R_{AA})$ was not used as a contraint for quadratic fitting of the data. Cases in which the data points in the PANIC plots show neither a clear linear nor a quadratic trend were not used for further analysis.

Usually the linear fits are performed without intercept assuming zero cross-relaxation for zero mixing time τ_m. Some of our data show a deviating behaviour. Thus there is indeed cross-relaxation for zero mixing time τ_m, which might be caused by strong coupling effects and cross-realaxation during the other elements in the pulse sequence. For fitting the data we always allow an intercept, but in most cases the values are small.

2.2 Distance determination

Distances are calculated using the approach of an internal reference based on the assumption of isotropic molecular tumbling which is uniform for the whole molecule.

$$r_{AB} \;=\; r_{ref} \cdot \left(\frac{\sigma_{AB}}{\sigma_{ref}}\right)^{-\frac{1}{6}} \tag{2.12}$$

For the tetrapeptide - $R,R-$cyclohexane-1,2-diol mixture data the distance between the diastereotopic protons H13a and H13b of the cyclohexyl-sidechain was used and set to $r_{13a,13b} = 1.75\,\mathring{A}$. For the cyclosporine A data the diastereotopic backbone protons of the amino-acid 3-Sar H3α_1 and H3α_2 were use as reference and their distance was set to $r_{3\alpha1,3\alpha2} = 1.75\,\mathring{A}$. The error of the distance Δr_{AB} is only calculated from the fitting error of the slope in the PANIC plot.

$$\Delta r_{AB} \;=\; \sqrt{\left[-\frac{r_{ref}}{6\sigma_{ref}\cdot\left(\frac{\sigma_{AB}}{\sigma_{ref}}\right)^{\frac{7}{6}}}\cdot\Delta\sigma_{AB}\right]^2 \;+\; \left[\frac{r_{ref}\cdot\sigma_{AB}}{6\sigma_{ref}^2\cdot\left(\frac{\sigma_{AB}}{\sigma_{ref}}\right)^{\frac{7}{6}}}\cdot\Delta\sigma_{ref}\right]^2} \tag{2.13}$$

3 Cyclosporine A

3.1 Proton assignment of cyclosporine A in C_6D_6

The proton assignment of cyclosporine A in C_6D_6 was taken from Kessler et al.[16], the given assignment was checked with ^{1}H, ^{1}H-PSYCHE[6], $F1$-PSYCHE-TOCSY[17] and ^{1}H,^{13}C-HSQC. If possible the diastereotopic notations *pro R* and *pro S* for diastereotopic protons as well as for chemically inequivalent methyl groups within valine and leucine residues are given. Protons marked with X are overlapped in $F1$ and are not used for the extraction of cross-relaxation rates.

Table 3.1: Proton assignment of cyclosporine A in C_6D_6

	Proton	Chem. Shift / ppm		Proton	Chem. Shift / ppm
	2-NH	8.2501		3-NMe	3.0664
	7-NH	7.9619		11-NMe	2.9671
	8-NH	7.6077		9-NMe	2.9212
	5-NH	7.4470		10-NMe	2.8419
	9-α	5.8634		1-δ_1 (*pro R*)	2.6575
	1-α	5.7216		5-β	2.6128
	1-ϵ	5.6394		4-NMe	2.5853
	4-α	5.5827		10-β_1 (*pro R*)	2.4151
	1-η	5.5211	X	4-β_1	2.2684
	6-α	5.3782	X	6-β_1 (*pro S*)	2.2659
	10-α	5.3298		11-β	2.2534
	11-α	5.2528		3-α_2	2.2011
	2-α	5.1142		9-β_1 (*pro R*)	2.1699
	5-α	4.8782	X	1-δ_2 (*pro S*)	2.1352
	8-α	4.8266	X	6γ	2.1254
	7-α	4.8031		1-γ	2.0627
	1-β	4.1917		10-γ	1.7831
	3-α_1	4.0027	X	2β_1 ; 2-β_2*	1.7716
	1-NMe	3.7166		1-ω	1.7407
X	1-OH	3.4500		7-β	1.6688
	6-NMe	3.2182	X	4-β_2**	1.5558

Table 3.1 – continuation

	Proton	Chem. Shift / ppm		Proton	Chem. Shift / ppm
	6-β_2 (*pro R*)	1.4468		6-δ_2 (*pro R*)	1.0500
	4-γ	1.3884		8-β	1.0296
	10-β_2 (*pro S*)	1.2924		4-δ_1	0.9789
X	9-γ*	1.2588		11-γ_1 (*pro R*)	0.9525
X	9-β_2 (*pro S*)*	1.2503	X	5-γ_2 (*pro R*)	0.9059
	10-δ_1	1.1600	X	9-δ_1	0.902
	10-δ_2	1.1518		4-δ_2	0.8974
X	5-γ_1 (*pro S*)	1.1379		2-γ	0.8613
X	6-δ_1 (*pro S*)	1.1356		9-δ_2	0.8256
X	1-γMe	1.1329		11-γ_2 (*pro S*)	0.641

*strongly coupled **distorted by H_2O peak

3.2 ^{1}H,^{1}H-distances extracted from 2D *gradient-selected F*1-PSYCHE-EASY-ROESY

Table 3.2: ^{1}H,^{1}H-distances extracted from 2D *gradient-selected* $F1$-PSYCHE-EASY-ROESY.

H	H'	σ / s^{-1}	r / $\AA$	H	H'	σ / s^{-1}	r / $\AA$
3-α_1	3-α_2	0.8967 ± 0.0106	1.75 (ref.)				
1−α	2-NH	0.2140 ± 0.0129	2.222 ± 0.023	6−α	7-NH	0.2439 ± 0.0019	2.174 ± 0.005
1−α	1−β	0.1168 ± 0.0022	2.458 ± 0.009	6−α	1−α	0.0746 ± 0.0026	2.649 ± 0.016
1−α	1−δ_1	0.0715 ± 0.0027	2.668 ± 0.018	6−α	6-NMe	0.0054 ± 0.0010	4.099 ± 0.126
1−α	6−α	0.0699 ± 0.0023	2.678 ± 0.016	6−α	1−δ_1	0.0444 ± 0.0013	2.888 ± 0.015
1−α	1−γMe	0.0298 ± 0.0034	3.087 ± 0.059	6−α	6−γ	0.0426 ± 0.0018	2.908 ± 0.022
1−α	7-NH	0.0330 ± 0.0033	3.034 ± 0.051	6−α	6−β_1	0.0322 ± 0.0132	3.047 ± 0.209
1−α	6−δ_2	0.0066 ± 0.0006	3.968 ± 0.061	6−α	6−β_2	0.0817 ± 0.0106	2.609 ± 0.057
1−α	1-NMe	0.0066 ± 0.0026	3.973 ± 0.258	6−α	6−δ_1	0.0211 ± 0.0007	3.269 ± 0.020
1−α	1−γ	0.0297 ± 0.0016	3.087 ± 0.028	6−α	6−δ_2	0.0299 ± 0.0004	3.085 ± 0.009
1−α	1−δ_2	0.0133 ± 0.0009	3.529 ± 0.040	7−α	7−β	0.0530 ± 0.0030	2.804 ± 0.027
2−α	2-NMe	0.0769 ± 0.0017	2.635 ± 0.011	7−α	8-NH	0.0660 ± 0.0054	2.703 ± 0.037
2−α	2−γ	0.0240 ± 0.0021	3.201 ± 0.047	7−α	7-NH	0.0321 ± 0.0051	3.049 ± 0.081
2−α	2-NH	0.0268 ± 0.0053	3.140 ± 0.104	7−α	5−γ_2	0.0056 ± 0.0003	4.076 ± 0.032
3−α_1	4-NMe	0.0879 ± 0.0007	2.577 ± 0.006	8−α	9-NMe	0.0750 ± 0.0016	2.646 ± 0.011
4−α	4−β_1	0.0998 ± 0.0045	2.523 ± 0.020	8−α	8−β	0.0479 ± 0.0004	2.851 ± 0.007
4−α	4−δ_1	0.0396 ± 0.0012	2.944 ± 0.016	8−α	8-NH	0.0284 ± 0.0034	3.112 ± 0.062
4−α	5-NH	0.0333 ± 0.0026	3.029 ± 0.040	8−α	11-NMe	0.0043 ± 0.0004	4.265 ± 0.074
4−α	4−γ	0.0303 ± 0.0029	3.078 ± 0.049	9−α	10−α	0.5485 ± 0.0023	1.899 ± 0.004
4−α	1−ω	0.0080 ± 0.0005	3.845 ± 0.037	9−α	9−δ_1	0.0345 ± 0.0008	3.011 ± 0.013
4−α	4-NMe	0.0064 ± 0.0014	3.989 ± 0.146	9−α	10−γ	0.0321 ± 0.0089	3.048 ± 0.141
5−α	6-NMe	0.0753 ± 0.0020	2.644 ± 0.013	9−α	9-NMe	0.0080 ± 0.0011	3.844 ± 0.085
5−α	5−γ_1	0.0265 ± 0.0034	3.148 ± 0.067	10−α	9−α	0.5787 ± 0.0067	1.882 ± 0.005
5−α	5−γ_2	0.0222 ± 0.0015	3.242 ± 0.037	10−α	11-NMe	0.0678 ± 0.0010	2.691 ± 0.008
5−α	5−β	0.0377 ± 0.0012	2.967 ± 0.017	10−α	10-NMe	0.0073 ± 0.0007	3.902 ± 0.063
5−α	5-NH	0.0344 ± 0.0035	3.013 ± 0.051	10−α	10−β_1	0.0410 ± 0.0010	2.926 ± 0.013

Table 3.2 – continuation

H	H'	σ / s^{-1}	r / $\AA$	H	H'	σ / s^{-1}	r / $\AA$
10−α	10−γ	0.0555 ± 0.0063	2.782 ± 0.053	9-NMe	9−α	0.0058 ± 0.0007	4.058 ± 0.078
10−α	10−β_2	0.0785 ± 0.0035	2.626 ± 0.020	9-NMe	8−α	0.1123 ± 0.0006	2.474 ± 0.005
10−α	6−δ_2	0.0131 ± 0.0008	3.538 ± 0.038	9-NMe	9−β_1	0.0332 ± 0.0012	3.032 ± 0.020
11−α	1-NMe	0.0980 ± 0.0026	2.531 ± 0.012	9-NMe	8−β	0.0048 ± 0.0002	4.188 ± 0.031
11−α	11-NMe	0.0070 ± 0.0020	3.927 ± 0.185	9-NMe	9−δ_1	0.0009 ± 0.0001	5.564 ± 0.118
11−α	10-NMe	0.0039 ± 0.0004	4.339 ± 0.074	9-NMe	9−δ_2	0.0011 ± 0.0002	5.333 ± 0.167
11−α	11−β	0.0298 ± 0.0072	3.086 ± 0.125	10-NMe	10−α	0.0051 ± 0.0008	4.141 ± 0.104
11−α	11−γ_1	0.0286 ± 0.0010	3.107 ± 0.018	10-NMe	11−α	0.0041 ± 0.0005	4.289 ± 0.088
11−α	11−γ_2	0.0278 ± 0.0026	3.122 ± 0.049	10-NMe	10−β_1	0.0236 ± 0.0035	3.210 ± 0.079
1-NMe	1−α	0.0059 ± 0.0006	4.038 ± 0.068	10-NMe	10−β_2	0.0249 ± 0.0017	3.181 ± 0.036
1-NMe	11−α	0.1177 ± 0.0015	2.455 ± 0.007	10-NMe	11−γ_2	0.0107 ± 0.0004	3.664 ± 0.024
1-NMe	1−β	0.0369 ± 0.0005	2.978 ± 0.009	11-NMe	7-NH	0.0143 ± 0.0002	3.489 ± 0.009
1-NMe	1−γ	0.0197 ± 0.0010	3.308 ± 0.029	11-NMe	8-NH	0.0070 ± 0.0004	3.926 ± 0.038
1-NMe	11−γ_1	0.0133 ± 0.0006	3.532 ± 0.030	11-NMe	10−α	0.0698 ± 0.0023	2.678 ± 0.015
3-NMe	2−α	0.0881 ± 0.0001	2.576 ± 0.005	11-NMe	11−α	0.0069 ± 0.0007	3.935 ± 0.063
3-NMe	3−α_2	0.0406 ± 0.0015	2.931 ± 0.018	11-NMe	10-NMe	0.0044 ± 0.0001	4.239 ± 0.020
4-NMe	5-NH	0.0201 ± 0.0006	3.296 ± 0.018	11-NMe	11−β	0.0787 ± 0.0005	2.625 ± 0.006
4-NMe	4−α	0.0071 ± 0.0003	3.924 ± 0.024	11-NMe	7−β	0.0045 ± 0.0003	4.231 ± 0.040
4-NMe	3−α_1	0.0715 ± 0.0015	2.668 ± 0.011	11-NMe	6−δ_2	0.0027 ± 0.0001	4.611 ± 0.030
4-NMe	4−β_2	0.0451 ± 0.0014	2.880 ± 0.016	11-NMe	11−γ_2	0.0089 ± 0.0003	3.772 ± 0.021
4-NMe	4−γ	0.0192 ± 0.0008	3.321 ± 0.023	8-NH	7-NH	0.0250 ± 0.0019	3.178 ± 0.040
4-NMe	5−γ_1	0.0071 ± 0.0003	3.917 ± 0.028	8-NH	11-NMe	0.0080 ± 0.0006	3.841 ± 0.045
6-NMe	6−α	0.0070 ± 0.0018	3.926 ± 0.168	8-NH	8−β	0.0296 ± 0.0010	3.090 ± 0.018
6-NMe	5−α	0.1118 ± 0.0013	2.476 ± 0.007	2-NH	1−α	0.1835 ± 0.0244	2.280 ± 0.051
6-NMe	6−β_1	0.0396 ± 0.0014	2.944 ± 0.018	2-NH	2−α	0.0267 ± 0.0067	3.142 ± 0.132
6-NMe	6−β_2	0.0284 ± 0.0100	3.112 ± 0.183	2-NH	1−β	0.0828 ± 0.0157	2.603 ± 0.082
6-NMe	5−γ_2	0.0066 ± 0.0003	3.968 ± 0.035	5-NH	2-NH	0.0189 ± 0.0021	3.329 ± 0.062
6-NMe	6−δ_2	0.0018 ± 0.0007	4.909 ± 0.311	5-NH	4−α	0.0352 ± 0.0063	3.002 ± 0.090
6-NMe	7−α	0.0029 ± 0.0003	4.556 ± 0.069	5-NH	5−α	0.0500 ± 0.0036	2.832 ± 0.034

Table 3.2 – continuation

H	H'	σ / s^{-1}	r / $\AA$	H	H'	σ / s^{-1}	r / $\AA$
5-NH	5−γ_1	0.0219 ± 0.0012	3.249 ± 0.031	11−β	11−α	0.0287 ± 0.0019	3.107 ± 0.036
7-NH	1−α	0.0391 ± 0.0061	2.949 ± 0.077	11−β	11-NMe	0.0536 ± 0.0006	2.798 ± 0.008
7-NH	6−α	0.4077 ± 0.0182	1.996 ± 0.015	11−β	7−β	0.0099 ± 0.0004	3.710 ± 0.023
7-NH	11-NMe	0.0153 ± 0.0015	3.449 ± 0.058	11−β	11−γ_1	0.0453 ± 0.0028	2.878 ± 0.030
7-NH	7−β	0.0462 ± 0.0020	2.868 ± 0.021	11−β	11−γ_2	0.0423 ± 0.0034	2.911 ± 0.039
1−δ_1	1−α	0.1142 ± 0.0026	2.467 ± 0.011	3−α_2	3−α_1	0.8788 ± 0.0104	1.756 ± 0.005
1−δ_1	1−ϵ	0.0810 ± 0.0047	2.612 ± 0.026	3−α_2	3-NMe	0.0548 ± 0.0011	2.788 ± 0.011
1−δ_1	1−η	0.0549 ± 0.0045	2.787 ± 0.038	9−β_1	9-NMe	0.0405 ± 0.0008	2.933 ± 0.011
1−δ_1	6−α	0.0618 ± 0.0008	2.733 ± 0.008	9−β_1	9−δ_2	0.0299 ± 0.0030	3.085 ± 0.052
1−δ_1	1−δ_2	0.5410 ± 0.0038	1.904 ± 0.004	1−γ	1−α	0.0311 ± 0.0046	3.064 ± 0.076
1−δ_1	1−γ	0.2546 ± 0.0165	2.159 ± 0.024	1−γ	1−ϵ	0.0797 ± 0.0077	2.620 ± 0.043
1−β	2-NH	0.0623 ± 0.0026	2.730 ± 0.020	1−γ	1−β	0.1121 ± 0.0160	2.475 ± 0.059
1−β	1−α	0.0998 ± 0.0045	2.523 ± 0.020	1−γ	1-NMe	0.0227 ± 0.0006	3.229 ± 0.016
1−β	1-NMe	0.0279 ± 0.0017	3.120 ± 0.032	1−γ	3-NMe	0.0037 ± 0.0005	4.380 ± 0.096
1−β	3-NMe	0.0019 ± 0.0002	4.866 ± 0.068	1−γ	1−δ_1	0.2461 ± 0.0101	2.171 ± 0.015
1−β	1−δ_2	0.0493 ± 0.0026	2.838 ± 0.025	1−γ	1−γMe	0.0403 ± 0.0129	2.935 ± 0.157
1−β	1−γ	0.0601 ± 0.0021	2.745 ± 0.017	1−ω	1−ϵ	0.0279 ± 0.0014	3.121 ± 0.026
1−β	1−γMe	0.0310 ± 0.0013	3.066 ± 0.023	1−ω	4−α	0.0076 ± 0.0005	3.879 ± 0.043
5−β	2-NH	0.0166 ± 0.0001	3.404 ± 0.008	1−ω	1−η	0.0394 ± 0.0004	2.946 ± 0.007
5−β	5-NH	0.0776 ± 0.0030	2.631 ± 0.018	1−ω	6-NMe	0.0009 ± 0.0001	5.562 ± 0.155
5−β	5−α	0.0364 ± 0.0025	2.985 ± 0.035	1−ω	6−δ_2	0.0007 ± 0.0001	5.821 ± 0.214
5−β	6-NMe	0.0041 ± 0.0009	4.292 ± 0.156	1−ω	4−δ_1	0.0020 ± 0.0002	4.845 ± 0.097
5−β	5−γ_1	0.0395 ± 0.0008	2.945 ± 0.012	7−β	7-NH	0.0422 ± 0.0010	2.913 ± 0.013
5−β	5−γ_2	0.0520 ± 0.0036	2.813 ± 0.033	7−β	7−α	0.0647 ± 0.0033	2.712 ± 0.023
10−β_1	10−α	0.0349 ± 0.0050	3.006 ± 0.072	7−β	11-NMe	0.0051 ± 0.0003	4.142 ± 0.038
10−β_1	10-NMe	0.0226 ± 0.0091	3.231 ± 0.217	7−β	9−δ_1	0.0040 ± 0.0002	4.319 ± 0.043
10−β_1	10−γ	0.0896 ± 0.0111	2.569 ± 0.053	7−β	2−γ	0.0047 ± 0.0003	4.199 ± 0.047
10−β_1	10−β_2	0.8823 ± 0.0164	1.755 ± 0.006	6−β_2	6−α	0.0811 ± 0.0035	2.612 ± 0.019
10−β_1	10−δ_2	0.0372 ± 0.0029	2.975 ± 0.039	6−β_2	6-NMe	0.0226 ± 0.0069	3.232 ± 0.165

Table 3.2 – continuation

H	H'	σ / s^{-1}	r / $\AA$	H	H'	σ / s^{-1}	r / $\AA$
6−β_2	6−β_1	0.8346 ± 0.0112	1.771 ± 0.005	11−γ_1	1-NMe	0.0129 ± 0.0007	3.551 ± 0.033
6−β_2	6−δ_2	0.0205 ± 0.0006	3.286 ± 0.017	11−γ_1	11−β	0.0620 ± 0.0127	2.732 ± 0.093
4−γ	4−α	0.0241 ± 0.0031	3.197 ± 0.068	11−γ_1	2−γ	0.0062 ± 0.0010	4.015 ± 0.111
4−γ	4-NMe	0.0150 ± 0.0008	3.458 ± 0.031	11−γ_1	11−γ_2	0.0284 ± 0.0005	3.111 ± 0.011
4−γ	4−δ_1	0.0311 ± 0.0039	3.064 ± 0.064	2−γ	2−α	0.0279 ± 0.0011	3.121 ± 0.021
4−γ	4−δ_2	0.0357 ± 0.0031	2.995 ± 0.044	2−γ	7−β	0.0030 ± 0.0002	4.523 ± 0.060
10−β_2	9−α	0.0328 ± 0.0026	3.037 ± 0.040	2−γ	11−γ_2	0.0016 ± 0.0003	5.014 ± 0.173
10−β_2	10−α	0.0834 ± 0.0181	2.600 ± 0.094	9−δ_2	9-NMe	0.0012 ± 0.0002	5.243 ± 0.118
10−β_2	10-NMe	0.0208 ± 0.0017	3.277 ± 0.045	9−δ_2	9−β_1	0.0217 ± 0.0012	3.253 ± 0.029
10−β_2	10−β_1	0.8682 ± 0.0132	1.759 ± 0.006	9−δ_2	9−δ_1	0.0133 ± 0.0005	3.533 ± 0.024
6−δ_2	1−α	0.0080 ± 0.0004	3.840 ± 0.030	11−γ_2	11−α	0.0316 ± 0.0023	3.057 ± 0.037
6−δ_2	6−α	0.0358 ± 0.0009	2.993 ± 0.013	11−γ_2	11-NMe	0.0100 ± 0.0001	3.705 ± 0.011
6−δ_2	10−α	0.0123 ± 0.0009	3.579 ± 0.043	11−γ_2	10-NMe	0.0107 ± 0.0003	3.661 ± 0.016
6−δ_2	6-NMe	0.0018 ± 0.0004	4.909 ± 0.199	11−γ_2	11−β	0.0580 ± 0.0071	2.762 ± 0.057
6−δ_2	11-NMe	0.0029 ± 0.0004	4.543 ± 0.110	11−γ_2	11−γ_1	0.0216 ± 0.0024	3.255 ± 0.060
6−δ_2	6−β_2	0.0307 ± 0.0032	3.071 ± 0.054	10−γ	9−α	0.0294 ± 0.0090	3.094 ± 0.159
6−δ_2	6−γ	0.0632 ± 0.0007	2.723 ± 0.007	10−γ	10−α	0.0255 ± 0.0015	3.168 ± 0.032
6−δ_2	4−β_2	0.0210 ± 0.0012	3.272 ± 0.032	10−γ	10−β_1	0.0542 ± 0.0209	2.794 ± 0.179
6−δ_2	6−δ_1	0.0174 ± 0.0010	3.376 ± 0.033	10−γ	10−δ_2	0.0359 ± 0.0004	2.993 ± 0.008
8−β	8-NH	0.0285 ± 0.0005	3.109 ± 0.011	10−δ_1	9−α	0.0148 ± 0.0009	3.467 ± 0.037
8−β	8−α	0.0527 ± 0.0013	2.806 ± 0.013	10−δ_1	10-NMe	0.0019 ± 0.0001	4.874 ± 0.063
8−β	9-NMe	0.0061 ± 0.0004	4.026 ± 0.044	10−δ_1	10−α	0.0290 ± 0.0009	3.101 ± 0.018
8−β	9−δ_1	0.0017 ± 0.0003	4.994 ± 0.150	10−δ_1	10−γ	0.0683 ± 0.0020	2.688 ± 0.014
4−δ_1	4−α	0.0434 ± 0.0011	2.899 ± 0.013	10−δ_1	10−β_2	0.0406 ± 0.0027	2.932 ± 0.033
4−δ_1	4−β_1	0.0223 ± 0.0008	3.240 ± 0.021	10−δ_2	10−β_1	0.0318 ± 0.0007	3.053 ± 0.012
4−δ_1	1−ω	0.0034 ± 0.0002	4.436 ± 0.050	10−δ_2	9−α	0.0163 ± 0.0012	3.412 ± 0.042
4−δ_1	4−γ	0.0218 ± 0.0073	3.251 ± 0.181	10−δ_2	10−α	0.0113 ± 0.0003	3.630 ± 0.018
4−δ_1	4−δ_2	0.0109 ± 0.0008	3.652 ± 0.045	4−δ_2	4−β_1	0.0278 ± 0.0035	3.122 ± 0.066
11−γ_1	11−α	0.0292 ± 0.0055	3.096 ± 0.098	4−δ_2	4−δ_1	0.0136 ± 0.0004	3.518 ± 0.019

Table 3.2 – continuation

H	H'	σ / s^{-1}	r / $\AA$	H	H'	σ / s^{-1}	r / $\AA$
4−δ_2	4−γ	0.0176 ± 0.0042	3.369 ± 0.134	4−δ_2	4−β_2	0.0231 ± 0.0010	3.220 ± 0.024

3.3 ^{1}H,^{1}H-distances extracted from 2D *gradient-selected F1-perfect*BASH-EASY-ROESY

Table 3.3: ^{1}H,^{1}H-distances extracted from 2D *gradient-selected F1-perfect*BASH-EASY-ROESY.

H	H'	σ / s^{-1}	r / $\AA$	H	H'	σ / s^{-1}	r / $\AA$
3-α_1	3-α_2	0.7347 ± 0.0181	1.75 (ref.)				
1−α	2-NH	0.2150 ± 0.0130	2.148 ± 0.023	4−α	1−δ_1	0.0079 ± 0.0004	3.726 ± 0.035
1−α	7-NH	0.0205 ± 0.0010	3.177 ± 0.028	4−α	4-NMe	0.0059 ± 0.0003	3.911 ± 0.037
1−α	6−α	0.0650 ± 0.0019	2.621 ± 0.017	4−α	4−β_1	0.0841 ± 0.0067	2.512 ± 0.035
1−α	1−β	0.1062 ± 0.0027	2.416 ± 0.014	4−α	3−α_2	0.0032 ± 0.0001	4.326 ± 0.034
1−α	1-NMe	0.0054 ± 0.0009	3.974 ± 0.112	4−α	1−δ_2	0.0109 ± 0.0004	3.529 ± 0.027
1−α	1−δ_1	0.0737 ± 0.0018	2.567 ± 0.015	4−α	1−γ	0.0068 ± 0.0003	3.820 ± 0.035
1−α	1−δ_2	0.0251 ± 0.0047	3.073 ± 0.096	4−α	1−ω	0.0067 ± 0.0002	3.826 ± 0.024
1−α	1−γ	0.0268 ± 0.0003	3.038 ± 0.014	4−α	4−β_2	0.0315 ± 0.0068	2.958 ± 0.107
1−α	7−β	0.0020 ± 0.0001	4.699 ± 0.039	4−α	4−γ	0.0225 ± 0.0008	3.128 ± 0.022
1−α	1−γMe	0.0206 ± 0.0022	3.174 ± 0.057	4−α	6−δ_1	0.0031 ± 0.0003	4.349 ± 0.078
1−α	6−δ_2	0.0059 ± 0.0002	3.908 ± 0.025	4−α	4−δ_1	0.0268 ± 0.0009	3.039 ± 0.021
1−α	11−γ_2	0.0015 ± 0.0001	4.897 ± 0.057	4−α	4−δ_2	0.0032 ± 0.0002	4.328 ± 0.040
2−α	2-NH	0.0216 ± 0.0021	3.151 ± 0.052	5−α	5-NH	0.0311 ± 0.0024	2.965 ± 0.041
2−α	3-NMe	0.0598 ± 0.0016	2.658 ± 0.016	5−α	6-NMe	0.0841 ± 0.0084	2.511 ± 0.043
2−α	11−γ_1	0.0009 ± 0.0001	5.386 ± 0.090	5−α	5−β	0.0370 ± 0.0009	2.880 ± 0.016
2−α	2−γ	0.0198 ± 0.0020	3.196 ± 0.055	5−α	5−γ_1	0.0235 ± 0.0028	3.106 ± 0.064
3−α_1	5-NH	0.0101 ± 0.0009	3.574 ± 0.052	5−α	5−γ_2	0.0227 ± 0.0025	3.125 ± 0.058
3−α_1	4-NMe	0.0786 ± 0.0013	2.540 ± 0.013	6−α	2-NH	0.0065 ± 0.0005	3.853 ± 0.050
4−α	5-NH	0.0319 ± 0.0008	2.952 ± 0.017	6−α	7-NH	0.2328 ± 0.0209	2.119 ± 0.033
4−α	1−β	0.0090 ± 0.0007	3.648 ± 0.051	6−α	8-NH	0.0054 ± 0.0007	3.965 ± 0.084

Table 3.3 – continuation

H	H'	σ / s^{-1}	r / $\AA$	H	H'	σ / s^{-1}	r / $\AA$
6−α	1−α	0.0651 ± 0.0011	2.621 ± 0.013	9−α	9−δ_2	0.0030 ± 0.0001	4.385 ± 0.039
6−α	6-NMe	0.0060 ± 0.0001	3.904 ± 0.019	10−α	9−α	0.5138 ± 0.0100	1.857 ± 0.010
6−α	1−δ_1	0.0387 ± 0.0017	2.858 ± 0.024	10−α	11-NMe	0.0616 ± 0.0005	2.646 ± 0.011
6−α	6−β_1	0.0307 ± 0.0011	2.971 ± 0.022	10−α	9-NMe	0.0011 ± 0.0006	5.143 ± 0.444
6−α	6−γ	0.0409 ± 0.0007	2.832 ± 0.014	10−α	10-NMe	0.0055 ± 0.0002	3.955 ± 0.032
6−α	6−β_2	0.0766 ± 0.0052	2.551 ± 0.031	10−α	10−β_1	0.0396 ± 0.0013	2.848 ± 0.019
6−α	6−δ_1	0.0198 ± 0.0006	3.197 ± 0.021	10−α	6−γ	0.0040 ± 0.0003	4.165 ± 0.054
6−α	6−δ_2	0.0252 ± 0.0007	3.070 ± 0.018	10−α	10−γ	0.0453 ± 0.0009	2.784 ± 0.014
6−α	5−γ_2	0.0015 ± 0.0001	4.936 ± 0.051	10−α	10−β_2	0.0672 ± 0.0080	2.607 ± 0.053
7−α	7-NH	0.0316 ± 0.0046	2.957 ± 0.073	10−α	6−δ_2	0.0111 ± 0.0003	3.520 ± 0.020
7−α	8-NH	0.0668 ± 0.0025	2.610 ± 0.019	11−α	1-NMe	0.0824 ± 0.0090	2.520 ± 0.047
7−α	6-NMe	0.0008 ± 0.0001	5.415 ± 0.082	11−α	11-NMe	0.0044 ± 0.0002	4.100 ± 0.029
7−α	7−β	0.0377 ± 0.0010	2.871 ± 0.017	11−α	10-NMe	0.0037 ± 0.0002	4.227 ± 0.045
7−α	4−β_2	0.0017 ± 0.0001	4.817 ± 0.063	11−α	11−β	0.0266 ± 0.0014	3.043 ± 0.029
7−α	5−γ_1	0.0005 ± 0.0001	5.812 ± 0.055	11−α	6−δ_2	0.0010 ± 0.0001	5.284 ± 0.092
7−α	8−β	0.0013 ± 0.0001	5.058 ± 0.099	11−α	11−γ_1	0.0264 ± 0.0027	3.046 ± 0.053
7−α	5−γ_2	0.0046 ± 0.0002	4.084 ± 0.039	11−α	11−γ_2	0.0256 ± 0.0030	3.062 ± 0.061
8−α	8-NH	0.0290 ± 0.0017	3.000 ± 0.031	1-NMe	1−α	0.0052 ± 0.0005	3.999 ± 0.070
8−α	11-NMe	0.0051 ± 0.0003	4.008 ± 0.044	1-NMe	11−α	0.0997 ± 0.0019	2.441 ± 0.013
8−α	9-NMe	0.0725 ± 0.0043	2.574 ± 0.028	1-NMe	2−α	0.0028 ± 0.0002	4.417 ± 0.057
8−α	7−β	0.0016 ± 0.0002	4.841 ± 0.108	1-NMe	1−β	0.0339 ± 0.0009	2.922 ± 0.018
8−α	8−β	0.0435 ± 0.0043	2.803 ± 0.048	1-NMe	3-NMe	0.0005 ± 0.0001	5.842 ± 0.104
9−α	10−α	0.4865 ± 0.0090	1.874 ± 0.010	1-NMe	11-NMe	0.0003 ± 0.0001	6.390 ± 0.188
9−α	11-NMe	0.0050 ± 0.0006	4.016 ± 0.079	1-NMe	10-NMe	0.0003 ± 0.0001	6.505 ± 0.151
9−α	9-NMe	0.0058 ± 0.0008	3.922 ± 0.092	1-NMe	1−δ_1	0.0015 ± 0.0002	4.913 ± 0.116
9−α	10-NMe	0.0014 ± 0.0002	4.976 ± 0.145	1-NMe	11−β	0.0023 ± 0.0002	4.589 ± 0.063
9−α	9−β_1	0.0273 ± 0.0011	3.029 ± 0.024	1-NMe	1−δ_2	0.0089 ± 0.0003	3.650 ± 0.023
9−α	10−γ	0.0388 ± 0.0012	2.857 ± 0.018	1-NMe	1−γ	0.0175 ± 0.0003	3.263 ± 0.016
9−α	9−δ_1	0.0296 ± 0.0007	2.989 ± 0.017	1-NMe	10−γ	0.0022 ± 0.0002	4.617 ± 0.061

Table 3.3 – continuation

H	H'	σ / s^{-1}	r / $\AA$	H	H'	σ / s^{-1}	r / $\AA$
1-NMe	1−γMe	0.0010 ± 0.0001	5.248 ± 0.031	7-NH	6−δ_2	0.0065 ± 0.0002	3.847 ± 0.025
1-NMe	6−δ_2	0.0004 ± 0.0001	6.075 ± 0.046	7-NH	5−γ_2	0.0036 ± 0.0001	4.244 ± 0.025
1-NMe	11−γ_1	0.0080 ± 0.0003	3.715 ± 0.031	8-NH	7-NH	0.0241 ± 0.0025	3.092 ± 0.055
1-NMe	11−γ_2	0.0005 ± 0.0001	5.875 ± 0.063	8-NH	11-NMe	0.0081 ± 0.0005	3.709 ± 0.042
6-NMe	8-NH	0.0011 ± 0.0001	5.158 ± 0.060	8-NH	9-NMe	0.0027 ± 0.0001	4.460 ± 0.030
6-NMe	6−α	0.0061 ± 0.0020	3.888 ± 0.213	8-NH	6−β_1	0.0147 ± 0.0009	3.360 ± 0.038
6-NMe	5−α	0.0961 ± 0.0012	2.456 ± 0.011	8-NH	6−γ	0.0489 ± 0.0010	2.749 ± 0.015
6-NMe	5−β	0.0049 ± 0.0004	4.031 ± 0.057	8-NH	7−β	0.0021 ± 0.0002	4.638 ± 0.072
6-NMe	6−β_1	0.0358 ± 0.0010	2.896 ± 0.018	8-NH	5−γ_1	0.0040 ± 0.0001	4.178 ± 0.019
6-NMe	6−γ	0.0055 ± 0.0002	3.962 ± 0.028	8-NH	8−β	0.0250 ± 0.0005	3.075 ± 0.016
6-NMe	1−ω	0.0008 ± 0.0001	5.464 ± 0.117	5-NH	2-NH	0.0228 ± 0.0025	3.121 ± 0.059
6-NMe	6−β_2	0.0189 ± 0.0007	3.222 ± 0.024	5-NH	4−α	0.0530 ± 0.0018	2.713 ± 0.019
6-NMe	6−δ_2	0.0011 ± 0.0001	5.174 ± 0.046	5-NH	5−α	0.0494 ± 0.0026	2.744 ± 0.026
6-NMe	5−γ_2	0.0064 ± 0.0002	3.857 ± 0.029	5-NH	1−β	0.0083 ± 0.0012	3.695 ± 0.088
2-NH	5-NH	0.0405 ± 0.0013	2.837 ± 0.019	5-NH	3−α_1	0.0097 ± 0.0007	3.602 ± 0.047
2-NH	1−α	0.3007 ± 0.0087	2.031 ± 0.013	5-NH	5−γ_1	0.0192 ± 0.0017	3.211 ± 0.049
2-NH	6−α	0.0136 ± 0.0010	3.404 ± 0.044	5-NH	5−γ_2	0.0016 ± 0.0001	4.851 ± 0.068
2-NH	2−α	0.0560 ± 0.0012	2.687 ± 0.015	1−β	2-NH	0.0382 ± 0.0029	2.864 ± 0.038
2-NH	1−β	0.0902 ± 0.0038	2.482 ± 0.020	1−β	5-NH	0.0054 ± 0.0005	3.966 ± 0.061
2-NH	5−γ_1	0.0029 ± 0.0001	4.400 ± 0.037	1−β	1−α	0.0921 ± 0.0029	2.474 ± 0.017
2-NH	2−γ	0.0080 ± 0.0003	3.721 ± 0.028	1−β	4−α	0.0119 ± 0.0011	3.481 ± 0.058
7-NH	8-NH	0.0307 ± 0.0020	2.970 ± 0.035	1−β	1-NMe	0.0306 ± 0.0030	2.972 ± 0.050
7-NH	1−α	0.0391 ± 0.0019	2.853 ± 0.026	1−β	3-NMe	0.0026 ± 0.0002	4.495 ± 0.054
7-NH	6−α	0.3220 ± 0.0088	2.008 ± 0.012	1−β	1−δ_1	0.0106 ± 0.0003	3.546 ± 0.024
7-NH	7−α	0.0673 ± 0.0035	2.607 ± 0.025	1−β	1−δ_2	0.0425 ± 0.0009	2.814 ± 0.015
7-NH	11-NMe	0.0180 ± 0.0011	3.246 ± 0.035	1−β	1−γ	0.0505 ± 0.0023	2.735 ± 0.023
7-NH	7−β	0.0434 ± 0.0009	2.804 ± 0.015	1−β	1−γMe	0.0242 ± 0.0009	3.091 ± 0.022
7-NH	6−δ_1	0.0039 ± 0.0002	4.185 ± 0.039				

3.4 ^{1}H,^{1}H-distances extracted from 1D *selective* and *gradient-selected continuous-wave*-ROESY

Table 3.4: ^{1}H,^{1}H-distances extracted from 1D *selective* and *gradient-selected continuous-wave*-ROESY.

H	H'	σ / s^{-1}	r / Å	H	H'	σ / s^{-1}	r / Å
3-α_1	3-α_2	0.9630 ± 0.0098	1.75 (ref.)				
1-α	1-β	0.1810 ± 0.0018	2.286 ± 0.005	10-α	9-α	0.7770 ± 0.0073	1.808 ± 0.004
1-α	2-NH	0.1200 ± 0.0049	2.447 ± 0.017	10-α	11-NMe	0.0949 ± 0.0003	2.566 ± 0.005
1-α	6-α	0.1050 ± 0.0013	2.505 ± 0.007	10-α	10-NMe	0.0083 ± 0.0003	3.854 ± 0.022
1-α	1-δ_1	0.0943 ± 0.0019	2.548 ± 0.010	10-α	10-β_1	0.0495 ± 0.0015	2.860 ± 0.015
1-α	1-γ	0.0399 ± 0.0008	2.941 ± 0.011	10-α	10-γ	0.0481 ± 0.0015	2.874 ± 0.015
1-α	7-NH	0.0167 ± 0.0010	3.399 ± 0.035	10-α	10-β_2	0.0458 ± 0.0054	2.897 ± 0.057
2-α	1-NMe	0.0027 ± 0.0001	4.633 ± 0.028	10-α	6-δ_2	0.0120 ± 0.0004	3.624 ± 0.021
2-α	9-NMe	0.0012 ± 0.0001	5.302 ± 0.068	11-α	1-NMe	0.0840 ± 0.0012	2.619 ± 0.008
2-α	3-NMe	0.0875 ± 0.0030	2.601 ± 0.016	11-α	11-NMe	0.0056 ± 0.0002	4.112 ± 0.030
2-α	2-γ	0.0159 ± 0.0005	3.456 ± 0.018	11-α	10-NMe	0.0060 ± 0.0002	4.068 ± 0.018
2-α	2-NH	0.0121 ± 0.0018	3.620 ± 0.092	11-α	11-β	0.0410 ± 0.0018	2.951 ± 0.022
3-α_1	4-NMe	0.1160 ± 0.0008	2.481 ± 0.005	11-α	11-γ_1	0.0153 ± 0.0015	3.478 ± 0.058
6-α	7-NH	0.1420 ± 0.0092	2.398 ± 0.026	11-α	11-γ_2	0.0223 ± 0.0008	3.266 ± 0.019
6-α	1-α	0.0890 ± 0.0020	2.594 ± 0.010	1-NMe	1-α	0.0063 ± 0.0006	4.034 ± 0.069
6-α	6-NMe	0.0057 ± 0.0002	4.097 ± 0.025	1-NMe	11-α	0.1420 ± 0.0031	2.398 ± 0.010
6-α	1-δ_1	0.0497 ± 0.0036	2.859 ± 0.035	1-NMe	1-β	0.0599 ± 0.0017	2.771 ± 0.014
6-α	6-γ	0.0432 ± 0.0026	2.926 ± 0.029	1-NMe	1-γ	0.0267 ± 0.0007	3.171 ± 0.015
6-α	6-β_2	0.0699 ± 0.0022	2.700 ± 0.015	1-NMe	11-γ_1	0.0083 ± 0.0004	3.855 ± 0.033
6-α	6-δ_1	0.0180 ± 0.0007	3.385 ± 0.024	1-NMe	3-NMe	0.0008 ± 0.0001	5.716 ± 0.067
6-α	6-δ_2	0.0258 ± 0.0003	3.189 ± 0.007	3-NMe	2-α	0.1550 ± 0.0009	2.364 ± 0.005
9-α	10-α	0.7670 ± 0.0121	1.811 ± 0.006	3-NMe	3-α_2	0.0541 ± 0.0017	2.818 ± 0.015
9-α	9-δ_1	0.0410 ± 0.0016	2.951 ± 0.020	6-NMe	6-α	0.0087 ± 0.0011	3.824 ± 0.082
9-α	10-γ	0.0410 ± 0.0016	2.951 ± 0.020	6-NMe	5-α	0.1990 ± 0.0031	2.268 ± 0.007
9-α	9-β_1	0.0182 ± 0.0025	3.379 ± 0.076	6-NMe	6-β_1	0.0552 ± 0.0027	2.809 ± 0.024
9-α	9-NMe	0.0059 ± 0.0002	4.083 ± 0.021	6-NMe	6-β_2	0.0209 ± 0.0022	3.303 ± 0.058

Table 3.4 – continuation

H	H'	σ / s^{-1}	r / $\AA$	H	H'	σ / s^{-1}	r / $\AA$
6-NMe	6-δ_2	0.0014 ± 0.0001	5.182 ± 0.059	7-NH	6-α	0.6840 ± 0.0313	1.846 ± 0.014
6-NMe	5-γ_2	0.0075 ± 0.0004	3.917 ± 0.032	7-NH	7-α	0.1380 ± 0.0079	2.410 ± 0.023
9-NMe	9-α	0.0045 ± 0.0003	4.261 ± 0.051	7-NH	11-NMe	0.0342 ± 0.0014	3.043 ± 0.021
9-NMe	2-α	0.0030 ± 0.0005	4.559 ± 0.129	7-NH	7-β	0.0606 ± 0.0028	2.765 ± 0.022
9-NMe	8-α	0.1600 ± 0.0026	2.351 ± 0.008	8-NH	7-NH	0.0176 ± 0.0028	3.398 ± 0.091
9-NMe	9-β_1	0.0357 ± 0.0009	3.021 ± 0.014	8-NH	7-α	0.4140 ± 0.0312	2.008 ± 0.025
9-NMe	8-β	0.0040 ± 0.0005	4.350 ± 0.084	8-NH	11-NMe	0.0148 ± 0.0005	3.499 ± 0.021
9-NMe	9-δ_2	0.0009 ± 0.0001	5.612 ± 0.105	8-NH	8-β	0.0392 ± 0.0010	2.974 ± 0.014
10-NMe	11-NMe	0.0044 ± 0.0003	4.278 ± 0.046	5-NH	4-α	0.0895 ± 0.0020	2.591 ± 0.011
10-NMe	10-β_1	0.0153 ± 0.0040	3.480 ± 0.153	5-NH	5-α	0.1110 ± 0.0092	2.501 ± 0.035
10-NMe	10-β_2	0.0130 ± 0.0040	3.572 ± 0.181	5-NH	5-γ_1	0.0210 ± 0.0006	3.299 ± 0.016
10-NMe	11-γ_2	0.0077 ± 0.0004	3.901 ± 0.034	8-β	8-NH	0.0188 ± 0.0017	3.362 ± 0.050
11-NMe	7-NH	0.0060 ± 0.0006	4.061 ± 0.072	8-β	8-α	0.1020 ± 0.0037	2.535 ± 0.016
11-NMe	8-NH	0.0037 ± 0.0008	4.415 ± 0.163	8-β	9-NMe	0.0067 ± 0.0005	3.990 ± 0.052
11-NMe	10-α	0.0668 ± 0.0027	2.721 ± 0.019	6-δ_2	1-α	0.0077 ± 0.0003	3.904 ± 0.030
11-NMe	11-α	0.0082 ± 0.0008	3.862 ± 0.066	6-δ_2	6-α	0.0376 ± 0.0009	2.995 ± 0.012
11-NMe	8-α	0.0136 ± 0.0014	3.547 ± 0.061	6-δ_2	10-α	0.0131 ± 0.0014	3.571 ± 0.065
11-NMe	9-NMe	0.0045 ± 0.0002	4.270 ± 0.037	6-δ_2	1-NMe	0.0005 ± 0.0001	6.056 ± 0.081
11-NMe	10-NMe	0.0052 ± 0.0001	4.164 ± 0.019	6-δ_2	6-NMe	0.0016 ± 0.0001	5.062 ± 0.046
11-NMe	11-β	0.0867 ± 0.0015	2.605 ± 0.009	6-δ_2	11-NMe	0.0044 ± 0.0001	4.285 ± 0.014
11-NMe	7-β	0.0040 ± 0.0003	4.359 ± 0.050	6-δ_2	6-γ	0.0698 ± 0.0027	2.701 ± 0.018
11-NMe	6-δ_2	0.0022 ± 0.0002	4.795 ± 0.065	6-δ_2	6-β_2	0.0178 ± 0.0016	3.393 ± 0.053
11-NMe	11-γ_2	0.0074 ± 0.0002	3.925 ± 0.020	6-β_2	6-α	0.1160 ± 0.0037	2.482 ± 0.014
2-NH	5-NH	0.0390 ± 0.0024	2.976 ± 0.031	6-β_2	6-NMe	0.0269 ± 0.0014	3.166 ± 0.027
2-NH	1-α	0.5630 ± 0.0269	1.907 ± 0.016	6-β_2	6-β_1	0.7580 ± 0.0170	1.815 ± 0.007
2-NH	2-α	0.1310 ± 0.0108	2.432 ± 0.034	6-β_2	6-γ	0.0781 ± 0.0062	2.651 ± 0.035
2-NH	1-β	0.1360 ± 0.0036	2.416 ± 0.012	6-β_2	6-δ_1	0.0141 ± 0.0006	3.527 ± 0.024
7-NH	8-NH	0.0324 ± 0.0010	3.070 ± 0.016	6-β_2	6-δ_2	0.0188 ± 0.0009	3.361 ± 0.026
7-NH	1-α	0.0752 ± 0.0035	2.668 ± 0.021	10-β_1	10-α	0.0443 ± 0.0024	2.913 ± 0.027

Table 3.4 – continuation

H	H'	σ / s^{-1}	r / $\AA$	H	H'	σ / s^{-1}	r / $\AA$
10-β_1	10-NMe	0.0259 ± 0.0002	3.186 ± 0.007	11-γ_2	11-γ_1	0.0116 ± 0.0007	3.641 ± 0.038
10-β_1	10-γ	0.0779 ± 0.0038	2.652 ± 0.022	7-β	7-NH	0.0184 ± 0.0010	3.375 ± 0.030
10-β_1	10-β_2	0.6700 ± 0.0077	1.853 ± 0.005	7-β	7-α	0.1150 ± 0.0050	2.485 ± 0.018
10-β_1	10-δ_2	0.0251 ± 0.0018	3.202 ± 0.039	7-β	11-NMe	0.0064 ± 0.0002	4.027 ± 0.017
10-β_1	6-δ_2	0.0037 ± 0.0003	4.405 ± 0.060	7-β	6-β_1	0.0224 ± 0.0026	3.263 ± 0.062
11-γ_2	11-α	0.0472 ± 0.0009	2.883 ± 0.010	7-β	5-γ_2	0.0033 ± 0.0002	4.499 ± 0.042
11-γ_2	11-NMe	0.0126 ± 0.0004	3.595 ± 0.021	7-β	2-γ	0.0041 ± 0.0002	4.325 ± 0.027
11-γ_2	10-NMe	0.0143 ± 0.0002	3.519 ± 0.010	4-γ	4-α	0.0224 ± 0.0043	3.265 ± 0.105
11-γ_2	11-β	0.0674 ± 0.0041	2.717 ± 0.028	4-γ	4-NMe	0.0145 ± 0.0009	3.509 ± 0.036

3.5 ^{1}H,^{1}H-distances extracted from 1D *selective* and *gradient-selected*-EASY-ROESY

Table 3.5: ^{1}H,^{1}H-distances extracted from 1D *selective* and *gradient-selected* EASY-ROESY.

H	H'	σ / s^{-1}	r / $\AA$	H	H'	σ / s^{-1}	r / $\AA$
3-α_1	3-α_2	0.7296 ± 0.0075	1.75 (ref.)				
1−α	2-NH	0.1806 ± 0.0030	2.2090 ± 0.007	6−α	6−δ_2	0.0241 ± 0.0003	3.0900 ± 0.009
1−α	7-NH	0.0164 ± 0.0011	3.2960 ± 0.036	9−α	10−α	0.4484 ± 0.0043	1.8980 ± 0.004
1−α	6−α	0.0621 ± 0.0010	2.6390 ± 0.008	9−α	9-NMe	0.0048 ± 0.0001	4.0440 ± 0.021
1−α	1−β	0.1052 ± 0.0006	2.4170 ± 0.005	9−α	10-NMe	0.0012 ± 0.0001	5.1220 ± 0.060
1−α	1-NMe	0.0050 ± 0.0004	4.0180 ± 0.049	9−α	9−β_1	0.0280 ± 0.0052	3.0130 ± 0.094
1−α	11-NMe	0.0014 ± 0.0001	4.9470 ± 0.076	9−α	10−γ	0.0401 ± 0.0022	2.8380 ± 0.027
1−α	1−δ_1	0.0664 ± 0.0019	2.6100 ± 0.013	9−α	9−δ_1	0.0322 ± 0.0003	2.9430 ± 0.007
1−α	1−δ_2	0.0235 ± 0.0024	3.1040 ± 0.053	9−α	9−δ_2	0.0030 ± 0.0003	4.3840 ± 0.079
1−α	1−γ	0.0297 ± 0.0018	2.9830 ± 0.030	10−α	9−α	0.4740 ± 0.0011	1.8800 ± 0.003
1−α	1−γMe	0.0233 ± 0.0016	3.1080 ± 0.037	10−α	11-NMe	0.0611 ± 0.0005	2.6460 ± 0.006
1−α	6−δ_2	0.0062 ± 0.0002	3.8740 ± 0.017	10−α	10-NMe	0.0052 ± 0.0001	3.9880 ± 0.019
2−α	2-NH	0.0295 ± 0.0030	2.9880 ± 0.051	10−α	10−β_1	0.0320 ± 0.0014	2.9460 ± 0.022
2−α	1-NMe	0.0020 ± 0.0001	4.6900 ± 0.025	10−α	10−γ	0.0421 ± 0.0019	2.8150 ± 0.022
2−α	6-NMe	0.0013 ± 0.0001	5.0130 ± 0.019	10−α	10−β_2	0.0823 ± 0.0056	2.5180 ± 0.029
2−α	3-NMe	0.0574 ± 0.0013	2.6730 ± 0.011	10−α	6−δ_2	0.0111 ± 0.0004	3.5180 ± 0.020
2−α	2−γ	0.0208 ± 0.0007	3.1660 ± 0.019	11−α	1-NMe	0.0824 ± 0.0011	2.5170 ± 0.007
3−α_1	4-NMe	0.0787 ± 0.0002	2.5370 ± 0.004	11−α	11-NMe	0.0054 ± 0.0007	3.9670 ± 0.086
6−α	7-NH	0.1989 ± 0.0055	2.1730 ± 0.011	11−α	10-NMe	0.0037 ± 0.0001	4.2140 ± 0.020
6−α	1−α	0.0642 ± 0.0008	2.6240 ± 0.007	11−α	11−β	0.0314 ± 0.0057	2.9560 ± 0.089
6−α	6-NMe	0.0048 ± 0.0002	4.0390 ± 0.022	11−α	11−γ_1	0.0286 ± 0.0012	3.0030 ± 0.021
6−α	1−δ_1	0.0307 ± 0.0011	2.9670 ± 0.019	11−α	11−γ_2	0.0258 ± 0.0010	3.0540 ± 0.020
6−α	6−γ	0.0393 ± 0.0014	2.8480 ± 0.018	1-NMe	1−α	0.0047 ± 0.0002	4.0610 ± 0.036
6−α	6−β_1	0.0266 ± 0.0070	3.0390 ± 0.133	1-NMe	11−α	0.1044 ± 0.0008	2.4200 ± 0.005
6−α	6−β_2	0.0906 ± 0.0116	2.4780 ± 0.053	1-NMe	1−β	0.0331 ± 0.0005	2.9310 ± 0.008
6−α	6−δ_1	0.0192 ± 0.0009	3.2090 ± 0.025	1-NMe	3-NMe	0.0005 ± 0.0001	5.9300 ± 0.066

Table 3.5 – continuation

H	H'	σ / s^{-1}	r / $\AA$	H	H'	σ / s^{-1}	r / $\AA$
1-NMe	1−γ	0.0229 ± 0.0005	3.1150 ± 0.011	10-NMe	11−α	0.0040 ± 0.0002	4.1730 ± 0.029
1-NMe	11−γ_1	0.0075 ± 0.0005	3.7570 ± 0.044	10-NMe	1-NMe	0.0002 ± 0.0001	6.8050 ± 0.119
3-NMe	2−α	0.0787 ± 0.0015	2.5360 ± 0.009	10-NMe	11-NMe	0.0030 ± 0.0001	4.3770 ± 0.024
3-NMe	1-NMe	0.0006 ± 0.0001	5.7300 ± 0.100	10-NMe	10−β_1	0.0108 ± 0.0006	3.5320 ± 0.034
3-NMe	3−α_2	0.0367 ± 0.0012	2.8800 ± 0.016	10-NMe	10−β_2	0.0125 ± 0.0008	3.4450 ± 0.038
4-NMe	5-NH	0.0241 ± 0.0007	3.0890 ± 0.016	10-NMe	11−γ_2	0.0073 ± 0.0002	3.7700 ± 0.017
4-NMe	4−α	0.0057 ± 0.0001	3.9300 ± 0.009	11-NMe	7-NH	0.0091 ± 0.0003	3.6330 ± 0.021
4-NMe	5−α	0.0043 ± 0.0001	4.1130 ± 0.019	11-NMe	8-NH	0.0061 ± 0.0003	3.8890 ± 0.030
4-NMe	3−α_1	0.0625 ± 0.0018	2.6360 ± 0.013	11-NMe	10−α	0.0607 ± 0.0018	2.6480 ± 0.014
4-NMe	6-NMe	0.0004 ± 0.0001	6.0140 ± 0.132	11-NMe	11−α	0.0065 ± 0.0002	3.8420 ± 0.023
4-NMe	3-NMe	0.0004 ± 0.0001	6.1890 ± 0.068	11-NMe	8−α	0.0096 ± 0.0002	3.5990 ± 0.015
4-NMe	4−β_2	0.0379 ± 0.0013	2.8650 ± 0.017	11-NMe	9-NMe	0.0033 ± 0.0001	4.2970 ± 0.013
4-NMe	4−γ	0.0193 ± 0.0008	3.2070 ± 0.022	11-NMe	10-NMe	0.0040 ± 0.0001	4.1690 ± 0.010
4-NMe	5−γ_1	0.0098 ± 0.0003	3.5910 ± 0.017	11-NMe	11−β	0.0672 ± 0.0003	2.6040 ± 0.005
4-NMe	4−δ_1	0.0010 ± 0.0001	5.2420 ± 0.045	11-NMe	7−β	0.0042 ± 0.0001	4.1370 ± 0.022
6-NMe	6−α	0.0056 ± 0.0011	3.9460 ± 0.127	11-NMe	6−δ_2	0.0027 ± 0.0001	4.4500 ± 0.039
6-NMe	5−α	0.0985 ± 0.0007	2.4430 ± 0.005	11-NMe	11−γ_2	0.0088 ± 0.0004	3.6540 ± 0.026
6-NMe	6−β_1	0.0360 ± 0.0012	2.8890 ± 0.017	11-NMe	1-NMe	0.0005 ± 0.0001	5.8900 ± 0.052
6-NMe	6−β_2	0.0169 ± 0.0012	3.2780 ± 0.038	2-NH	5-NH	0.0353 ± 0.0024	2.8990 ± 0.034
6-NMe	6−δ_2	0.0011 ± 0.0001	5.2000 ± 0.073	2-NH	1−α	0.3358 ± 0.0171	1.9920 ± 0.017
6-NMe	5−γ_2	0.0068 ± 0.0004	3.8190 ± 0.040	2-NH	2−α	0.0760 ± 0.0066	2.5510 ± 0.037
9-NMe	9−α	0.0038 ± 0.0001	4.2000 ± 0.019	2-NH	1−β	0.0874 ± 0.0043	2.4920 ± 0.021
9-NMe	8−α	0.0880 ± 0.0010	2.4900 ± 0.006	2-NH	3-NMe	0.0019 ± 0.0001	4.7180 ± 0.061
9-NMe	11-NMe	0.0027 ± 0.0001	4.4390 ± 0.026	2-NH	2−γ	0.0057 ± 0.0009	3.9240 ± 0.106
9-NMe	10-NMe	0.0006 ± 0.0001	5.6820 ± 0.081	5-NH	2-NH	0.0167 ± 0.0016	3.2840 ± 0.053
9-NMe	9−β_1	0.0288 ± 0.0006	2.9990 ± 0.012	5-NH	4−α	0.0557 ± 0.0028	2.6870 ± 0.023
9-NMe	8−β	0.0049 ± 0.0003	4.0230 ± 0.039	5-NH	5−α	0.0475 ± 0.0014	2.7600 ± 0.015
9-NMe	9−δ_2	0.0011 ± 0.0001	5.2080 ± 0.064	5-NH	3−α_1	0.0064 ± 0.0043	3.8530 ± 0.427
10-NMe	10−α	0.0038 ± 0.0004	4.2130 ± 0.079	5-NH	5−γ_1	0.0174 ± 0.0002	3.2620 ± 0.009

Table 3.5 – continuation

H	H'	σ / s^{-1}	r / $\AA$	H	H'	σ / s^{-1}	r / $\AA$
7-NH	8-NH	0.0314 ± 0.0010	2.9560 ± 0.017	6−δ_2	10−α	0.0118 ± 0.0002	3.4780 ± 0.011
7-NH	7−α	0.0636 ± 0.0037	2.6280 ± 0.026	6−δ_2	6-NMe	0.0013 ± 0.0001	5.0070 ± 0.039
7-NH	6−α	0.3365 ± 0.0123	1.9910 ± 0.013	6−δ_2	11-NMe	0.0034 ± 0.0001	4.2840 ± 0.012
7-NH	1−α	0.0454 ± 0.0034	2.7800 ± 0.035	6−δ_2	6−β_2	0.0226 ± 0.0040	3.1230 ± 0.092
7-NH	11-NMe	0.0166 ± 0.0008	3.2870 ± 0.026	6−δ_2	6−δ_1	0.0150 ± 0.0002	3.3430 ± 0.009
7-NH	7−β	0.0450 ± 0.0008	2.7840 ± 0.009	7−β	7-NH	0.0302 ± 0.0005	2.9750 ± 0.009
7-NH	6−δ_2	0.0057 ± 0.0006	3.9250 ± 0.070	7−β	1−α	0.0022 ± 0.0002	4.6110 ± 0.078
8-NH	7-NH	0.0191 ± 0.0019	3.2110 ± 0.054	7−β	7−α	0.0741 ± 0.0036	2.5620 ± 0.021
8-NH	11-NMe	0.0064 ± 0.0002	3.8530 ± 0.025	7−β	11-NMe	0.0052 ± 0.0001	3.9920 ± 0.010
8-NH	8−β	0.0261 ± 0.0004	3.0480 ± 0.009	7−β	11−β	0.0197 ± 0.0008	3.1950 ± 0.022
1−β	2-NH	0.0315 ± 0.0018	2.9540 ± 0.028	7−β	5−γ_2	0.0037 ± 0.0001	4.2140 ± 0.020
1−β	1−α	0.0881 ± 0.0013	2.4890 ± 0.007	7−β	2−γ	0.0039 ± 0.0001	4.1890 ± 0.019
1−β	1-NMe	0.0260 ± 0.0034	3.0500 ± 0.067	8−β	8-NH	0.0258 ± 0.0006	3.0550 ± 0.014
1−β	3-NMe	0.0016 ± 0.0001	4.8760 ± 0.041	8−β	8−α	0.0611 ± 0.0019	2.6450 ± 0.015
1−β	6−γ	0.0285 ± 0.0013	3.0050 ± 0.023	8−β	9-NMe	0.0061 ± 0.0002	3.8900 ± 0.017
1−β	1−γ	0.0550 ± 0.0013	2.6920 ± 0.012	8−β	9−δ_1	0.0023 ± 0.0002	4.5570 ± 0.065
1−β	1−γMe	0.0240 ± 0.0008	3.0920 ± 0.018	10−β_1	10−α	0.0356 ± 0.0061	2.8950 ± 0.083
4−γ	4−α	0.0233 ± 0.0009	3.1060 ± 0.021	10−β_1	10−γ	0.0572 ± 0.0043	2.6750 ± 0.034
4−γ	4-NMe	0.0107 ± 0.0003	3.5350 ± 0.017	10−β_1	10−β_2	0.7203 ± 0.0183	1.7540 ± 0.008
6−β_2	6−α	0.0799 ± 0.0022	2.5300 ± 0.012	10−β_1	10−δ_2	0.0292 ± 0.0016	2.9930 ± 0.028
6−β_2	6-NMe	0.0213 ± 0.0009	3.1540 ± 0.023	10−β_1	6−δ_2	0.0038 ± 0.0001	4.1980 ± 0.024
6−β_2	6−β_1	0.7166 ± 0.0155	1.7550 ± 0.007	11−γ_2	11−α	0.0340 ± 0.0007	2.9180 ± 0.011
6−β_2	6−γ	0.0400 ± 0.0029	2.8390 ± 0.035	11−γ_2	11-NMe	0.0098 ± 0.0001	3.5880 ± 0.008
6−β_2	6−δ_1	0.0205 ± 0.0023	3.1740 ± 0.059	11−γ_2	9-NMe	0.0004 ± 0.0001	6.1060 ± 0.073
6−β_2	6−δ_2	0.0202 ± 0.0041	3.1810 ± 0.107	11−γ_2	10-NMe	0.0103 ± 0.0002	3.5630 ± 0.013
6−δ_2	7-NH	0.0039 ± 0.0004	4.1830 ± 0.064	11−γ_2	11−β	0.0539 ± 0.0011	2.7020 ± 0.010
6−δ_2	1−α	0.0071 ± 0.0002	3.7870 ± 0.020	11−γ_2	11−γ_1	0.0181 ± 0.0005	3.2410 ± 0.016
6−δ_2	6−α	0.0300 ± 0.0004	2.9790 ± 0.009				

3.6 Further comparisons of extracted ^{1}H,^{1}H-distances using different methods

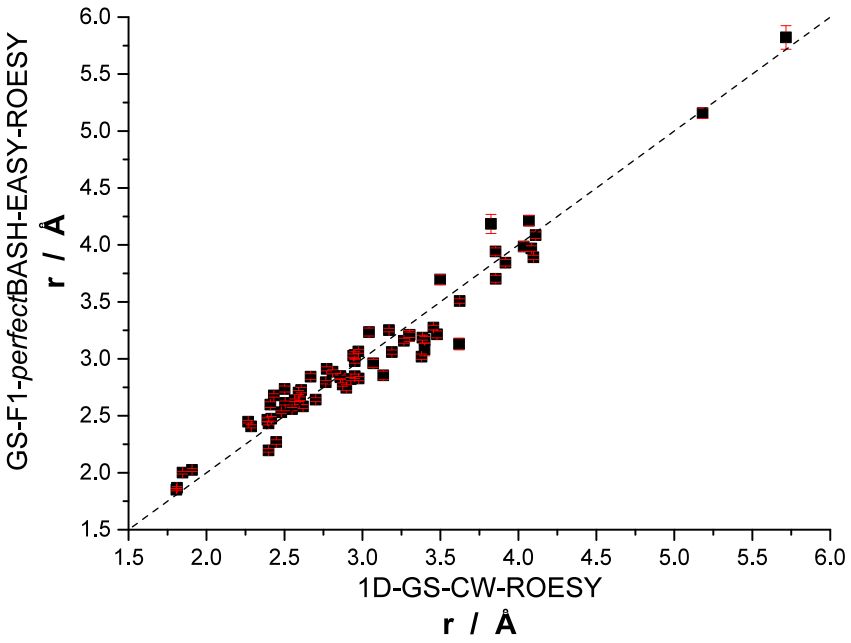

Figure 3.1: Comparison between ^{1}H,^{1}H-distances extracted from the 2D *gradient-selected* $F1$-*perfect*BASH-EASY-ROESY and 1D *selective* and *gradient-selected continuous-wave*-ROESY. RMSD = 0.159 $\AA$

3.7 Selected ^{1}H,^{1}H-distances extracted from the *gradient-selected F*1-PSYCHE-EASY-ROESY and *gradient-selected F*1-*perfect*BASH-EASY-ROESY and comparison with a model

The spatial structure of cyclosporine A and its dynamics have been studied extensively under various conditions[18–30]. These structural investigations were performed using NOE effects, $J-$coupling constants, chemical shift values and RDCs. However, most of the studies investigate cyclosporine A dissolved chloroform or water. We selected geometries in cyclosporine A, which should be largely independent of possible conformational changes for our comparison. However, a possible bias from utilizing another solvent (C_6D_6) than the one used to extract the NOE restraints ($CDCl_3$)[18,19] cannot be ruled out at this point.

Cyclosporine A contains a few diastereotopic protons in the four $N-$methyl-leucine amino acids MeLeu-4, MeLeu-6, MeLeu-9 and MeLeu-10 as well as $1-\delta_1/1-\delta_2$ in MeBmt-1 and $3-\alpha_1/3-\alpha_2$ in Sar-3. From our spectra we could extract six distances between diastereotopic protons, whose diagonal-peaks and NOE cross-peaks were not extensively overlapped by other protons or distorted in other ways. The NOE between the two $\alpha-$protons in Sar-3 were used for internal calibration and were set to 1.75 $\AA$. For the remaining NOE contacts, we found similar values between 1.75 $\AA$ and 1.77 $\AA$, except for the diastereotopic proton pair of MeBmt-1 $1-\delta_1/1-\delta_2$. Here we have found a proton distance of 1.90 $\AA$, which however can be explained by the conformational flexibility of this sidechain in the intermediate time regime, as previously described[19]. The exchange process also manifests itself in a broadened linewidth for $1-\delta_1$ with unresolved multiplet structure in the 1D 1H-spectrum.

The characteristic values of the $^3J_{\alpha\beta}-$coupling constants of three $N-$methyl-leucine amino acids MeLeu-4, MeLeu-6 and MeLeu-9 and the two $N-$methyl-valine amino acids Val-5 and MeVal-11 indicate the preferred conformation about the C_α – C_β bond. The large ($^3J_{\alpha\beta} \geq 10$ Hz) and the small ($^3J_{\alpha\beta} \leq 4$ Hz) $J-$coupling constant to each $\beta-$proton in MeLeu correspond to torsion angles close to 180° and 60° between the $\alpha,\beta-$protons, which can be translated to a large expected proton-distance $r \approx 3.05$ $\AA$ for the 180° arrangement and $r \approx 2.50$ $\AA$ for the 60° arrangement respectively. The large $J-$coupling constant ($^3J_{\alpha\beta} \geq 10$ Hz) in Val-5 and MeVal-11 indicates a 180° arrangement of the $\alpha-$ and $\beta-$protons. From the mixing-time series of the *gradient-selected* F1-PSYCHE-EASY-ROESY we could find appropriate values (table 3.6), although some NOE cross-peaks of the 180° arrangement were too weak to be integrated accurately. Previous structural investigations[18,19] indicated trans-conformations about the $N-$methylated peptide bonds, except for MeLeu-9/MeLeu-10. A strong NOE between these two $\alpha-$protons implies a cis-conformation. The peptide trans-conformation leads to a strong NOE between the $N-$methyl and the $\alpha-$protons of adjacent amino acids. From these NOEs we could determine 12 proton distances between 2.46 $\AA$ and 2.69 $\AA$ for these residues, which fits with the expected value of approximately $r \approx 2.60$ $\AA$, which we derived from an energy minimized $N-$methylated peptide fragment with $all-trans-$conformation, using r^{-3} averaging[31] to account for the fast methyl group rotation. Thanks to the attenuated t_1-noise due to *gradient selection*, we were able to observe further weak NOE responses between $N-$methyl and $\alpha-$protons of the same amino acid. From the energy minimized $N-$methylated peptide fragment we would expect an interproton distance around 3.90 $\AA$ for this pair, if a $trans-$conformation about the peptide

bond exists. Although these NOE contacts are weak, the constructed PANIC plots show good linearity and we could extract 10 proton distances between 3.84 $\AA$ and 4.14 $\AA$. It should be noted, that the spectral width in the indirect dimension $F1$ is restricted to the $\alpha-$ and amide-proton region, when *perfect*BASH homonuclear decoupling[32] is applied. Thus the distances from the reverse cross peaks could not be determined, using this mixing-time series.

Table 3.6: Selected ^{1}H,^{1}H-distances between the $\alpha-$ and $\beta-$protons of the leucine and valine amino acids as well as between $\alpha-$proton and $N-$methyl protons of cyclosporine A in benzene-d_6 determined with the mixing-time series of the *gradient-selected* $F1$-PSYCHE-EASY-ROESY and *gradient-selected* $F1$-*perfect*BASH-EASY-ROESY experiments. All other extracted proton-proton distances can be found in the previous chapters.

H	**H'**	**r / Å**		$\mathbf{r_{model}}$ / Å[a]
		PSYCHE	*perfect*BASH	
4$-\alpha$	4$-\beta_1$ (*pro S*)	2.52 ± 0.02	2.51 ± 0.04	2.50
6$-\alpha$	6$-\beta_2$ (*pro R*)	2.61 ± 0.06	2.55 ± 0.03	
6$-\beta_2$ (*pro R*)	6$-\alpha$	2.61 ± 0.02	–	
10$-\alpha$	10$-\beta_2$ (*pro S*)	2.63 ± 0.02	2.61 ± 0.05	
10$-\beta_2$ (*pro S*)	10$-\alpha$	2.60 ± 0.09	–	
4$-\alpha$	4$-\beta_2$ (*pro R*)	–	2.96 ± 0.11	3.05
6$-\alpha$	6$-\beta_1$ (*pro S*)	3.05 ± 0.21	2.97 ± 0.02	
10$-\alpha$	10$-\beta_1$ (*pro R*)	2.93 ± 0.01	2.84 ± 0.02	
10$-\beta_1$ (*pro R*)	10$-\alpha$	3.01 ± 0.07	–	
5$-\alpha$	5$-\beta$	2.97 ± 0.02	2.88 ± 0.02	
5$-\beta$	5$-\alpha$	2.99 ± 0.04	–	
11$-\alpha$	11$-\beta$	3.09 ± 0.12	3.04 ± 0.03	
11$-\beta$	11$-\alpha$	3.11 ± 0.04	–	
2$-\alpha$	3-NMe	2.64 ± 0.01	2.66 ± 0.02	2.59 - 2.65
3-NMe	2$-\alpha$	2.58 ± 0.01	–	
3$-\alpha_1$ (*pro S*)	4-NMe	2.58 ± 0.01	2.54 ± 0.01	
4-NMe	3$-\alpha_1$ (*pro S*)	2.67 ± 0.01	–	
5$-\alpha$	6-NMe	2.64 ± 0.01	2.51 ± 0.04	
6-NMe	5$-\alpha$	2.48 ± 0.01	2.46 ± 0.01	
8$-\alpha$	9-NMe	2.65 ± 0.01	2.57 ± 0.03	
9-NMe	8$-\alpha$	2.47 ± 0.01	–	
10$-\alpha$	11-NMe	2.69 ± 0.01	2.65 ± 0.01	
11-NMe	10$-\alpha$	2.68 ± 0.02	–	
11$-\alpha$	1-NMe	2.53 ± 0.01	2.52 ± 0.05	
1-NMe	11$-\alpha$	2.46 ± 0.01	2.44 ± 0.01	
1$-\alpha$	1-NMe	3.97 ± 0.26	3.97 ± 0.11	3.86 - 3.90

Table 3.6 – continuation

H	**H'**	**r / Å** PSYCHE	**r / Å** *perfect*BASH	$\mathbf{r_{model}}$ / Å[a]
1-NMe	1−α	4.04 ± 0.07	3.99 ± 0.07	3.86 - 3.90
4−α	4-NMe	3.99 ± 0.15	3.91 ± 0.04	
4-NMe	4−α	3.92 ± 0.02	–	
6−α	6-NMe	4.10 ± 0.13	3.90 ± 0.02	
6-NMe	6−α	3.93 ± 0.17	3.89 ± 0.21	
9−α	9-NMe	3.84 ± 0.09	3.92 ± 0.09	
9-NMe	9−α	4.06 ± 0.08	–	
10−α	10-NMe	3.90 ± 0.06	3.96 ± 0.03	
10-NMe	10−α	4.14 ± 0.10	–	
11−α	11-NMe	3.93 ± 0.19	4.10 ± 0.03	
11-NMe	11−α	3.94 ± 0.06	–	

[a]Determined with an energy minimized (MMFF94)[33] peptide fragment of cyclosporine A with $all - trans-$conformation around the amide bonds as a model compound. The fragments contain either the amino acids 4-MeLeu to 7-Ala or the amino acids 8-Ala to 11-MeVal.

3.8 Representative PANIC plots of cyclosporine A

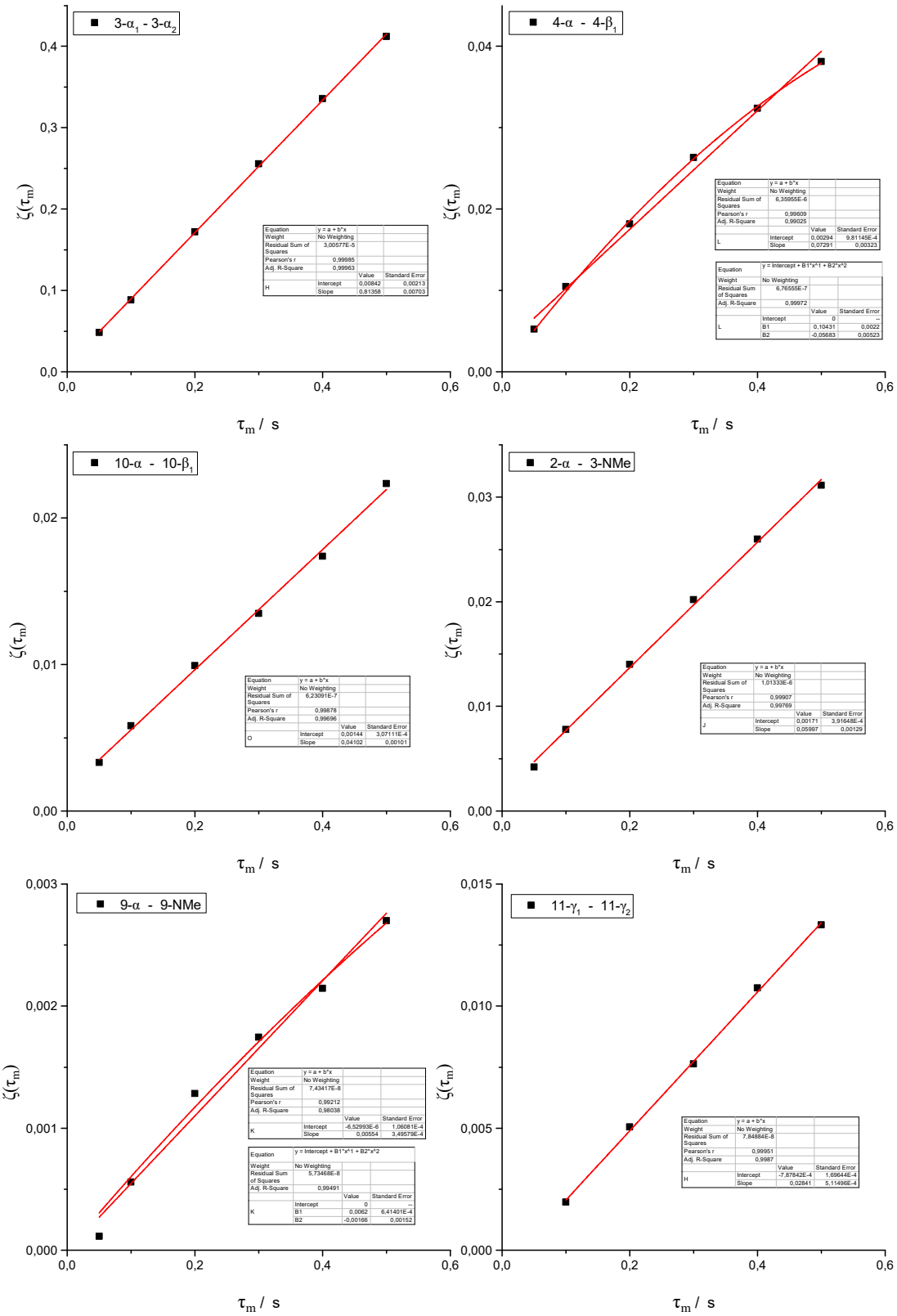

Figure 3.2: Representative PANIC plots from a mixing-time series of the *gradient-selected* $F1$-PSYCHE-EASY-ROESY experiment of cyclosporine A. The plots were constructed via normalization of the NOE cross-peak integral with the diagonal-peak integral with the same chemical shift in $F1$ (same integration row). In some cases the points in the plot differ from the expected linear behavior. In such cases a linear as well as a quadratic fit was applied.

4 Monitoring chemical exchange of cyclosporine A

4.1 Extraction of exchange rates from 2D *gradient-selected F*1-PSYCHE-EASY-ROESY

For the extraction of exchange rates we assume that we have only slow chemical exchange of two components A and B in chemical equilibrium. Such an assumption seems justified, since we can observe two signal sets with sharp lines in the 1D-^{1}H-spectrum. We define for our system the kinetic matrix **K**:

$$\mathbf{K} = \begin{pmatrix} -R_{AA} & k_{BA} \\ k_{AB} & -R_{BB} \end{pmatrix} \tag{4.1}$$

The matrix elements are defined as:

$$\begin{aligned} R_{AA} &= R_{2,A} + x_B k_{ex} \\ R_{BB} &= R_{2,B} + x_A k_{ex} \\ k_{AB} &= x_B k_{ex} \\ k_{BA} &= x_A k_{ex} \end{aligned} \tag{4.2}$$

Herein $R_{2,A} = \frac{1}{T_{2,A}}$ and $R_{2,B} = \frac{1}{T_{2,B}}$ are the transversal relaxation rates, which include auto-relaxation rates and all cross-relaxation processes of each component ($R_{2,A} = \delta_A + \sum_i \sigma_{iA}$). This is valid, if the chemical exchange is much slower than cross-relaxation. The parameters x_A and x_B are the populations of the components A and B. Applying the same procedure as described in literature[3,10] and chapter 2.1 we get the four expressions for the integrated intensities $I(\tau_m)$ of the diagonal- and cross-peaks, but now caused by chemical exchange:

$$\begin{aligned} I_{AA}\left(\Omega_{1,A}, \Omega_{2,A}, \tau_m\right) &= \frac{1}{2} w_T M_0 \beta_A D\, a_{AA}\left(\tau_m\right) \\ I_{BB}\left(\Omega_{1,B}, \Omega_{2,B}, \tau_m\right) &= \frac{1}{2} w_T M_0 \beta_B D\, a_{BB}\left(\tau_m\right) \\ I_{AB}\left(\Omega_{1,A}, \Omega_{2,B}, \tau_m\right) &= \frac{1}{2} w_T M_0 \beta_A D\, a_{AB}\left(\tau_m\right) \\ I_{BA}\left(\Omega_{1,B}, \Omega_{2,A}, \tau_m\right) &= \frac{1}{2} w_T M_0 \beta_B D\, a_{BA}\left(\tau_m\right) \end{aligned} \tag{4.3}$$

Again we use the mixing coefficients $a(\tau_m)$, which describe the intensity of the integrated diagonal- and cross-peaks for a given mixing time τ_m in equilibrium and the absence of fur-

ther exchange processes,

$$
\begin{aligned}
a_{AA}(\tau_m) &= \frac{1}{2} x_A \exp(-R_L \tau_m) \cdot \\
&\quad \left[\left(1 - \frac{R_{AA} - R_{BB}}{R_C} \right) + \left(1 + \frac{R_{AA} - R_{BB}}{R_C} \right) \exp(-R_C \tau_m) \right] \\
a_{BB}(\tau_m) &= \frac{1}{2} x_B \exp(-R_L \tau_m) \cdot \\
&\quad \left[\left(1 - \frac{R_{BB} - R_{AA}}{R_C} \right) + \left(1 + \frac{R_{BB} - R_{AA}}{R_C} \right) \exp(-R_C \tau_m) \right] \\
a_{AB}(\tau_m) &= a_{BA}(\tau_m) = -x_A x_B \frac{k_{ex}}{R_C} \exp(-R_L \tau_m) \cdot [1 - \exp(-R_C \tau_m)]
\end{aligned}
\tag{4.4}
$$

whereby we now redefine R_C and R_L now for the case of chemical exchange:

$$
\begin{aligned}
R_C &= \sqrt{(R_{2,A} - R_{2,B} + (x_B - x_A) k_{ex})^2 + 4 x_A x_B k_{ex}^2} \\
R_L &= \frac{1}{2} (R_{2,A} + R_{2,B} + k_{ex}) - \frac{1}{2} R_C
\end{aligned}
\tag{4.5}
$$

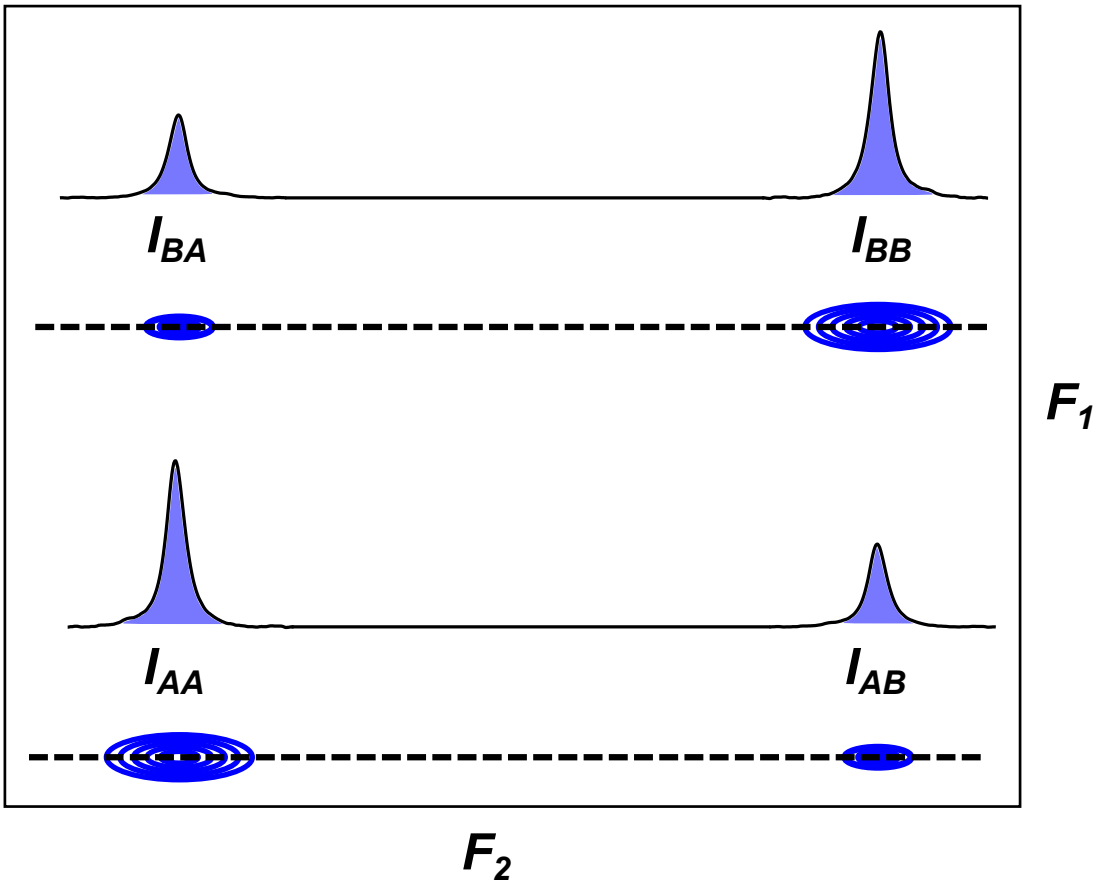

Figure 4.1: Quantificantion of the chemical-exchange peaks from the 2D *gradient-selected* $F1$-*pure-shift*-EASY-ROESY spectra by extracting and integrating $F2$-traces at the peak maximum in $F1$ to extract chemical-exchange rates k_{AB} and k_{BA}.

We analyse the chemical exchange process in the same way, as we did for the cross-relaxation

rates. To this end we quantify the ROESY spectra by extracting and integrating traces along the direct dimension $F2$. Now we could fit the integrated intensities against the mixing-time τ_m and extract the exchange rates from the fit-function. However, this would be error prone because we have the mixing-time dependent diffusion factor D and β to account for effects from PSYCHE homonuclear decoupling. Hence we take advantage from the internal normalization by division of the cross-peak intensity by the diagonal-peak intensity to eliminate these factors as we did for the cross-relaxation:

$$\begin{aligned} \widetilde{\zeta}_{A\to B}\left(\tau_m\right) &= \frac{I_{AB}\left(\tau_m\right)}{I_{AA}\left(\tau_m\right)} \\ &= \frac{\frac{1}{2}M_0\beta_A D\frac{1}{R_{2,A}}\cdot a_{AB}\left(\tau_m\right)}{\frac{1}{2}M_0\beta_A D\frac{1}{R_{2,A}}\cdot a_{AA}\left(\tau_m\right)} \end{aligned} \tag{4.6}$$

Insertion of the expressions for a_{AB} and a_{AA} yields:

$$\widetilde{\zeta}_{A\to B}\left(\tau_m\right) \;=\; \frac{2x_B k_{ex}}{R_C}\cdot\frac{1 \;-\; \exp\left(-R_C\tau_m\right)}{1 \;+\; \exp\left(-R_C\tau_m\right) \;+\; \frac{R_{AA}-R_{BB}}{R_C}\left(1 \;-\; \exp\left(-R_C\tau_m\right)\right)} \tag{4.7}$$

Evaluation of this expression in a Taylor series discarding all terms with higher order than three we get:

$$\begin{aligned} \widetilde{\zeta}_{A\to B}\left(\tau_m\right) \approx\; & x_B k_{ex}\tau_m \;+\; \frac{1}{2}x_B k_{ex}\left(R_{AA}-R_{BB}\right)\tau_m^2 \\ & +\; \frac{1}{12}x_B k_{ex}\left(3\left(R_{AA}-R_{BB}\right)^2 - R_C^2\right)\tau_m^3 \;+\; \cdots \end{aligned} \tag{4.8}$$

If we assume $R_{2,A} \;\approx\; R_{2,B}$ the expression further simplifies to:

$$\widetilde{\zeta}_{A\to B}\left(\tau_m\right) \;\approx k_{AB}\tau_m \;+\; \frac{1}{2}\left(k_{AB}^2 \;-\; k_{AB}k_{BA}\right)\tau_m^2 \;+\; \cdots \tag{4.9}$$

A similar expression can be found, when the exchange cross-peak of the component B I_{BA} is normalised by its corresponding diagonal-peak I_{BB}, which gives access to the exchange rate k_{BA} of the reversed process:

$$\begin{aligned} \widetilde{\zeta}_{B\to A}\left(\tau_m\right) &= \frac{I_{BA}\left(\tau_m\right)}{I_{BB}\left(\tau_m\right)} \\ &\approx\; k_{BA}\tau_m \;-\; \frac{1}{2}\left(k_{BA}^2 \;-\; k_{AB}k_{BA}\right)\tau_m^2 \;+\; \cdots \end{aligned} \tag{4.10}$$

Now, the size of k_{AB}/k_{BA} and the differences $k_{AB}^2 \;-\; k_{AB}k_{BA}\left(k_{BA}^2 \;-\; k_{AB}k_{BA}\right)$ relative to the acquired mixing-times τ_m determine if either the linear fitting of the data is sufficient or the second-order term should be included to extract the exchange rates k_{AB} and k_{BA} from the plot.

Since we have acquired our 2D *Pure Shift* EASY-ROESY and 1D-EASY-ROESY experiments with mixing-times up to 500 ms (250 ms in *perfect*BASH, short compared to the inverse of the exchange rates), our resulting plots show a linear trend. Hence we can extract the exchange rates from the slope of a linear-fit of the normalised peak-integrals to the mixing-time τ_m (Figure 4.2). For longer mixing-times $\tau_m > 500\,ms$ the plot is expected to deviate from its linear behaviour and then the second-order term should be included. If both exchange rates k_{AB} and k_{BA} are determined experimentally, the populations x_A and x_B of the components A and B can be calculated (bearing in mind, that $R_{2,A} \approx R_{2,B}$ was assumed):

$$\begin{aligned} x_A &= \frac{k_{BA}}{k_{AB} + k_{BA}} \\ x_B &= \frac{k_{AB}}{k_{AB} + k_{BA}} \end{aligned} \tag{4.11}$$

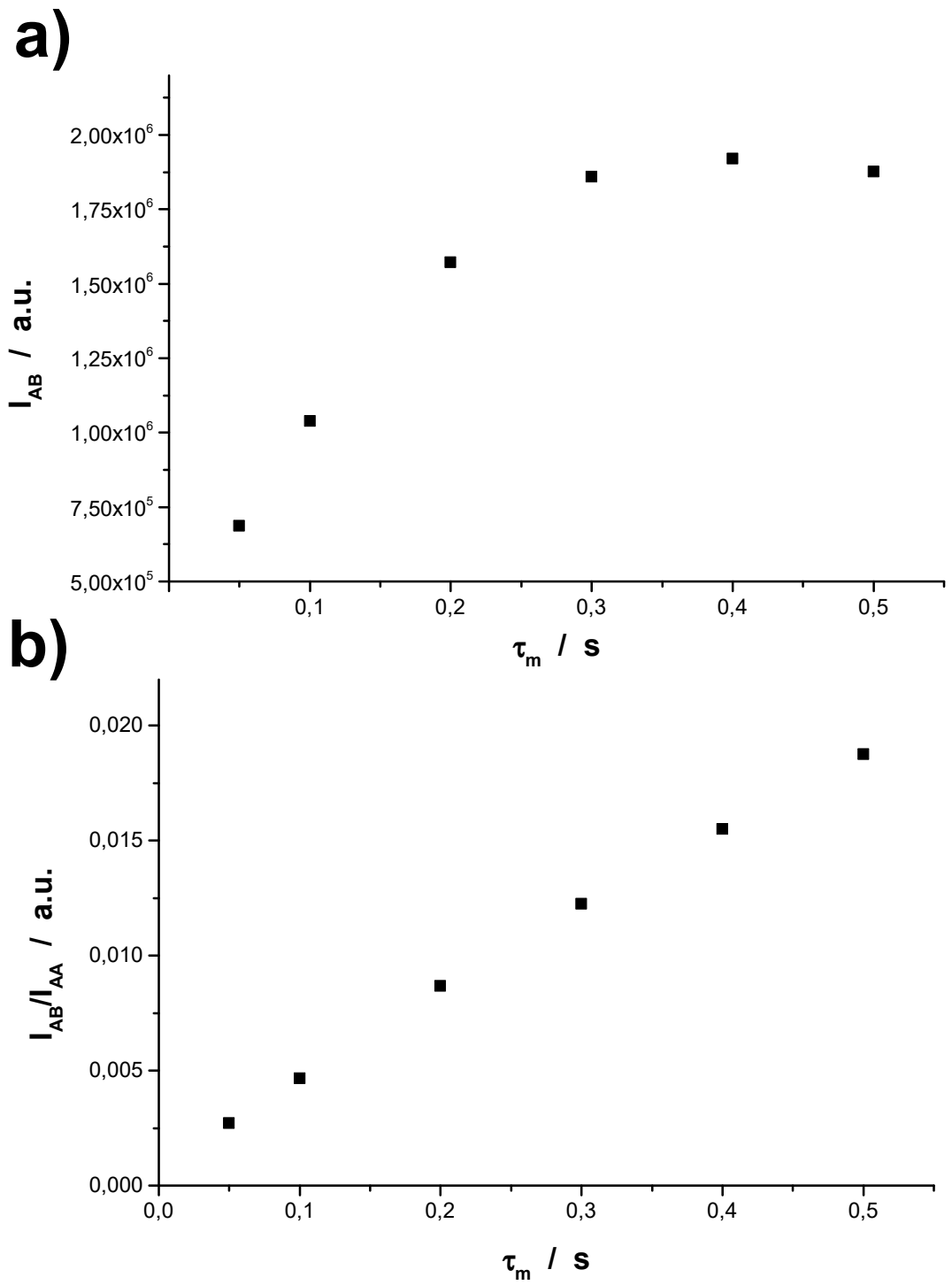

Figure 4.2: Evolution of the chemical exchange cross-peak integral (a) of the protons 4-NMe of cyclosporine A with the mixing-time τ_m. The integrals were extracted from the mixing-time series of the 2D *gradient-selected* $F1$-PSYCHE-EASY-ROESY experiment via $F2$-trace integration. In (b) the normalised integral of the chemical exchange cross-peak is plotted against the mixing-time τ_m.

4.2 Extracted exchange rates of cyclosporine A

Table 4.1: Exchange rates k_{AB}, k_{BA} and the population x_B of the minor conformer extracted from the 2D *gradient-selected* $F1$-PSYCHE-EASY-ROESY, the 2D *gradient-selected* $F1$-*perfect*BASH-EASY-ROESY and the 1D *selective* and *gradient-selected*-EASY-ROESY. The errors of the exchange rates k_{AB}, k_{BA} are only calculated from the fitting error of the slope in the PANIC plot. The error of the population x_B is calculated from the error of the exchange rates.

Proton	**PSYCHE**			***perfect*BASH**			**1D-EASY-ROESY**
	k_{AB} / s^{-1}	k_{BA} / s^{-1}	x_B	k_{AB} / s^{-1}	k_{BA} / s^{-1}	x_B	k_{AB} / s^{-1}
2-NH	–	–	–	0.038 ± 0.001	1.072 ± 0.049	0.034 ± 0.002	0.038 ± 0.004
7-NH	–	–	–	–	1.162 ± 0.070	–	–
5-NH	–	–	–	0.039 ± 0.001	1.290 ± 0.068	0.029 ± 0.002	0.028 ± 0.002
1−α	0.031 ± 0.002	–	–	0.034 ± 0.002	–	–	0.033 ± 0.002
2−α	0.033 ± 0.002	–	–	0.039 ± 0.002	–	–	0.033 ± 0.001
3−α_1	0.029 ± 0.002	–	–	0.034 ± 0.001	–	–	0.028 ± 0.001
3−α_2	0.025 ± 0.002	1.887 ± 0.228	0.013 ± 0.002	–	1.166 ± 0.034	–	–
5−α	0.031 ± 0.001	1.039 ± 0.068	0.029 ± 0.002	0.041 ± 0.001	1.033 ± 0.055	0.038 ± 0.002	–
6−α	0.030 ± 0.001	–	–	–	–	–	0.029 ± 0.003
7−α	0.032 ± 0.002	1.078 ± 0.050	0.029 ± 0.003	0.042 ± 0.002	1.179 ± 0.068	0.034 ± 0.002	–
8−α	0.030 ± 0.002	–	–	–	–	–	–
10−α	0.028 ± 0.002	1.080 ± 0.076	0.026 ± 0.002	0.040 ± 0.001	0.944 ± 0.078	0.041 ± 0.003	0.029 ± 0.003
11−α	0.035 ± 0.003	–	–	0.038 ± 0.003	–	–	0.036 ± 0.001

Table 4.1 – continuation

Proton	PSYCHE			*perfect*BASH			1D-EASY-ROESY
	k_{AB} / s^{-1}	k_{BA} / s^{-1}	x_B	k_{AB} / s^{-1}	k_{BA} / s^{-1}	x_B	k_{AB} / s^{-1}
1-NMe	0.035 ± 0.001	1.064 ± 0.045	0.032 ± 0.002	0.041 ± 0.001	1.164 ± 0.022	0.034 ± 0.001	0.038 ± 0.001
3-NMe	0.033 ± 0.001	1.136 ± 0.034	0.029 ± 0.001	–	–	–	0.036 ± 0.001
4-NMe	0.036 ± 0.001	1.046 ± 0.011	0.033 ± 0.001	–	–	–	0.040 ± 0.001
6-NMe	0.033 ± 0.001	–	–	0.038 ± 0.001	–	–	0.037 ± 0.001
9-NMe	0.037 ± 0.002	1.004 ± 0.018	0.035 ± 0.002	–	–	–	0.039 ± 0.001
10-NMe	0.031 ± 0.002	0.909 ± 0.051	0.033 ± 0.002	–	–	–	–

4.3 Observing Overhauser contacts of the minor conformer of cyclosporine A with the 2D *gradient-selected F*1-*perfect*BASH-EASY-ROESY

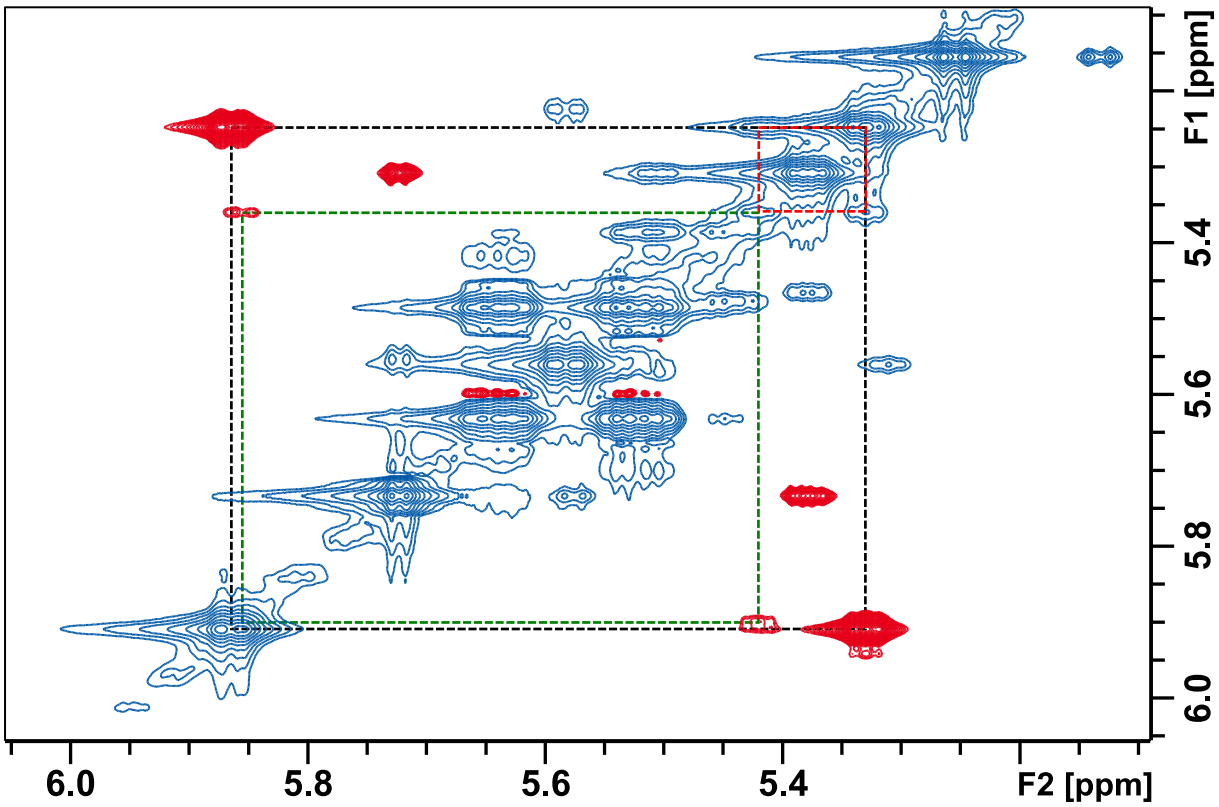

Figure 4.3: $\alpha-$Proton region of the 2D *gradient-selected* $F1$-*perfect*BASH-EASY-ROESY. NOE contact of the protons 9-α and 10-α (black square), the chemical exchange between the major conformer of cyclosporine A and its minor conformer visible as clear exchange cross-peaks at proton 10-α (red square) and the 9-α/10-α NOE contact of the minor conformer of cyclosporine A (green square).

5 Further comments on the pulse sequences

5.1 Analysis of the 2D *gradient-selected* $F1$-PSYCHE-EASY-ROESY pulsesequence

In this section we analyse the main properties of the 2D *gradient-selected* $F1$-PSYCHE-EASY-ROESY pulse sequence and the effects of its elements on the magnetisation. This includes the *gradient-selection* over the mixing-time, the intensity attenuation by diffusion, potential spin-site dependent effects of the PSYCHE homonuclear decoupling (β-factor) and the necessity of the final $z-$filter to obtain double absorption line shapes with the States-TPPI implementation as stated in the main text. The theoretical examination is based on the analysis of the classic 2D-NOESY experiment described by Jeener *et al.* [3] using the same formalism, whereby we include homonuclear decoupling (*pure shift*) in the t_1-evolution time, the gradient en- and decoding step as well as the final $z-$filter. For treating the gradient en- and decoding we use the formalism of Stott *et al.* [4]. The PSYCHE homonuclear decoupling and the EASY-ROESY mixing are only treated in a simplified manner. Further we assume in our analysis perfect coherence selection by gradients and *phase-cycling*. For simplicity the analysis is exemplary performed for one phase-cycling step, with pulse phases defined in the caption of Figure 5.1.

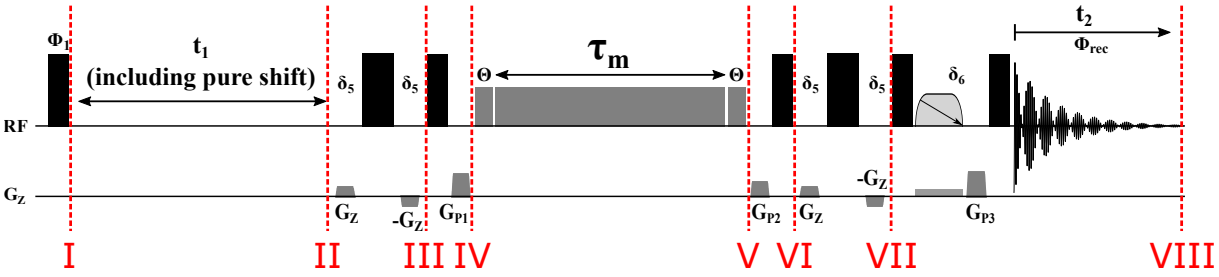

Figure 5.1: Simplified pulse sequence scheme for the 2D *gradient-selected* $F1$-PSYCHE-EASY-ROESY experiment with States-TPPI selection[5]. Narrow and wide rectangles represent hard 90° and 180° pulses, respectively. The broad rectangle in gray is the simplified ROESY spinlock of τ_m duration, the gray rectangles before and after the spinlock are hard pulses, which rotate the magnetisation by the desired angle Θ. The Thrippleton-Keeler element is indicated by a single trapezoid with diagonal arrow. The gradients G_z are for phase en- and decoding, G_{P1} to G_{P3} are purge gradients. The delay δ_5 is the duration of the en- or decoding gradient G_z and a recovery delay. The delay δ_6 consists of the lengths of the Thrippleton-Keeler element, the purge gradient G_{P3} and two recovery delays. Scalar coupling refocusing is achieved before the ROESY mixing step (time point III), while chemical shifts have evolved for t_1. The evolution of scalar couplings is neglected between the time points II and III as well as VI and VII. All pulse phases are x except for $\Phi_1 = -x$ and $\Phi_{rec} = -x$. Here are only the pulse phases shown, which are used in the following analyis. Full phase-cycling can be found in the detailed description in chapter **??**.

At the beginning we define the initial magnetisation as the equilibrium $z-$magnetisation, which can be described by a column vector of the initial magnetisations of all protons k in the system in the thermal equilibrium. The parameter k is the control variable of the protons in the indirect dimension $F1$, the later introduced parameter l is the control variable of the protons in the direct dimension $F2$.

$$M_z = M_0 \tag{5.1}$$

The excitation pulse (time point I) with $-x$ phase rotates the magnetisation vector M_z onto the $y-$axis. If we assume a perfect 90° excitation pulse M_y equals M_0.

$$M_z \quad \xrightarrow{90°_{-x}} \quad M_y \;=\; -\frac{i}{2}\left(M_+ \,-\, M_-\right) \tag{5.2}$$

The transversal magnetisation M_y evolves subsequently during t_1. Herein we combine the evolution of the two transverse components M_y and M_x in the complex transverse magnetisation M_+ and M_-. The following examination is, however, only performed with the M_+ component of the total magnetisation for simplicity. This gives us at time point II:

$$M_+\left(II\right) \;=\; -\frac{i}{2}\boldsymbol{\beta}\,\exp\left(-i\boldsymbol{\Omega}'t_1\right)\cdot M_0 \tag{5.3}$$

Since the timing in the experiment is chosen in a way that homonuclear $J-$coupling evolution is refocused during t_1, for simplicity we assume here, that all spin-spin coupling effects are absent. Hence we only need to include the evolution by chemical shifts Ω_k and the decay by transverse relaxation rate $R_{2,k} = \frac{1}{T_{2,k}}$ during t_1 in the spectral matrix defined by $\boldsymbol{\Omega}'$. In equation 5.3 we have further introduced the matrix $\boldsymbol{\beta}$ with diagonal elements β_k to consider effects introduced by the element for spin-subset selection to achieve homonuclear decoupling (*pure shift*) in $F1$. The matrix $\boldsymbol{\beta}$ accounts for the sensitivity attenuation and potential spin-site dependent T_2- and offset-weighting effects introduced by the PSYCHE homonuclear decoupling[6] element. The t_1-evolution time including the *pure shift* element is followed by a gradient encoding step, which introduces a spatially dependent phase factor and changes M_+ to M_- due to the 180° pulse:

$$M_-\left(III\right) \;=\; -\frac{i}{2}\boldsymbol{\beta}\,\exp\left(i\Phi_z\right)\,\exp\left(-i\boldsymbol{\Omega}'t_1\right)\cdot M_0 \tag{5.4}$$

with

$$\Phi_z \;=\; -\gamma\cdot G_z\cdot z\cdot\tau_G \tag{5.5}$$

Herein γ is the gyromagnetic ratio, G_z is the applied gradient strength, τ_G is the applied duration and z is the position in the active volume of the sample. During the gradient encoding and decoding steps, we again neglect $J-$coupling and chemical shift evolution, to simplify the analysis. The gradient encoding is followed by a second 90° pulse, which rotates the y-component of the evolved and gradient encoded magnetisation onto the z-axis. The following purge gradient dephases all residual transverse parts, thus we only take the imaginary part of our complex transverse magnetisation:

$$M_z\left(IV\right) \;=\; -\boldsymbol{\beta}\,\mathfrak{Im}\left[\frac{i}{2}\exp\left(i\Phi_z\right)\,\exp\left(-i\boldsymbol{\Omega}'t_1\right)\right]\cdot M_0 \tag{5.6}$$

In the EASY-ROESY experiment[7] the mixing is realised by two symmetrically shifted spin-locks with a locking-angle differing from 90° (usually 45° to 60°), for minimizing the offset dependency of the transverse cross-relaxation rate and possible Hartmann-Hahn magnetisation

transfer. Thus transversal as well as longitudinal cross-relaxation take place simultaneously during the mixing-time τ_m. For simplicity, we treat both periods of spin-locking as one step, thereby assuming neglectably small offset dependence[36] and the adiabatic ramp-pulses as hard pulses with negligible duration, which rotate the magnetisation by the desired angle Θ. Further we neglect TOCSY transfer and the offset dependency of the transversal cross-relaxation. However, we have to consider both the transversal and longitudinal relaxation pathways using the differential equations. Hence we decompose the magnetisation matrix in expression in 5.6 into its longitudinal M_z and transversal components M_y during the mixing process and treat them independently.

$$\begin{aligned} M_z\left(IV\,;\,\tau_m=0\right) &= w_L \cdot M_z\left(IV\right) \;=\; -w_L\boldsymbol{\beta}\,\mathfrak{Im}\left[\frac{i}{2}\exp\left(i\Phi_z\right)\exp\left(-i\boldsymbol{\Omega}'t_1\right)\right]\cdot M_0 \\ M_y\left(IV\,;\,\tau_m=0\right) &= w_T \cdot M_z\left(IV\right) \;=\; -w_T\boldsymbol{\beta}\,\mathfrak{Im}\left[\frac{i}{2}\exp\left(i\Phi_z\right)\exp\left(-i\boldsymbol{\Omega}'t_1\right)\right]\cdot M_0 \end{aligned} \tag{5.7}$$

For the whole EASY-ROESY mixing process the weights for longitudinal w_L and transversal w_T cross relaxation along the diagonal are[8,9]:

$$\begin{aligned} w_L &= \cos^2\Theta \\ w_T &= \sin^2\Theta \\ \tan\Theta &= \frac{\gamma B_1}{\Omega\;-\;\Omega_{RF}} \end{aligned} \tag{5.8}$$

The mixing process is described by the differential equations for longitudinal and transversal relaxation. The matrices $\mathbf{L}$ and $\mathbf{T}$ for the longitudinal and transversal part, respectively, contain for simplification only auto- and dipole-dipole relaxation[3,10,11]. Potential chemical exchange effects and TOCSY transfer during the mixing-time τ_m are neglected. The former is discussed in chapter 4.

$$\frac{dM_z}{dt} \;=\; -\mathbf{L}\cdot\left\{M_z \;-\; M_0\right\} \tag{5.9}$$

$$\frac{dM_y}{dt} \;=\; -\mathbf{T}\cdot\left\{M_y\right\} \tag{5.10}$$

Inserting the expressions for M_z (a) and M_y (b) (equation 5.7) into the solutions of the differential equations in 5.9 and 5.10 we get:

$$M_z\left(V;\tau_m\right) \;=\; \left[1\;-\;\exp\left(-\mathbf{L}\tau_m\right)\left\{w_L\boldsymbol{\beta}D\,\mathfrak{Im}\left[\frac{i}{2}\exp\left(i\Phi_z\right)\exp\left(-i\boldsymbol{\Omega}'t_1\right)\right]\;+\;1\right\}\right]\cdot M_0 \tag{5.11}$$

and

$$M_y\left(V;\tau_m\right) \;=\; -\exp\left(-\mathbf{T}\tau_m\right)\left\{w_T\boldsymbol{\beta}D\,\mathfrak{Im}\left[\frac{i}{2}\exp\left(i\Phi_z\right)\exp\left(-i\boldsymbol{\Omega}'t_1\right)\right]\right\}\cdot M_0 \tag{5.12}$$

In experiments with gradient selection, molecular diffusion is an extra source of intensity loss. To take this into account, a diffusional attenuation factor $D \;=\; f\left(\Delta\right)$ (Δ is the diffusion time and $\Delta \;\approx\; \tau_m$) is included, which can be approximated by the Stejskal-Tanner Equation and is discussed in chapter 5.2.
At the end of the mixing process, both parts of the magnetisation are again aligned on the z-axis by the second adiabatic ramp-pulse. All residual transverse parts are dephased by the second purge gradient. The subsequent third 90° pulse rotates the magnetisation back to the transverse plane. Again we only consider the M_+ part of the transverse magnetisation.

$$\begin{aligned} M_+\left(VI\right) \;=\; -\frac{i}{2}\Big[1 \;-\; &\exp\left(-\mathbf{L}\tau_m\right)\left\{w_L\boldsymbol{\beta}D\,\mathfrak{Im}\left[\frac{i}{2}\exp\left(i\Phi_z\right)\exp\left(-i\boldsymbol{\Omega}'t_1\right)\right] \;+\; 1\right\} \\ &-\exp\left(-\mathbf{T}\tau_m\right)\left\{w_T\boldsymbol{\beta}D\,\mathfrak{Im}\left[\frac{i}{2}\exp\left(i\Phi_z\right)\exp\left(-i\boldsymbol{\Omega}'t_1\right)\right]\right\}\Big]\cdot M_0 \end{aligned} \tag{5.13}$$

Then the encoded magnetisation is decoded by a subsequent gradient decoding step with the same duration and gradient strength, which we describe by a second spatially dependent phase factor:

$$\begin{aligned} M_-\left(VII\right) \;=\; -\frac{i}{2}\exp\left(i\Phi'_z\right)\Big[\; & \\ 1 \;-\; &\exp\left(-\mathbf{L}\tau_m\right)\left\{w_L\boldsymbol{\beta}D\,\mathfrak{Im}\left[\frac{i}{2}\exp\left(i\Phi_z\right)\exp\left(-i\boldsymbol{\Omega}'t_1\right)\right] \;+\; 1\right\} \\ &-\exp\left(-\mathbf{T}\tau_m\right)\left\{w_T\boldsymbol{\beta}D\,\mathfrak{Im}\left[\frac{i}{2}\exp\left(i\Phi_z\right)\exp\left(-i\boldsymbol{\Omega}'t_1\right)\right]\right\}\Big]\cdot M_0 \end{aligned} \tag{5.14}$$

In order to obtain absorption mode lineshapes, the $z-$filter introduced thereafter is necessary. It preserves only the imaginary part of the expression in equation 5.14, which finally evolves during the detection period t_2 described by the spectral density matrix $\boldsymbol{\Omega}$. In contrast to the spectral density matrix $\boldsymbol{\Omega}'$ during t_1 the spectral density matrix $\boldsymbol{\Omega}$ in the detection period t_2 contains chemical shifts and spin-spin couplings.

$$\begin{aligned} &M_+\left(VIII\right) \;= \\ &-\frac{i}{2}\exp\left(-i\boldsymbol{\Omega}t_2\right)\mathfrak{Im}\Big\{\frac{i}{2}\exp\left(i\Phi'_z\right) \\ &\Big[1 \;-\; \exp\left(-\mathbf{L}\tau_m\right)\left\{w_L\boldsymbol{\beta}D\,\mathfrak{Im}\left[\frac{i}{2}\exp\left(i\Phi_z\right)\exp\left(-i\boldsymbol{\Omega}'t_1\right)\right] \;+\; 1\right\} \\ &-\;\exp\left(-\mathbf{T}\tau_m\right)\left\{w_T\boldsymbol{\beta}D\,\mathfrak{Im}\left[\frac{i}{2}\exp\left(i\Phi_z\right)\exp\left(-i\boldsymbol{\Omega}'t_1\right)\right]\right\}\Big]\Big\}\cdot M_0 \end{aligned} \tag{5.15}$$

The final expression can be decomposed into three parts. The first one has oscillatory terms exclusively in t_2 and gives rise to axial-peaks:

$$M_{+,ax}\,(VIII) \;=\; -\frac{i}{2}\exp\left(-i\boldsymbol{\Omega}t_2\right)\mathfrak{Im}\Big\{\frac{i}{2}\exp\left(i\Phi'_z\right)\left[1\;-\;\exp\left(-\mathbf{L}\tau_m\right)\right]\Big\}\cdot M_0 \tag{5.16}$$

In equation 5.16 we have a spatially dependent phase factor $\exp\left(i\Phi'_z\right)$. Even without further examination, we see that this spatially dependent phase factor does not vanish. Hence this term does not contribute to the detected signal, as it remains dephased and thus is not detectable. This is the feature of the gradient selection, as axial peaks are suppressed intrinsically.

The remaining two parts have oscillatory terms in both t_1 and t_2:

$$\begin{aligned}
&M_{+,rest}\,(VIII) \;=\\
&\frac{i}{8}\exp\left(-i\boldsymbol{\Omega}t_2\right)\mathfrak{Im}\Big\{\\
&i\exp\left(i\Phi'_z\right)\exp\left(-\mathbf{L}\tau_m\right)w_L\boldsymbol{\beta}D\,\mathfrak{Im}\left[i\exp\left(i\Phi_z\right)\exp\left(-i\boldsymbol{\Omega}'t_1\right)\right]\Big\}\cdot M_0\\
&+\;\frac{i}{8}\exp\left(-i\boldsymbol{\Omega}t_2\right)\mathfrak{Im}\Big\{\\
&i\exp\left(i\Phi'_z\right)\exp\left(-\mathbf{T}\tau_m\right)w_T\boldsymbol{\beta}D\,\mathfrak{Im}\left[i\exp\left(i\Phi_z\right)\exp\left(-i\boldsymbol{\Omega}'t_1\right)\right]\Big\}\cdot M_0
\end{aligned} \tag{5.17}$$

For the further evaluation we have to write out the spectral density matrix $\boldsymbol{\Omega}'$ during t_1 in its eigenbase as described by Jeener *et al.* [3]. Herein the matrix $\boldsymbol{\Omega}'$ contains only the evolution by chemical shifts Ω_k due to the application of *pure-shift* and the decay by transversal relaxation $R_{2,k} = \frac{1}{T_{2,k}}$, $\vec{e}_k$ are unity vectors of all protons k in $F1$.

$$\begin{aligned}
&M_{+,rest}\,(VIII) \;=\; \sum_k\\
&\frac{i}{8}\exp\left(-i\boldsymbol{\Omega}t_2\right)\mathfrak{Im}\Big\{\\
&i\exp\left(i\Phi'_z\right)\exp\left(-\mathbf{L}\tau_m\right)w_L\boldsymbol{\beta}D\,\mathfrak{Im}\left[i\exp\left(-i\Omega_k t_1 - R_{2,k}t_1\right)\exp\left(i\Phi_z\right)\cdot\vec{e}_k\right]\Big\}\cdot M_0\\
&+\;\frac{i}{8}\exp\left(-i\boldsymbol{\Omega}t_2\right)\mathfrak{Im}\Big\{\\
&i\exp\left(i\Phi'_z\right)\exp\left(-\mathbf{T}\tau_m\right)w_T\boldsymbol{\beta}D\,\mathfrak{Im}\left[i\exp\left(-i\Omega_k t_1 - R_{2,k}t_1\right)\exp\left(i\Phi_z\right)\cdot\vec{e}_k\right]\Big\}\cdot M_0
\end{aligned} \tag{5.18}$$

Taking the imaginary part of the precession during t_1:

$$
\begin{aligned}
&M_{+,rest}\,(VIII) \;=\; \sum_{k} \\
&\frac{i}{8}\exp\left(-i\mathbf{\Omega}t_2\right)\mathfrak{Im}\Big\{i\exp\left(i\Phi'_z\right)\exp\left(-\mathbf{L}\tau_m\right)w_L\boldsymbol{\beta}D \\
&\exp\left(-R_{2,k}t_1\right)\cdot\vec{e}_k\cdot\left[\cos\left(\Omega_k t_1\right)\cos\left(\Phi_z\right)+\sin\left(\Omega_k t_1\right)\sin\left(\Phi_z\right)\right]\Big\}\cdot M_0 \\
&+\;\frac{i}{8}\exp\left(-i\mathbf{\Omega}t_2\right)\mathfrak{Im}\Big\{i\exp\left(i\Phi'_z\right)\exp\left(-\mathbf{T}\tau_m\right)w_T\boldsymbol{\beta}D \\
&\exp\left(-R_{2,k}t_1\right)\cdot\vec{e}_k\cdot\left[\cos\left(\Omega_k t_1\right)\cos\left(\Phi_z\right)+\sin\left(\Omega_k t_1\right)\sin\left(\Phi_z\right)\right]\Big\}\cdot M_0
\end{aligned}
\tag{5.19}
$$

Expanding the cosine and sine expressions of the spatially dependent phase factor in terms of exponentials we obtain:

$$
\begin{aligned}
&M_{+,rest}\,(VIII) \;=\; \sum_{k} \\
&\frac{i}{8}\exp\left(-i\mathbf{\Omega}t_2\right)\mathfrak{Im}\Big\{i\exp\left(i\Phi'_z\right)\exp\left(-\mathbf{L}\tau_m\right)w_L\boldsymbol{\beta}D\exp\left(-R_{2,k}t_1\right)\cdot\vec{e}_k \\
&\left[\frac{1}{2}\cos\left(\Omega_k t_1\right)\left(e^{i\Phi_z}+e^{-i\Phi_z}\right)\;+\;\frac{1}{2i}\sin\left(\Omega_k t_1\right)\left(e^{i\Phi_z}-e^{-i\Phi_z}\right)\right]\Big\}\cdot M_0 \\
&+\;\frac{i}{8}\exp\left(-i\mathbf{\Omega}t_2\right)\mathfrak{Im}\Big\{i\exp\left(i\Phi'_z\right)\exp\left(-\mathbf{T}\tau_m\right)w_T\boldsymbol{\beta}D\exp\left(-R_{2,k}t_1\right)\cdot\vec{e}_k \\
&\left[\frac{1}{2}\cos\left(\Omega_k t_1\right)\left(e^{i\Phi_z}+e^{-i\Phi_z}\right)\;+\;\frac{1}{2i}\sin\left(\Omega_k t_1\right)\left(e^{i\Phi_z}-e^{-i\Phi_z}\right)\right]\Big\}\cdot M_0
\end{aligned}
\tag{5.20}
$$

Choosing $\Phi'_z \;=\; \pm\Phi_z$ for the spatially dependent phase factor of the gradient decoding step one half of the exponential phase factor terms vanish and thus can be refocused. The other terms with non vanishing exponential phase factor remain dephased. Hence only one half of the gradient encoded magnetisation can be recovered, which is a familiar property of gradient selected experiments[4].

$$
\begin{aligned}
&M_{+,rest}\,(VIII) \;=\; \sum_{k} \\
&\frac{i}{8}\exp\left(-i\mathbf{\Omega}t_2\right)\mathfrak{Im}\Big\{\exp\left(-\mathbf{L}\tau_m\right)w_L\boldsymbol{\beta}D\exp\left(-R_{2,k}t_1\right)\cdot\vec{e}_k \\
&\left[\frac{i}{2}\cos\left(\Omega_k t_1\right)\left(e^{2i\Phi_z}+1\right)\;+\;\frac{1}{2}\sin\left(\Omega_k t_1\right)\left(e^{2i\Phi_z}-1\right)\right]\Big\}\cdot M_0 \\
&+\;\frac{i}{8}\exp\left(-i\mathbf{\Omega}t_2\right)\mathfrak{Im}\Big\{\exp\left(-\mathbf{T}\tau_m\right)w_T\boldsymbol{\beta}D\exp\left(-R_{2,k}t_1\right)\cdot\vec{e}_k \\
&\left[\frac{i}{2}\cos\left(\Omega_k t_1\right)\left(e^{2i\Phi_z}+1\right)\;+\;\frac{1}{2}\sin\left(\Omega_k t_1\right)\left(e^{2i\Phi_z}-1\right)\right]\Big\}\cdot M_0
\end{aligned}
\tag{5.21}
$$

Considering only the refocused terms and omitting all terms which stay dephased in expres-

sion 5.21 we obtain:

$$
\begin{aligned}
&M_{+,rest}\,(VIII) \;=\; \sum_{k} \\
&\frac{i}{8}\exp\left(-i\boldsymbol{\Omega}t_2\right)\mathfrak{Im}\Big\{\exp\left(-\mathbf{L}\tau_m\right)w_L\boldsymbol{\beta}D\exp\left(-R_{2,k}t_1\right)\cdot\vec{e}_k \\
&\left[\frac{i}{2}\cos\left(\Omega_k t_1\right) \;-\; \frac{1}{2}\sin\left(\Omega_k t_1\right)\right]\Big\}\cdot M_0 \\
&+\;\frac{i}{8}\exp\left(-i\boldsymbol{\Omega}t_2\right)\mathfrak{Im}\Big\{\exp\left(-\mathbf{T}\tau_m\right)w_T\boldsymbol{\beta}D\exp\left(-R_{2,k}t_1\right)\cdot\vec{e}_k \\
&\left[\frac{i}{2}\cos\left(\Omega_k t_1\right) \;-\; \frac{1}{2}\sin\left(\Omega_k t_1\right)\right]\Big\}\cdot M_0
\end{aligned}
\tag{5.22}
$$

Finally taking the imaginary part of the term in the brackets we get:

$$
\begin{aligned}
&M_{+,rest}\,(VIII) \;=\; \sum_{k} \\
&\frac{i}{16}w_L\boldsymbol{\beta}D\;\exp\left(-i\boldsymbol{\Omega}t_2\right)\exp\left(\mathbf{L}\tau_m\right)\cdot\vec{e}_k\cdot\exp\left(-R_{2,k}t_1\right)\cos\left(\Omega_k t_1\right)\cdot M_0 \\
&+\;\frac{i}{16}w_T\boldsymbol{\beta}D\;\exp\left(-i\boldsymbol{\Omega}t_2\right)\exp\left(\mathbf{T}\tau_m\right)\cdot\vec{e}_k\cdot\exp\left(-R_{2,k}t_1\right)\cos\left(\Omega_k t_1\right)\cdot M_0
\end{aligned}
\tag{5.23}
$$

From the last calculation step, we can rationalize the requirement of the final $z-$filter before the detection period to obtain 2D spectrum with double absorption lineshapes after conducting the Fourier transformations (FT) along t_2 and t_1. When taking the imaginary part of the expression in the bracket, we see that only the cosine modulated part of t_1 survives and the sine modulated term vanishes. Now imagine, we would take both the cosine and the sine term - what is indeed the case when dropping the final $z-$filter - and subsequently conduct double FT. The real part after FT contains double absorption and double dispersive parts and we would obtain a 2D spectrum with the unfavourable *phase-twisted* line shapes. Hence the $z-$filter is necessary to select only the cosine modulation of t_1 to obtain a 2D spectrum with double absorption line shapes after double FT when using the gradient selection technique. However, to allow sign discrimination in the indirect dimension $F1$, which is indeed impossible if we only use the cosine modulation for FT, we need the equivalent sine modulation during t_1. This is achieved by a phase shift of the excitation pulse.

After writing out the spectral density matrix $\boldsymbol{\Omega}$ during t_2 in its eigenbase, as we did for t_1, we can conduct the Fourier transformation first along t_2 and subsequently along t_1. The parameter l is the control variable of the protons in the direct dimension $F2$. Herein we use the States or States-TPPI processing protocol to retain only the double absorption part by combining the sine and the cosine modulation in t_1. Thus we finally obtain after a 90° phase correction ($\vec{e}_l$ and

$\vec{e}_k$ are unity vectors of all protons l in $F2$ and all protons k in $F1$):

$$
\begin{aligned}
&S_+\left(\omega_{F1}, \omega_{F2}, \tau_m\right) \;=\; \sum_k \sum_l \\
&\frac{1}{2} w_L M_0 \boldsymbol{\beta} D \, \frac{R_{2,k}}{R_{2,k}^2 \;+\; \left(\omega_{F1} - \Omega_k\right)^2} \cdot \vec{e}_l \cdot \exp\left(\mathbf{L}\tau_m\right) \cdot \vec{e}_k \cdot \frac{R_{2,l}}{R_{2,l}^2 \;+\; \left(\omega_{F2} - \Omega_l\right)^2} \\
&+\; \frac{1}{2} w_T M_0 \boldsymbol{\beta} D \, \frac{R_{2,k}}{R_{2,k}^2 \;+\; \left(\omega_{F1} - \Omega_k\right)^2} \cdot \vec{e}_l \cdot \exp\left(\mathbf{T}\tau_m\right) \cdot \vec{e}_k \cdot \frac{R_{2,l}}{R_{2,l}^2 \;+\; \left(\omega_{F2} - \Omega_l\right)^2}
\end{aligned}
\tag{5.24}
$$

In the last expression we omitted the factor $\frac{1}{8}$, which was introduced by considering only the M_+ component of the transversal magnetisation three times with factor $\frac{1}{2}$. We see, that the factors $\boldsymbol{\beta}$ and D, which have been introduced to account for intensity attenuation by the *pure shift* element and diffusion, will influence all cross peaks k, l in the same way as the diagonal peak at position k, k (at the same $F1$ frequency). This property offers the opportunity to eliminate these effects by internal normalization to the diagonal peak at the same $F1$ frequency, if the latter is resolved. This is analysed with a simple example in chapter 2.1.

5.2 Evaluation of diffusional intensity attenuation: Stejskal-Tanner Equation

To analyse the intensity attenuation by diffusion the 2D *gradient-selected* $F1$-PSYCHE-EASY-ROESY pulse sequence can be described approximately as a stimmulated echo (STE) sequence with symmetrical bipolar gradient pulses. The Stejskal-Tanner equation including gradient shapes is given by[12],

$$D\left(\Delta,\, \delta,\, G_5\right) \,=\, \exp\left[-\gamma^2 4\delta^2\sigma^2 G_5^2\left(\Delta \,+\, \frac{\left(2\kappa - 2\lambda - 1\right)\delta}{2} \,-\, \frac{\tau}{2}\right)\right] \tag{5.25}$$

in which Δ is the diffusion time, δ is the duration of the en- and decoding gradients (p_{18}) and τ is a recovery delay (d_{16}) after the gradient pulse. The parameters σ, κ and λ are introduced to account for shaped gradients.

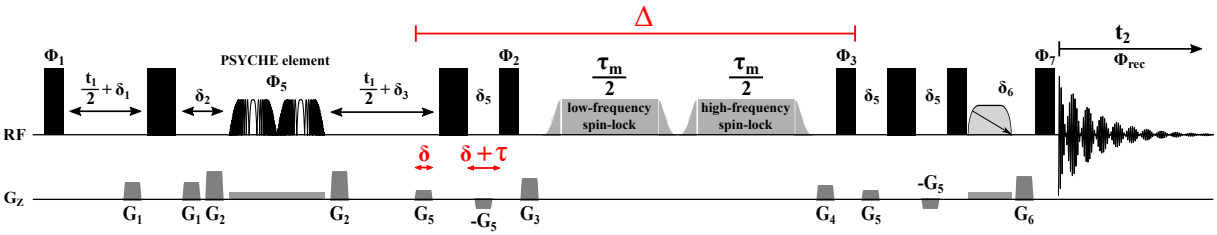

Figure 5.2: Pulse sequence scheme for the 2D *gradient-selected* $F1$-PSYCHE-EASY-ROESY experiment including the time parameters for the Stejskal-Tanner equation.

Using the acquisition parameters of the 2D *gradient-selected* $F1$-PSYCHE-EASY-ROESY experiment, the gradient shape parameters[12] for a smoothed squared gradient (SMSQ) and the diffusion coefficient of cyclosporine A in benzene-d_6 (determined with a STE-DOSY experiment at 300 K) we can calculate diffusional intensity attenuation curves (Figure 5.3) depending on the applied encoding gradient strength $G_{encod.} = G_5$ and on the mixing time τ_m. In 5.25 $p_{16} = 1\,ms$ is the duration of the purge-gradient pulses before the ROESY spin-lock and $p_{41} = 1\,ms$ is the duration of the half-gaussian adiabatic ramp-pulses.

$$\begin{aligned}
\Delta &= 2p_{18} + 4d_{16} + 2p_{16} + \tau_m + 4p_{41} + 68\,\mu s \;=\; \tau_m + 8.468\,ms \\
\delta &= p_{18} \;=\; 800\,\mu s \\
\tau &= d_{16} + 10\,\mu s \;=\; 210\,\mu s \\
\sigma &= 0.9 \\
\kappa &= \frac{422}{1215} + \frac{23}{1080\pi^2} \;\approx\; 0.3495 \\
\lambda &= 0.5 \\
D &= (5.445 \,\pm\, 0.014) \times 10^{-9}\,\frac{m^2}{s}
\end{aligned} \tag{5.26}$$

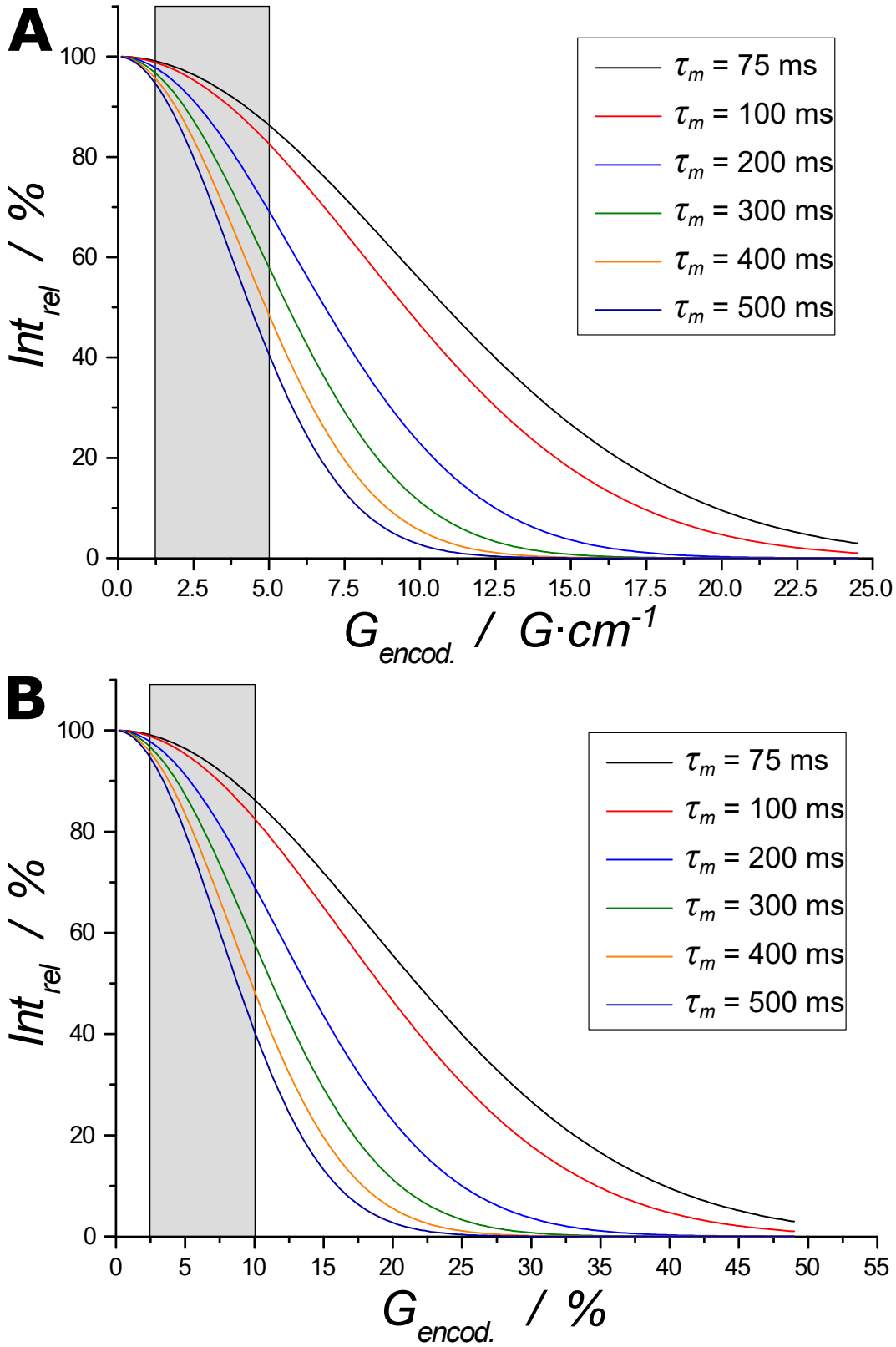

Figure 5.3: Diffusional intensity attenuation curves calculated with the Stejskal-Tanner equation depending on the applied encoding gradient strength $G_{encod.} = G_5$ and the ROESY mixing time τ_m. In the top plot the absolute gradient strength in G·cm^{-1} and in the bottom plot the strength is given as a fraction of the maxiumum strength of 50 G·cm^{-1} of a common gradient coil. The grey area defines the encoding gradient strength, which should be at least applied to clean up the spectrum on one hand and to limit the intensity loss by diffusion on the other hand.

5.3 Sensitivity comparisons

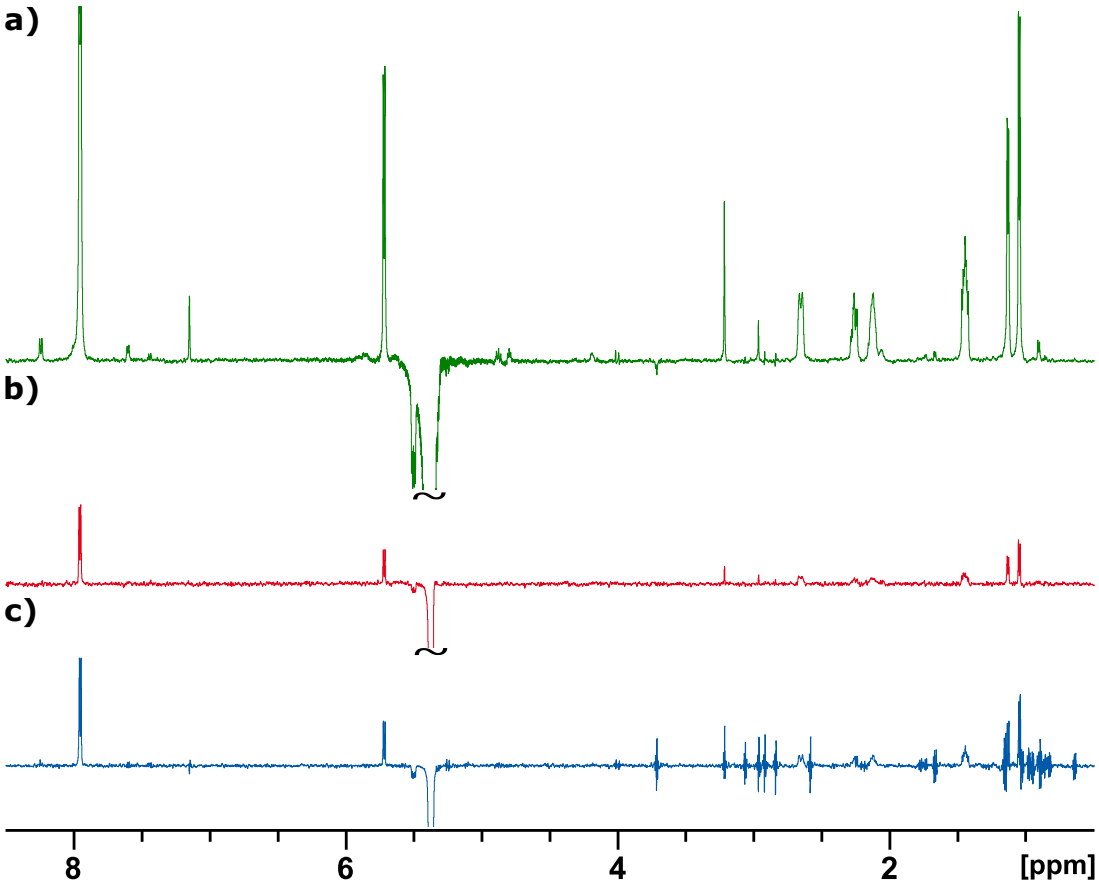

Figure 5.4: Comparison of $F2$-traces extracted (c) from the 2D $F1$-PSYCHE-EASY-ROESY spectrum, (b) from the 2D *gradient-selected* $F1$-PSYCHE-EASY-ROESY spectrum and (a) from the 2D *gradient-selected* $F1$-*perfect*BASH-EASY-ROESY spectrum of cyclosporine A in C_6D_6 at the chemical shift of H-6α (5.3782 ppm). The traces are scaled according to the different RG values.

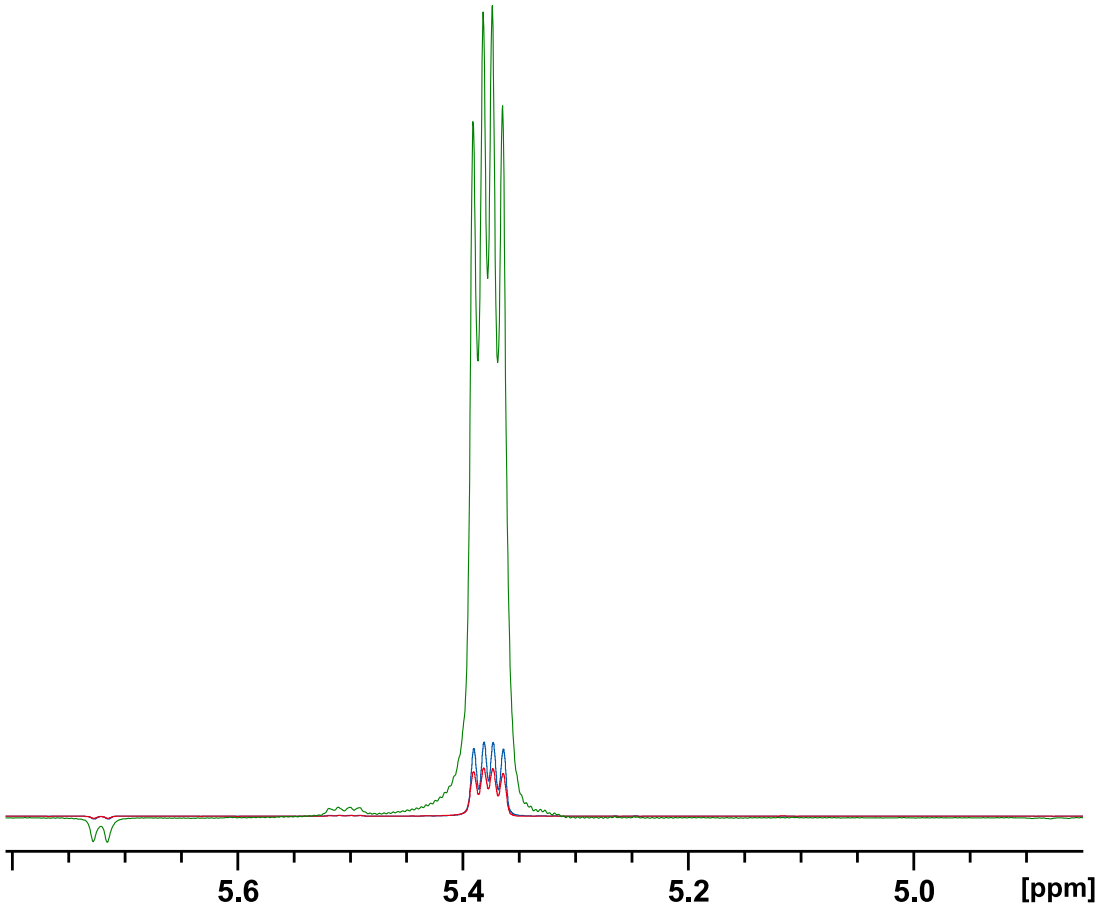

Figure 5.5: Comparison of $F2$-traces extracted from the 2D $F1$-PSYCHE-EASY-ROESY spectrum (blue), from the 2D *gradient-selected* $F1$-PSYCHE-EASY-ROESY spectrum (red) and from the 2D *gradient-selected* $F1$-*perfect*BASH-EASY-ROESY spectrum (green) of cyclosporine A in C_6D_6 at the chemical shift of H-6α (5.3782 ppm). The traces are scaled according to the different RG values. In the traces only the diagonal-peak is shown and phased positive. Obvious is the intensity loss between the two homonuclear decoupling methods *perfect*BASH and PSYCHE. Further the intensity loss by approximately the factor two between the *gradient-selected* and the not *gradient-selected* version is visible.

5.4 1D *gradient-selected* CW-ROESY (GS-CW-ROESY): Description

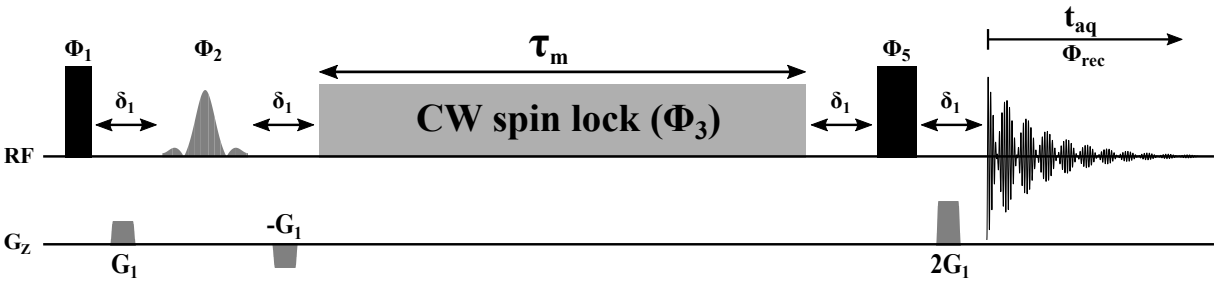

Figure 5.6: Pulse sequence scheme for the 1D *gradient-selected* CW-ROESY experiment. Narrow and wide rectangles represent hard 90° and 180° pulses, respectively. The grey broad rectangle is the *continuous-wave* (CW) spin lock of τ_m duration. Grey shapes are selective pulses. The gradient G_1 is used for coherence selection and for phase en- and decoding. The delay $\delta_1 = p_{16} + d_{16}$, where p_{16} is the durations of the gradient pulse and d_{16} is a recovery delay. Phase cycling: All pulse phases are x unless denoted otherwise. $\Phi_1 = x\ -x$, $\Phi_2 = x\ x\ y\ y\ -x\ -x\ -y\ -y$, $\Phi_3 = y$, $\Phi_5 = 4(x)\ 4(-x)$, and $\Phi_{rec} = x\ -x\ -x\ x\ x\ -x\ -x\ x$.

The pulse sequence (Figure 5.6) of the 1D *gradient-selected* CW-ROESY (GS-CW-ROESY) is based on the Tr-ROESY implementation with gradient-selection published by J. Furrer *et al.* [34]. In this implementation we use a *continuous-wave* spin-lock for mixing instead of a train of phase-alternating 180° low-power pulses. The *pulsed field gradient selected selective spin-echo* for selection of one or one group of proton resonances, using a selective, shaped 180° pulse, is implemented with bipolar gradients. This arrangement leads to a dephasing of the selected proton resonance, with the phase-factor along z depending on the gradient strength $2G_1$. This phase factor is reversed after the CW-ROESY mixing element by a gradient pulse with twofold strength within a hard pulse spin-echo affecting all spins. With such an implementation and with carefully adjusted gradients clean ROESY spectra can be acquired without interfering substraction artefacts. However, as discussed for the 2D *gradient-selected* $F1$-PSYCHE-EASY-ROESY, only half of the excited magnetisation can be rephased and the intensities of the resulting proton signals are attenuated by molecular diffusion. Hence for quite long selective refocusing pulses (> 50 ms) and long mixing-times τ_m this arrangement might be unfavourable because of the loss in sensitivity.

5.5 1D *gradient-selected* EASY-ROESY: Description

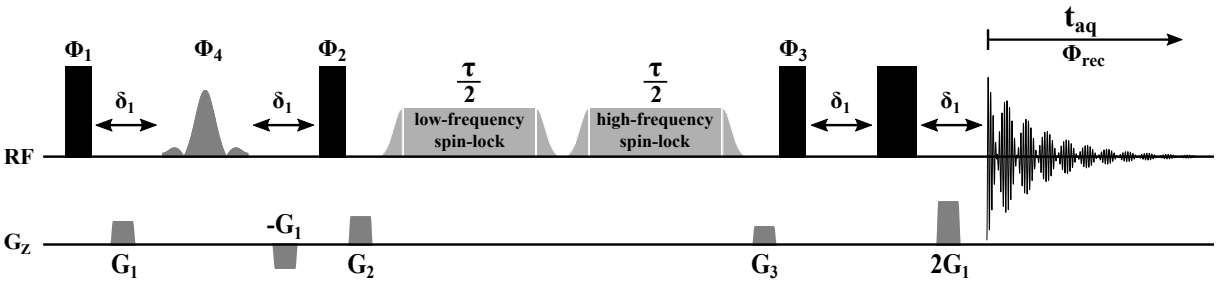

Figure 5.7: Pulse sequence scheme for the 1D *gradient-selected* EASY-ROESY experiment. Narrow and wide rectangles represent hard 90° and 180° pulses, respectively. Broad rectangles in grey are low- and high-frequency spinlocks (SL) of $\tau_m/2$ duration, half-Gaussian shaped pulses are used as adiabatic ramps. Grey shapes are selective pulses. The gradients G_1 are used for coherence selection and for phase en- and decoding, the gradients G_2 and G_3 are purge gradients. The delay $\delta_1 = p_{17} + d_{16}$, where p_{17} is the durations of the gradient pulse and d_{16} is a recovery delay. Phase cycling: All pulse phases are x unless denoted otherwise. $\Phi_1 = x\ -x$, $\Phi_2 = 16(x)\ 16(-x)$, $\Phi_3 = 8(x)\ 8(-x)$, $\Phi_4 = x\ x\ y\ y\ -x\ -x\ -y\ -y$ and $\Phi_{rec} = x\ -x\ -x\ x\ x\ -x\ -x\ x\ -x\ x\ x\ -x\ -x\ x\ x\ -x\ -x\ x\ x\ -x\ -x\ x\ x\ -x\ -x\ x\ x\ -x\ -x\ x\ x\ -x\ -x\ x$.

The pulse sequence (Figure 5.7) of the 1D *gradient-selected* EASY-ROESY was built from the 2D EASY-ROESY sequence from the Bruker pulse sequence library (*roesyadjsphpr*) by replacing the t_1-evolution time by a *pulsed field-gradient selected selective spin-echo* with bipolar gradients and the hard pulse spin-echo with the decoding gradients after the mixing element. In comparison with the already published 1D-EASY-ROESY implementation by Boros *et al.* [35], we implemented the pulse sequence with gradient selection over the EASY-ROESY mixing-element in the same way as described for the GS-CW-ROESY experiment to attenuate substraction artefacts and to get cleaner spectra. Further, we use no Thrippleton-Keeler elements in the mixing element before and after the spin-locks. The low- and high-frequency irradiation offsets are shifted symmetrically relative to the carrier frequency (O1P), which should be set to the center of the whole proton spectrum. The offset for selective refocusing to select one proton is defined with CNST1.

5.6 Dependency of the spin-lock angle in EASY-ROESY experiments

When we probe transversal cross-relaxation with ROESY experiments, we have to consider two extra pathways of spin polarization besides transversal cross-relaxation, namely longitudinal cross-relaxation (NOESY) and Hartmann-Hahn transfer (TOCSY). Complete suppression of both transfer pathways simultaneously is unattainable. The relation between longitudinal (L) and transversal (T) cross-relaxation can be adjusted with the spin-lock angle Θ relative to the direction of the B_0-field[8,9]:

$$\sigma_{eff} \;=\; w_L\sigma_L \;+\; w_T\sigma_T \;=\; \cos^2(\Theta)\sigma_L \;+\; \sin^2(\Theta)\sigma_T \tag{5.27}$$

In motional regimes near the zero-crossing of the longitudinal cross-relaxation one might be tempted to improve the intensities of the cross-peaks in the ROESY spectra by choosing a large spin-lock angle Θ, which turns the spin-lock axis more towards the transversal plane and increases the transversal part of the effective cross-realaxation rate. However, this is accompanied with the risk of substantial TOCSY transfer[36]. This gives rise to additional TOCSY cross-peaks in the resulting EASY-ROESY spectra and influences the intensity of NOE cross-peaks between protons which share dipolar coupling through space and scalar coupling via chemical bonds. Thus one has to find a compromise between maximizing ROESY and limiting TOCSY polarization transfer, when adjusting the spin-lock angle. Usually a spin-lock angle of $\Theta = 45°$ is the best choice, if TOCSY is an issue. In the present study the mixing-time series of the 2D *gradient-selected* $F1$-PSYCHE-EASY-ROESY experiment was acquired with a spin-lock angle of 50° and 5.5 kHz RF field, all other EASY-ROESY experiments were performed with 45° and 5 kHz RF field. This parameter setting leads to different cross-relaxation rates. Nevertheless, the interproton distances calculated by internal calibration (equation 2.12) show a high consistency, suggesting these contributions to the cross-relaxation rates at least partially cancel themselves in the subsequent calculations.

However we subject this issue to a more detailed analysis with the aim to estimate the errors that may arise. For this, for selected protons we acquired mixing-time series with the *gradient-selected*-1D-EASY-ROESY experiment and spin-lock angles of 45° to 50° and 60°. We chose the protons 1-β (1-MBmt) and 10-β_1 (10-MLeu), which are within one scalar coupling network and the N-methyl group of 11-MVal, which should be less influenced by TOCSY. For internal calibration the distance between the protons 3-α_1 and 3-α_2 was used and set to $r_{3\alpha1,3\alpha2} \;=\; 1.75\,\mathring{A}$. The extracted cross-relaxation rates and the calculated distances from the NOEs of the selected protons are summarized in table 5.1.

Table 5.1: Cross-relaxation rates and ^{1}H,^{1}H-distances extracted from 1D *gradient-selected* EASY-ROESY experiments under variation of the spin-lock angle Θ.

H	**H'**	σ / s^{-1}			**r** / $\AA$		
		Θ = 45°	Θ = 50°	Θ = 60°	Θ = 45°	Θ = 50°	Θ = 60°
3-α_1	3-α_2	0.7100 ± 0.0048	0.8701 ± 0.0065	0.9614 ± 0.0110	1.75 (ref.)	1.75 (ref.)	1.75 (ref.)
3-α_1	4-NMe	0.0787 ± 0.0002	0.0918 ± 0.0003	0.1046 ± 0.0003	2.516 ± 0.003	2.537 ± 0.032	2.524 ± 0.005
11-NMe	7-NH	0.0089 ± 0.0003	0.0108 ± 0.0003	0.0116 ± 0.0009	3.619 ± 0.019	3.627 ± 0.049	3.641 ± 0.049
11-NMe	8-NH	0.0062 ± 0.0003	0.0067 ± 0.0002	0.0090 ± 0.0003	3.846 ± 0.029	3.925 ± 0.053	3.796 ± 0.020
11-NMe	10-α	0.0602 ± 0.0017	0.0699 ± 0.0011	0.0868 ± 0.0022	2.631 ± 0.013	2.655 ± 0.034	2.604 ± 0.012
11-NMe	11-α	0.0064 ± 0.0002	0.0070 ± 0.0002	0.0089 ± 0.0012	3.821 ± 0.022	3.892 ± 0.052	3.805 ± 0.088
11-NMe	8-α	0.0075 ± 0.0001	0.0114 ± 0.0005	0.0134 ± 0.0006	3.722 ± 0.011	3.594 ± 0.051	3.557 ± 0.026
11-NMe	10-NMe	0.0040 ± 0.0001	0.0044 ± 0.0001	0.0057 ± 0.0002	4.141 ± 0.012	4.216 ± 0.055	4.104 ± 0.023
11-NMe	11-β	0.0675 ± 0.0003	0.0787 ± 0.0002	0.0968 ± 0.0010	2.582 ± 0.003	2.603 ± 0.032	2.557 ± 0.007
11-NMe	7-β	0.0053 ± 0.0001	0.0064 ± 0.0001	0.0079 ± 0.0005	3.940 ± 0.015	3.958 ± 0.051	3.886 ± 0.039
11-NMe	6-δ_2	0.0039 ± 0.0003	0.0037 ± 0.0002	0.0054 ± 0.0006	4.157 ± 0.049	4.331 ± 0.068	4.134 ± 0.077
11-NMe	11-γ_2	0.0119 ± 0.0003	0.0133 ± 0.0006	0.0142 ± 0.0001	3.448 ± 0.014	3.501 ± 0.051	3.521 ± 0.008
10-β_1	10-α	0.0346 ± 0.0012	0.0478 ± 0.0063	0.0521 ± 0.0030	2.885 ± 0.017	2.829 ± 0.072	2.835 ± 0.028
10-β_1	10-γ	0.0572 ± 0.0043	0.0698 ± 0.0036	0.0893 ± 0.0025	2.654 ± 0.033	2.656 ± 0.040	2.592 ± 0.013
10-β_1	10-β_2	0.6020 ± 0.0068	0.6775 ± 0.0127	0.7692 ± 0.0175	1.793 ± 0.004	1.818 ± 0.023	1.810 ± 0.008
10-β_1	10-δ_2	0.0430 ± 0.0015	0.0437 ± 0.0015	0.0490 ± 0.0016	2.783 ± 0.016	2.871 ± 0.039	2.864 ± 0.017
10-β_1	6-δ_2	0.0038 ± 0.0001	0.0045 ± 0.0011	0.0053 ± 0.0002	4.164 ± 0.023	4.192 ± 0.174	4.153 ± 0.025
1-β	2-NH	0.0464 ± 0.0022	0.0488 ± 0.0044	0.0611 ± 0.0039	2.748 ± 0.022	2.818 ± 0.055	2.761 ± 0.030
1-β	1-α	0.0881 ± 0.0013	0.1060 ± 0.0019	0.1234 ± 0.0016	2.470 ± 0.007	2.477 ± 0.032	2.456 ± 0.007
1-β	1-NMe	0.0286 ± 0.0009	0.0373 ± 0.0012	0.0428 ± 0.0010	2.979 ± 0.015	2.948 ± 0.040	2.930 ± 0.012
1-β	3-NMe	0.0016 ± 0.0001	0.0019 ± 0.0002	0.0024 ± 0.0001	4.837 ± 0.040	4.838 ± 0.091	4.735 ± 0.044
1-β	1-δ_2	0.0285 ± 0.0013	0.0390 ± 0.0006	0.0479 ± 0.0015	2.981 ± 0.022	2.926 ± 0.037	2.875 ± 0.016
1-β	1-γ	0.0550 ± 0.0013	0.0651 ± 0.0013	0.0752 ± 0.0010	2.671 ± 0.011	2.687 ± 0.035	2.667 ± 0.008
1-β	1-γMe	0.0305 ± 0.0010	0.0349 ± 0.0013	0.0445 ± 0.0011	2.947 ± 0.016	2.981 ± 0.042	2.911 ± 0.013

As expected the effective cross-relaxation rates increase when raising the locking angle from 45° to 50° and 60° as the spin-locking axis is closer to the transversal plane. The calculated distances, performed via internal calibration using the diastereotopic proton pair 3-α_1/3-α_2, seem to be less influenced by the applied locking-angle neither for the protons 10-β_1 and 1-β nor for the proton 11-NMe, which should be differently biased by TOCSY mixing effects. Proton distances from long-range NOE contacts differ more, when the spin-lock angle is changed. However, these proton distances are in general more sensitive to experimental and systematic errors like spin-diffusion effects. The limited dataset presented here does not show a clear systematic error introduced by the parameters used herein (variation of the spin-lock angle from 45° to 60°). Rather, the observed distribution of derived interproton distances and their estimated experimental uncertainties may allow for a more robust estimation of the experimental error of the calculated interproton distance.

5.7 Evaluation of offset effects in EASY-ROESY experiments

In the EASY-ROESY experiment the attenuation of Hartmann-Hahn polarization transfer is performed on one hand by adjusting the spin-lock angle Θ and with *off-resonance* locking outside the common chemical shift range of protons. To average out offset effects the spin-lock is applied twice with irradiation at the low-frequency edge for one half of the mixing-time and subsequently at the high-frequency edge for the second half[36]. This irradiation offset shifting to the low- and high-frequency is performed symmetrically relative to a midpoint, which should be ideally the center of the whole proton spectrum. In the EASY-ROESY implementations the placement of this midpoint is under the control of the experimenter. Herein the midpoint is defined via CNST0 in the 2D *gradient-selected* $F1$-*perfect*BASH-EASY-ROESY experiment and in all other EASY-ROESY experiments by the carrier frequency offset O1P. We also subject this parameter to a more detailed analysis with the aim to estimate the errors that may arise, when the midpoint for symmetrical offset shifting is placed away from the center of the whole proton spectrum. For this we acquire mixing time series for several selected protons with the *gradient-selected*-1D-EASY-ROESY experiment and set the midpoint either to the exact center of the proton spectrum $\Omega = 4.453$ ppm or to the chemical shift of the selected protons. We chose the protons $1{-}\beta$ (1-MBmt), 2-NH (2-Abu) and $11{-}\gamma_2$ (11-MVal), whereby the chemical shift of $1{-}\beta$ ($\Omega = 4.1907$) is close to the center at 4.453 ppm. The protons 2-NH ($\Omega = 8.2444$ ppm) and $11{-}\gamma_2$ ($\Omega = 0.6427$ ppm) have the highest and the lowest chemical shifts of all protons in cyclosporine A, respectively. For internal calibration the distance between the protons 3-α_1 and 3-α_2 was used and set to $r_{3\alpha1,3\alpha2} = 1.75\,\mathring{A}$. The extracted cross-relaxation rates and the calculated distances from the NOEs of the selected protons are summarized in table 5.2.

Table 5.2: Cross-relaxation rates and ^{1}H,^{1}H-distances extracted from 1D *gradient-selected* EASY-ROESY experiments under variation of the midpoint for symmetrical offset shifting to the low- and high-frequency for spin-locking.

H	**H'**	σ / s^{-1}	r / $\AA$	δ / ppm	σ / s^{-1}	r / $\AA$	δ / ppm
3−α_1	3−α_2	0.8287 ± 0.0591	1.75 (ref.)	4.453	0.8434 ± 0.0035	1.75 (ref.)	4.0060
3−α_1	4-NMe	0.0945 ± 0.0010	2.513 ± 0.005	4.453	0.0932 ± 0.0004	2.526 ± 0.003	4.0060
1−β	2-NH	0.0560 ± 0.0032	2.742 ± 0.026	4.453	0.0539 ± 0.0015	2.768 ± 0.013	4.1907
1−β	1−α	0.0924 ± 0.0029	2.522 ± 0.013	4.453	0.0933 ± 0.0006	2.526 ± 0.003	4.1907
1−β	1-NMe	0.0313 ± 0.0003	3.022 ± 0.006	4.453	0.0314 ± 0.0003	3.028 ± 0.005	4.1907
1−β	1−δ_2	0.0456 ± 0.0024	2.838 ± 0.025	4.453	0.0382 ± 0.0014	2.931 ± 0.018	4.1907
1−β	1−γ	0.0560 ± 0.0014	2.742 ± 0.012	4.453	0.0577 ± 0.0019	2.736 ± 0.015	4.1907
1−β	1−γMe	0.0329 ± 0.0003	2.996 ± 0.006	4.453	0.0353 ± 0.0003	2.970 ± 0.005	4.1907
2-NH	5-NH	0.0419 ± 0.0017	2.878 ± 0.020	4.453	0.0383 ± 0.0019	2.930 ± 0.024	8.2444
2-NH	1−α	0.3834 ± 0.0045	1.990 ± 0.005	4.453	0.3467 ± 0.0121	2.029 ± 0.012	8.2444
2-NH	2−α	0.0729 ± 0.0037	2.624 ± 0.023	4.453	0.0710 ± 0.0030	2.643 ± 0.019	8.2444
2-NH	1−β	0.0877 ± 0.0023	2.545 ± 0.012	4.453	0.0888 ± 0.0010	2.547 ± 0.005	8.2444
11−γ_2	11−α	0.0378 ± 0.0006	2.928 ± 0.009	4.453	0.0394 ± 0.0008	2.916 ± 0.010	0.6427
11−γ_2	11-NMe	0.0114 ± 0.0001	3.575 ± 0.007	4.453	0.0114 ± 0.0002	3.588 ± 0.009	0.6427
11−γ_2	10-NMe	0.0113 ± 0.0001	3.583 ± 0.009	4.453	0.0113 ± 0.0002	3.592 ± 0.009	0.6427
11−γ_2	11−β	0.0574 ± 0.0005	2.731 ± 0.005	4.453	0.0583 ± 0.0010	2.732 ± 0.008	0.6427
11−γ_2	11−γ_1	0.0179 ± 0.0003	3.317 ± 0.010	4.453	0.0172 ± 0.0004	3.348 ± 0.012	0.6427

The dataset does not seem to show any systematic influence of the cross-relaxation rates nor the derived distances on the choice of spin-lock offset. Neither the protons with chemical shift close to the center (1-β and 3-α_1) nor the protons with the highest and lowest chemical shift 2-NH and 11-γ_2 show significant changes beyond experimental and systematic errors.

5.8 2D *F*1-PSYCHE-EASY-ROESY: Spin-site dependent attenuation

In the theoretical description of the 2D *gradient-selected* $F1$-PSYCHE-EASY-ROESY experiment in chapter 5.1 we introduced a parameter β_k to account for effects introduced by the PSYCHE[6] element for homonuclear decoupling (*pure shift*) in $F1$. The low-flip angle leads to a signal attenuation, which should be equal for all protons. In this chapter we are interested in deviations from this average value equally for all protons introduced by proton specific T_2-weighting and potential offset effects. To get an idea how this β parameter scales the signal intensity and which kind of errors may occur, if these effects are neglected, we subject this matter to a brief analysis. We acquired 1D *pure shift* ^{1}H spectra of cyclosporine A under quantitative conditions (sufficiently long recovery delay d_1) either using PSYCHE[6] or Zangger-Sterk[37] for homonuclear decoupling and compared the relative signal integrals. With a Zangger-Sterk homonuclear decoupled 1D-^{1}H spectrum it was shown by Kaltschnee *et al.* [38] that reliable integrals can be obtained after applying some corrections. Both spectra were acquired with the *interferogram-based* acquisition mode in an extra pseudo *pure shift* dimension. Herein the whole FID is collected in independently and consecutively acquired *data-chunks*, whose duration is short compared to the inverse of the J_{HH}-coupling constant. Zangger-Sterk homonuclear decoupling can also be performed using the *real-time* decoupling[39], if the duration of the selective refocusing pulse in the Zangger-Sterk element is quite short. However, as we have used rather long selective refocusing pulses (65 ms) to achieve nearly broadband homonuclear decoupling the *real-time* decoupling would not work. As described in the Zangger-Sterk-NOESY paper of Kaltschnee *et al.* [38] the proton signal amplitudes are influenced by T_2 relaxation during the homonuclear decoupling block and the *data-chunking* in *interferogram-based* 1D *pure shift* ^{1}H spectra. If the duration of the *data-chunks* is very short $\Delta \leq 5$ ms the latter influence of the *data-chunking* becomes small and could be neglected. The influence of T_2 relaxation during the homonuclear decoupling block on the proton signal integral can be corrected as described in the paper[38].

$$\begin{aligned} I_{rel} &= I_{rel,corr} \cdot A\left(T_2\right) \\ &\text{with} \\ A\left(T_2\right) &= \exp\left(-\frac{p_{sel}+\delta_1+\delta_2+\delta_3}{T_2}\right) \end{aligned} \tag{5.28}$$

Herein I_{rel} is the relative integral extracted from the spectrum and $I_{rel,corr}$ is the T_2-corrected relative integral. The attenuation factor $A\left(T_2\right)$ depends on the T_2-relaxation time constant, the duration of the selective refocusing pulse p_{sel} and the timing parameters δ_1 through δ_3, which are defined as:

$$\begin{aligned} \delta_1 &= p_{16} + d_{16} + \frac{1}{4SW_1} \\ \delta_2 &= 2p_{16} + 3d_{16} + \frac{1}{4SW_1} \\ \delta_3 &= p_{16} + 2d_{16} \end{aligned} \tag{5.29}$$

Herein p_{16} is the duration of the gradient for coherence selection and d_{16} a recovery delay.

Now we analyse this matter for the case of PSYCHE homonuclear decoupling. The T_2-relaxation time constants of the protons used for the T_2-correction were determined using a series of CPMG experiments (*cpmg* pulse programme from the Bruker pulse sequence library) under variation of the T_2 relaxation period and subsequent mono exponential fitting of the integrals. For protons, which are overlapped in the 1D ^{1}H spectrum, the T_2-relaxation time constants were determined using a CPMG experiment with *interferogram-based* Zangger-Sterk homonuclear decoupling. In table 5.3 the results from our analysis are summarized. Herein I_{rel} are the normalised relative integrals from the 1D PSYCHE ^{1}H or 1D Zangger-Sterk ^{1}H spectra before the T_2 correction, $A(T_2)$ are the attenuation factors used for T_2 correction, calculated from the T_2 value as described in the paper of Kaltschnee *et al.* [38] and $I_{rel,corr}$ are the relative integrals after T_2 correction. The integrals are normalised to the integral of proton $2{-}\alpha$, which is set to 1. The T_2 correction for PSYCHE is a more sophisticated task, as the finally detected magnetisation is determined by the magnetisation recovered during the PSYCHE element. In a rough approximation we either include or not include the duration of the PSYCHE element ($p_{sel} = 30\,ms$) in the T_2 correction as an upper limit and lower limit, respectively. For p_{16} and d_{16} we use the experimental values of 1 ms and 200 μs, respectively.

Table 5.3: Relative integrals I_{rel}, T_2-attenuation factors $A(T_2)$ and corrected relative integrals $I_{rel,corr}$ determined from a 1D ^{1}H-PSYCHE spectrum and a 1D ^{1}H-Zangger-Sterk spectrum.

Proton	T_2 / **s**	**PSYCHE**						**Zangger-Sterk**		
		I_{rel}[a]	$A(T_2)$[a]	$I_{rel,corr}$[a]	I_{rel}[b]	$A(T_2)$[b]	$I_{rel,corr}$[b]	I_{rel}	$A(T_2)$	$I_{rel,corr}$
2-NH	0.155	0.561	0.955	0.579	0.561	0.786	0.657	0.712	0.597	0.997
7-NH	0.205	0.690	0.966	0.703	0.690	0.834	0.761	0.837	0.677	1.033
8-NH	0.249	0.692	0.972	0.700	0.692	0.861	0.738	0.830	0.726	0.956
5-NH	0.197	0.698	0.964	0.712	0.698	0.828	0.775	0.755	0.667	0.946
$9{-}\alpha$	0.140	0.887	0.950	0.919	0.887	0.767	1.064	0.785	0.565	1.161
$1{-}\alpha$	0.216	0.916	0.967	0.932	0.916	0.842	1.000	0.899	0.691	1.086
$1{-}\epsilon$	0.277	0.824	0.975	0.832	0.824	0.875	0.866	0.897	0.750	1.000
$4{-}\alpha$	0.206	0.966	0.966	0.984	0.966	0.835	1.064	0.831	0.678	1.024
$1{-}\eta$	0.267	0.968	0.974	0.979	0.968	0.870	1.023	0.995	0.742	1.121
$6{-}\alpha$	0.239	0.921	0.971	0.934	0.921	0.856	0.990	0.956	0.716	1.116
$10{-}\alpha$	0.218	0.910	0.968	0.925	0.910	0.843	0.993	0.807	0.694	0.972
$11{-}\alpha$	0.437	0.972	0.984	0.972	0.972	0.919	0.973	1.104	0.833	1.107
$2{-}\alpha$	0.444	1.000	0.984	1.000	1.000	0.920	1.000	1.000	0.836	1.000
$5{-}\alpha$	0.369	0.971	0.981	0.974	0.971	0.904	0.987	1.039	0.805	1.078

Table 5.3 – continuation

Proton	T_2 / s	PSYCHE						Zangger-Sterk		
		I_{rel}[a]	$A(T_2)$[a]	$I_{rel,corr}$[a]	I_{rel}[b]	$A(T_2)$[b]	$I_{rel,corr}$[b]	I_{rel}	$A(T_2)$	$I_{rel,corr}$
8−α	0.340	0.971	0.979	0.975	0.971	0.897	0.996	0.921	0.791	0.973
7−α	0.392	0.967	0.982	0.969	0.967	0.910	0.977	1.016	0.816	1.041
3−α_1	0.220	0.896	0.968	0.911	0.896	0.844	0.976	0.898	0.695	1.080
1-NMe	0.359	2.937	0.980	2.948	2.937	0.902	2.996	2.908	0.801	3.034
6-NMe	0.440	2.979	0.984	2.979	2.979	0.919	2.981	3.003	0.834	3.008
3-NMe	0.436	2.959	0.984	2.960	2.959	0.918	2.964	2.994	0.832	3.004
11-NMe	0.438	2.938	0.984	2.939	2.938	0.919	2.941	2.965	0.833	2.973
9-NMe	0.417	2.900	0.983	2.903	2.900	0.915	2.916	2.893	0.826	2.928
10-NMe	0.551	2.970	0.987	2.960	2.970	0.935	2.922	3.145	0.865	3.038
1−δ_1	0.207	0.756	0.966	0.771	0.756	0.836	0.833	0.836	0.680	1.028
4-NMe	0.453	2.896	0.984	2.895	2.896	0.921	2.891	3.021	0.838	3.010
10−β_1	0.237	0.712	0.970	0.722	0.712	0.855	0.767	0.925	0.714	1.083
1−γ	0.231	0.855	0.970	0.868	0.855	0.851	0.924	0.820	0.708	0.968
1−ω	0.400	2.718	0.982	2.722	2.718	0.911	2.743	2.939	0.819	2.998
7−β	0.292	2.643	0.976	2.665	2.643	0.880	2.761	2.738	0.761	3.008
6−β_2	0.215	0.659	0.967	0.671	0.659	0.841	0.720	0.860	0.690	1.041
4−γ	0.290	0.763	0.976	0.769	0.763	0.880	0.797	0.919	0.760	1.011
10−β_2	0.225	0.730	0.969	0.741	0.730	0.848	0.792	0.869	0.701	1.035
10−δ_1	0.278	2.330	0.975	2.353	2.330	0.875	2.450	2.554	0.751	2.843
10−δ_2	0.273	2.348	0.974	2.372	2.348	0.873	2.475	2.686	0.746	3.007
6−δ_2	0.273	2.497	0.974	2.522	2.497	0.873	2.632	2.636	0.746	2.951
8−β	0.320	2.582	0.978	2.599	2.582	0.891	2.667	2.782	0.779	2.983
4−δ_1	0.347	2.496	0.980	2.507	2.496	0.898	2.555	2.781	0.794	2.925
11−γ_1	0.186	2.295	0.962	2.347	2.295	0.819	2.578	2.313	0.651	2.970
4−δ_2	0.331	2.655	0.979	2.670	2.655	0.894	2.732	2.855	0.786	3.036
2−γ	0.434	2.443	0.984	2.444	2.443	0.918	2.448	2.930	0.832	2.943
9−δ_2	0.338	2.408	0.979	2.420	2.408	0.896	2.472	2.821	0.790	2.985
11−γ_2	0.322	2.470	0.978	2.486	2.470	0.891	2.550	2.712	0.780	2.905

Table 5.3 – continuation

Proton	T_2 / s	PSYCHE						Zangger-Sterk		
		I_{rel}[a]	$A(T_2)$[a]	$I_{rel,corr}$[a]	I_{rel}[b]	$A(T_2)$[b]	$I_{rel,corr}$[b]	I_{rel}	$A(T_2)$	$I_{rel,corr}$

[a] duration of PSYCHE element not included in the T_2-correction

[b] duration of PSYCHE element included in the T_2-correction

The corrected integral values in the Zangger-Sterk column are quite close to the expected value of 1 (or 3 for methyl protons) as expected, based on the work of Kaltschnee *et al.* [38]. The integral values of the PSYCHE homonuclear decoupling differ significantly (up to 23 %) from the expected value irrespective of the inclusion of the duration of the PSYCHE element in the T_2-correction. The plot of the relative T_2-corrected integrals $I_{rel,corr}$ against the T_2-relaxation time constants (shown in figure 5.8) indicates, that a T_2-weighting effect of the PSYCHE integrals after correction remains. The Zangger-Sterk integrals, plotted for comparison, do not show this effect. Thus PSYCHE seems not to give reliable integrals, T_2-weighting with the duration of the homodecoupling block only is not the exclusive problem. There might be additional effects, which attenuate the integral spin-site dependent and are not analysed in detail herein. Nevetheless we can conclude, the way in which the ROESY data are analysed to extract accurate cross-relaxation rates is essential. To eliminate such spin-site dependence in our data analysis, we normalise the cross-peak integrals with the corresponding diagonal-peak in the same row (same chemical shift in $F1$). Then these weighting effects, which we consider with the β_k-factor and which we assume to be only dependent on the spin-site in $F1$, are eliminated. This would be not the case if the cross-peak integrals are either normalised by the corresponding diagonal-peak in the same column (same chemical shift in $F2$), normalised by both diagonal-peaks in $F1$ and $F2$, as described in the paper of Macura *et al.* [15], or not normalised.

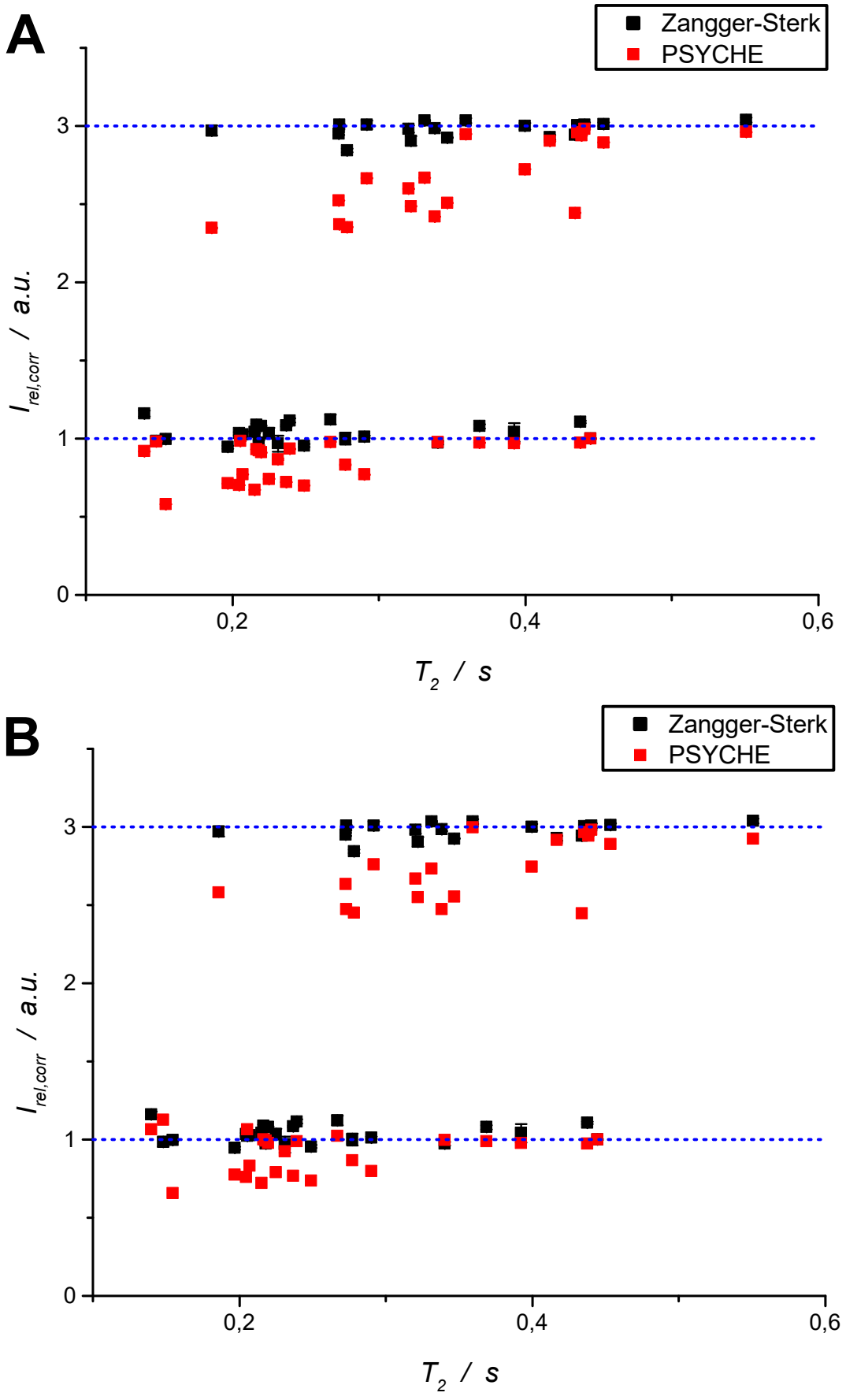

Figure 5.8: Illustration of the dependency of the corrected relative integrals $I_{rel,corr}$ from the transversal relaxation time T_2 (A and B). The integrals were either determined with a 1D ^{1}H-Zangger-Sterk spectrum (black squares) or with a 1D ^{1}H-PSYCHE spectrum (red squares). The horizontal dashed lines are the expected values of 3 for methyl protons or 1 for all other protons. In (A) the duration of the PSYCHE element was not included in the T_2 correction as an lower correction limit, in (B) the duration was included as an upper correction limit.

5.9 Explanation of COSY-like artefacts in *F*1-PSYCHE-EASY-ROESY experiments

In the main text we discuss additional responses in EASY-ROESY experiments with PSYCHE homonuclear decoupling in the indirect dimension $F1$. These are observed at the average chemical shift $\frac{\Omega_2+\Omega_1}{2}$ in $F1$ of two scalar coupled protons with quite low chemical shift difference $\Delta\Omega_{F1} = \Omega_2 - \Omega_1$ and have a distorted anti-phase doublet appearance as shown in Figure 5.9. These additional responses, which we call COSY artefacts or COSY responses in the following, are not restricted to the $F1$-PSYCHE-EASY-ROESY and its *gradient-selected* version. Indeed these artefacts are an intrinsic property of all homonuclear 2D-experiments (TOCSY, NOESY, CLIP-COSY) with PSYCHE homonuclear decoupling in the indirect dimension $F1$ and results from insufficiently attenutated COSY polarization transfer. Below we briefly analyse the origin of these COSY responses and under which conditions we can observe them. A similar analysis was previously done by Sinnaeve[40] to explain artefacts at methyl-protons in PSYCHEDELIC spectra of partially aligned analytes.

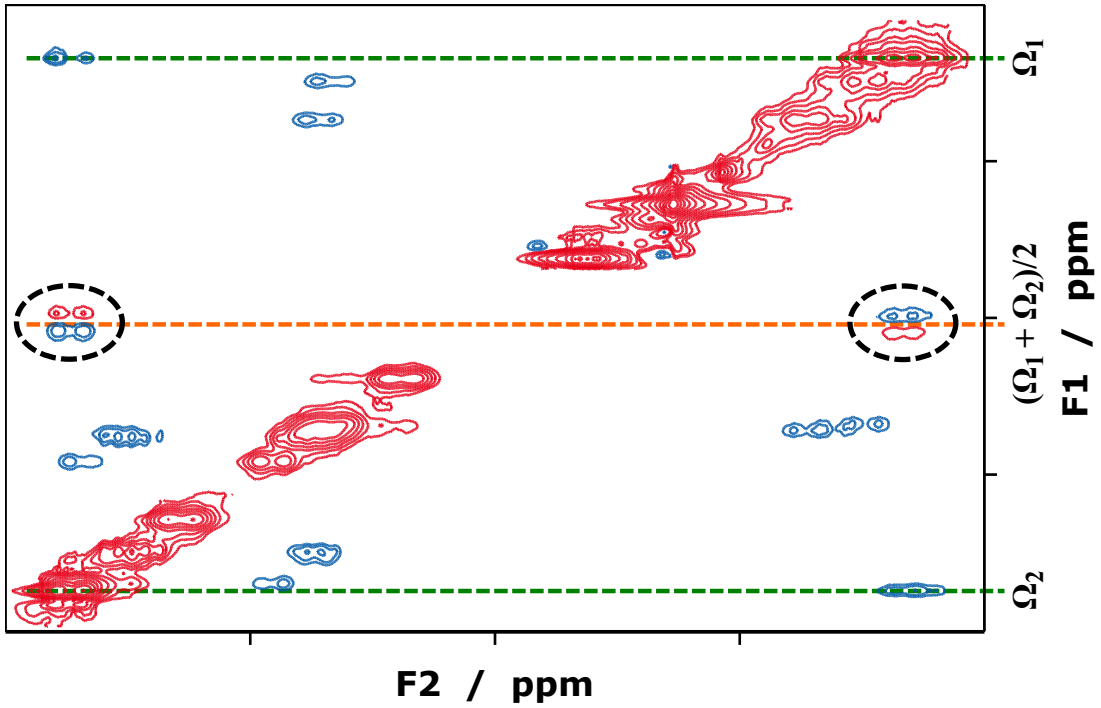

Figure 5.9: Additional COSY responses (dashed black circles) in the $F1$-PSYCHE-EASY-ROESY spectrum, which appear at the average chemical shift $\frac{\Omega_2+\Omega_1}{2}$ in $F1$ (dashed orange line) of two scalar coupled protons.

For simplicity we assume an instantaneous flip by the angle β, when the frequency sweep of the adiabatic PSYCHE pulse bundle matches the offset frequency Ω_i of the corresponding proton. We apply our analysis to a simple scalar coupled two-spin-$\frac{1}{2}$-system I and S, neglecting all relaxation. Further we restrict our analysis to the *single-quantum* terms with index "$-$", which are selected by phase-cycling or gradients and are of significant relative intensity. If the flip angle β is low, we can neglect all terms with higher order than two with respect to β. Then

three main terms, generated by the PSYCHE element, remain:

$$\begin{aligned} \frac{i}{2}\, I_+ S_\beta \quad \xrightarrow{\text{"PSYCHE"}} \quad & \frac{i}{4}\,\beta^2\, I_- S_\beta \\ & \frac{i}{8}\,\beta^2\, I_\beta S_- \\ & \frac{i}{8}\,\beta^2\, I_\alpha S_- \end{aligned} \tag{5.30}$$

In the first term the spin state of the coupling partner S is inverted and no polarization transfer has taken place, hence this is the wanted term, as PSYCHE should be a spin state selective inversion element. In the second and the third term polarization has been transfered from the I spin to the S spin and the spin state of the I spin is once inverted and once preserved. These two terms are the unwanted COSY terms.

If we start our analysis after the the 90° excitation pulse and include chemical shift as well as $J-$coupling evolution during t_1 the three terms transform to:

$$\begin{aligned} \frac{i}{2}\, I_- S_\alpha \quad & \xrightarrow{\frac{t_1}{2}+\delta_1\,-\,180^\circ\,-\,\delta_2} \quad \exp\left[i\Omega_1\left(\frac{t_1}{2}+\delta_1-\delta_2\right)+\pi J\left(\frac{t_1}{2}+\delta_1+\delta_2\right)\right]\,\frac{i}{2}\, I_+ S_\beta \\ & \xrightarrow{\text{"PSYCHE"}} \\ & \xrightarrow{\frac{t_1}{2}+\delta_3} \\ & \frac{i}{4}\,\beta^2 \exp\left(i\Omega_1 t_1\right)\, I_- S_\beta \\ & \frac{i}{8}\,\beta^2 \exp\left(i\frac{\Omega_1+\Omega_2}{2}t_1 + i\Delta\Omega\delta_3\right)\, I_\beta S_- \\ & \frac{i}{8}\,\beta^2 \exp\left[i\left(\frac{\Omega_1+\Omega_2}{2}-2\pi J\right)t_1 + i\left(\Delta\Omega-2\pi J\right)\delta_3\right]\, I_\alpha S_- \end{aligned} \tag{5.31}$$

Herein we use the timing conditions $\frac{t_1}{2}+\delta_1+\delta_2 = \frac{t_1}{2}+\delta_3$ for refocusing of scalar-coupling and $\delta_1-\delta_2+\delta_3 = 0$ for chemical shift evolution during t_1. The wanted term has experienced only net chemical shift evolution during t_1, whereas the coupling evolution is fully refocused. This term will give us the wanted singlet response at $\omega_{F1} = \Omega_1$ after Fourier transformation along t_1. The two unwanted COSY terms have evolved with the average chemical shift $\frac{\Omega_2+\Omega_1}{2}$ during t_1, which will result in a peak at the average chemical shifts of I and S in $F1$. In the term, whose I spin-state is preserved, the $J-$coupling evolution is not refocused, which will produce a doublet appearance in $F1$. Further both terms contain a constant phase factor depending on the chemical shift difference, the $J-$coupling constant and the time parameter δ_3, which will lead to phase distortions of these COSY responses in $F1$.

Now we discuss the attenuation of such COSY responses using the *spatio-temporal-averaging* concept and when this will fail to attenuate these terms sufficiently. The PSYCHE element is applied as frequency-swept pulses during magnetic field gradients to attenuate such COSY responses. Herein the time points, when the frequency sweep matches the offset frequencies Ω_1

and Ω_2 of the protons are the crucial parameters, which define, whether the term is preserved, sufficiently attenuated or only partly attenuated. If no polarization has been transferred, which is the case for the first term in 5.30, the durations during which the gradients dephase and rephase (indicated as green areas in Figure 5.10a), respectively are equal. This is the case, if we assume an *instantaneous flip* from the transversal plane to the longitudinal axis (case (a) in Figure 5.10). In the second case (b) the time points are not symmetrical and hence the durations are not equal, as indicated in Figure 5.10 (b) with green and red areas.

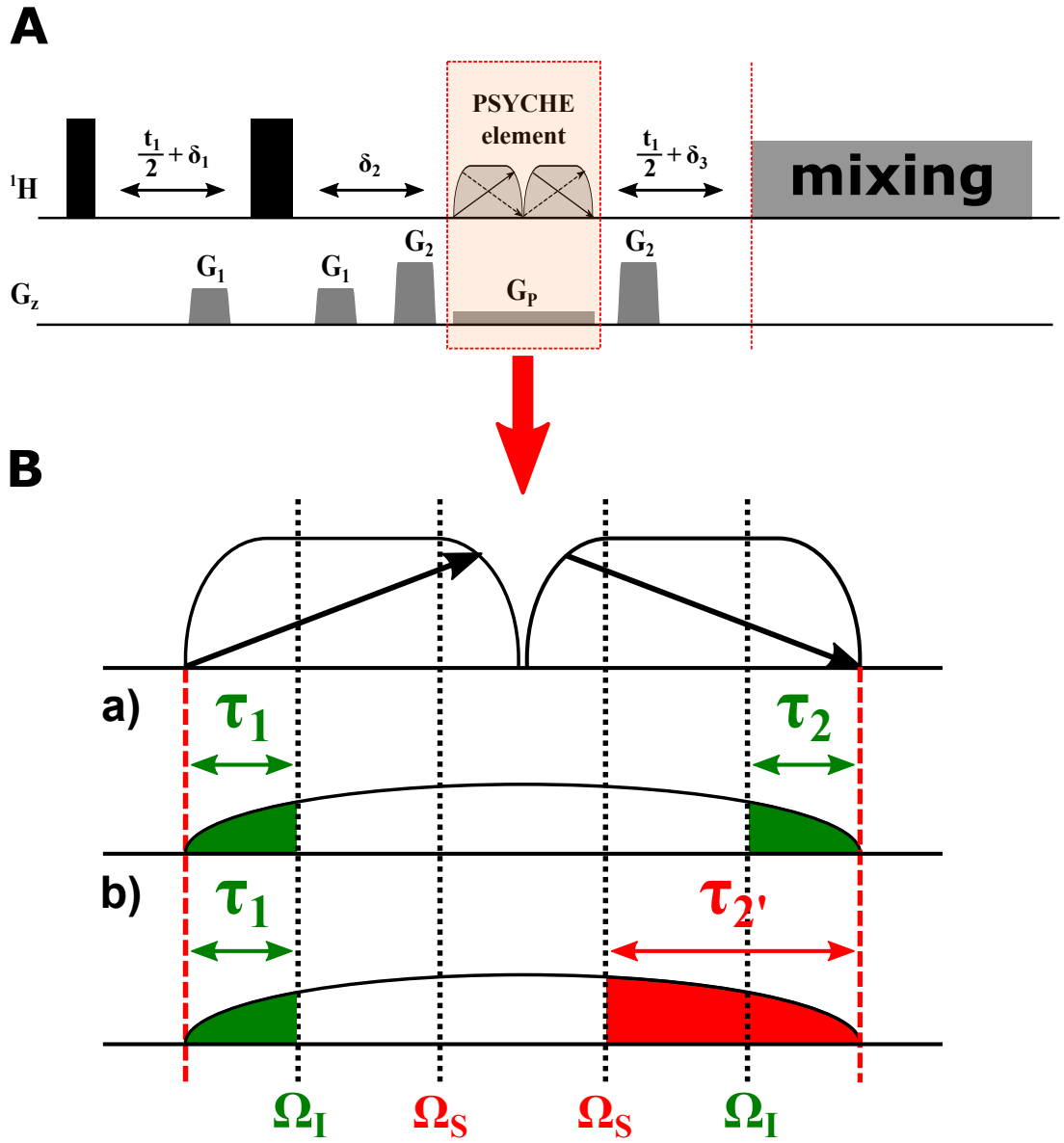

Figure 5.10: Pulse sequence of the 1D-^{1}H-PSYCHE experiments (A) and (B) schematic illustration of the working principle of the PSYCHE element to preserve the wanted term without polarization transfer (a) and attenuate the term with COSY transfer (b).

For further discussions we introduce the spatially dependent phase factor Φ generated by z-gradients:

$$\Phi \;=\; \exp\left(-i\,p\,\gamma\,G\,\tau\,z\right) \tag{5.32}$$

Herein p is the coherence order, which changes between +1, 0 and -1 during the PSYCHE element, γ is the gyromagnetic ratio, G is the applied gradient strength, τ is the applied duration and z is the position in the active volume of the sample. First we look, what happens for the wanted term during both effective gradient durations τ_1 and τ_2 (case (a) in Figure 5.10):

$$\frac{i}{4}\,\beta^2 \exp\left(i\Omega_1 t_1\right)\; I_- S_\beta \exp\left[i\left(-\gamma G\,\tau_1 z\;+\;\gamma G\,\tau_2 z\right)\right] \tag{5.33}$$

Here the durations τ_1 and τ_2 are equal and the gradient phase factors cancel each other and thus vanish. Hence this term is fully rephased. Now let us investigate, what happens to the terms, which underwent polarization transfer:

$$\begin{aligned}
&\frac{i}{8}\,\beta^2 \exp\left(i\frac{\Omega_1+\Omega_2}{2}t_1 + i\Delta\Omega\delta_3\right)\; I_\beta S_- \exp\left[i\gamma G\,z\left(\tau_{2'}\;-\;\tau_1\right)\right] \\
&\frac{i}{8}\,\beta^2 \exp\left(i\left(\frac{\Omega_1+\Omega_2}{2} - 2\pi J\right)t_1 + i\left(\Delta\Omega - 2\pi J\right)\delta_3\right)\; I_\alpha S_- \exp\left[i\gamma G\,z\left(\tau_{2'}\;-\;\tau_1\right)\right]
\end{aligned} \tag{5.34}$$

Here the durations τ_1 and $\tau_{2'}$ are not equal and the gradient phase factors do not cancel completely. Hence this term a gradient phase-factor depending on the difference $\tau_{2'} - \tau_1$. If we express the durations τ in terms of the offset frequencies Ω, the duration of the PSYCHE element τ_P and its frequency sweepwidth ΔF, we get:

$$\begin{aligned}
\tau_1 &= \frac{\Omega_1 \tau_P}{2\Delta F} \\
\tau_{2'} &= \frac{\Omega_2 \tau_P}{2\Delta F} \\
\tau_{2'} - \tau_1 &= \frac{\left(\Omega_2 - \Omega_1\right)\tau_P}{2\Delta F}
\end{aligned} \tag{5.35}$$

To quantify the efficiency of attenuation we further define the attenuation factor A. We get this factor by integrating over all positions z in the active volume of the sample with the length L after insertion of the third expression in equation 5.35:

$$A \;=\; \frac{1}{L}\int\limits_{-\frac{L}{2}}^{\frac{L}{2}} \exp\left[\frac{i\gamma G\,z\left(\Omega_2\;-\;\Omega_1\right)\tau_P}{2\Delta F}\right]\; dz \tag{5.36}$$

Performing the integration and tidying up we finally get for A:

$$\begin{aligned}
A &= \frac{\sin\left(c\Delta\Omega\tau_P\right)}{c\Delta\Omega\tau_P} \\
\text{with}\;\; c &= \frac{\gamma G_P L}{4\Delta F}
\end{aligned} \tag{5.37}$$

From the last expression we see, that the attenuation factor A behaves similarly to the expressions found for the *zero-quantum-coherence suppression* applying the Thrippleton-Keeler filter[41]. Assuming a detection volume with sharp cutoffs, it is described by a *sinc*-function depending on the chemical shift differences $\Delta\Omega$ and the duration of the PSYCHE element τ_P. Hence, the chemical shift differences $\Delta\Omega$ and the duration of the PSYCHE element are the crucial parameters, which define whether we can observe the additional COSY responses in homonuclear 2D-spectra with PSYCHE homonuclear decoupling in the indirct dimension $F1$ or not. In case of small chemical shift differences $\Delta\Omega$, the typically applied duration of 30 ms for the PSYCHE element the unwanted terms partly survive as the attenuation factor A will be not low enough to push the intensity below noise-level. It should be noted, that the equations derived herein only describe the effects within our approximations (e.g. instantaneous hard flip-angle, weak-coupling limit), but they do not describe all effects. During the PSYCHE element there might be spin-locking effects, which transfer weak coupling to strong coupling.

5.10 2D *gradient-selected F*1-PSYCHE-EASY-ROESY: Alternative implementations

As stated in the main text, there are alternative solutions to implement *gradient selection* into the 2D PSYCHE-EASY-ROESY experiment. In this section we discuss two alternative 2D *gradient-selected* $F1$-PSYCHE-EASY-ROESY pulse sequences and their potential drawbacks compared to the implementation presented in the main manuscript.

5.10.1 Implementation with gradient-encoding before t_1-evolution

One might also imagine to place the gradient encoding step before the t_1-evolution. This implementation is derived from the semi-selective gradient selected ROESY experiment proposed by Dalvit *et al.* [42], in which the selective refocusing pulse would be replaced by a hard 180° pulse and the $z-$filter moved to the end of the pulse sequence. Indeed, such an implementation has some unfavorable properties in the combined pure shift and gradient selection approach introduced here. First the intensity attenuation by molecular diffusion would be enhanced, since the diffusion time is lengthened by the t_1-evolution and the duration of the pure shift element. In homonuclear 2D experiments with the pure shift implementation in the indirect dimension $F1$ the benefit from the resolution gain by homonuclear decoupling itself is only obtained for quite high spectral resolution in the indirect dimension. Thus longer maximum t_1-evolution periods in the order of 100 ms are necessary to achieve such a high spectral resolution after Fourier transformation. Secondly as the t_1-evolution time is incremented the diffusion attenuation is incremented as well, which leads to an extra line broadening in the indirect dimension after Fourier transformation. Further we found experimentally, that the performance towards the suppression of t_1-noise was less efficient.

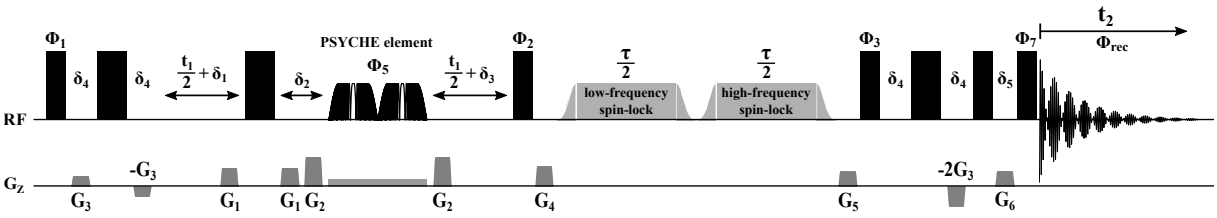

Figure 5.11: Pulse sequence scheme for the 2D *gradient-selected* $F1$-PSYCHE-EASY-ROESY experiment with gradient encoding before t_1-evolution. Narrow and wide rectangles represent hard 90° and 180° pulses, respectively. The double trapezoid corresponds to low-power chirp pulses of small flip angle, which sweep frequency in opposite directions simultaneously (PSYCHE element). Broad rectangles in grey are low- and high-frequency spinlocks of $\tau_m/2$ duration, half-Gaussian shaped pulses were used as adiabatic ramps. The gradients G_1 and G_2 are used for coherence selection, the gradients G_3 are for phase en- and decoding, G_4 to G_6 are purge gradients. The delays δ_1 through δ_5 are $\delta_1 = p_{17} + d_{16}$, $\delta_2 = 2p_{17} + 3d_{16}$, $\delta_3 = p_{17} + 2d_{16}$, $\delta_4 = p_{18} + d_{16}$ and $\delta_5 = p_{19} + d_{16}$, where p_{16} to p_{19} are the lengths of the gradients and d_{16} is a recovery delay. Scalar coupling refocusing is achieved before the ROESY mixing step, while chemical shifts have evolved for t_1. Phase cycling: All pulse phases are x unless denoted otherwise, $\Phi_1 = x\ -x$, $\Phi_2 = 8(x)\ 8(-x)$, $\Phi_3 = 4(x)\ 4(-x)$, $\Phi_5 = x\ x\ y\ y\ -x\ -x\ -y\ -y$, $\Phi_7 = 2(-x\ -x\ x\ x)$ and $\Phi_{rec} = -x\ x\ -x\ x\ x\ -x\ x\ -x\ x\ -x\ x\ -x\ -x\ x\ -x\ x$.

5.10.2 Implementation without Thrippleton-Keeler-filter

In principle the pulse sequence for the 2D *gradient-selected* $F1$-PSYCHE-EASY-ROESY experiment presented in the main text needs no Thrippleton-Keeler-element[41] in the final $z-$filter. A $z-$filter with a strong purge-gradient should be sufficient for suitable spectra. However, we found unfavorable line shapes with this implementation (Figure 5.13), which results from scalar J-coupling evolution during the gradient decoding step. These anti-phase coherences are transfered to zero- and double-quantum coherences in the $z-$filter. The double-quantum coherences are dephased by the purge gradient. This is not the case for the zero-quantum coherences, which are subsequently transferred back to anti-phase coherences. During detection these coherences lead to dispersive mode line-shapes after Fourier transformation.

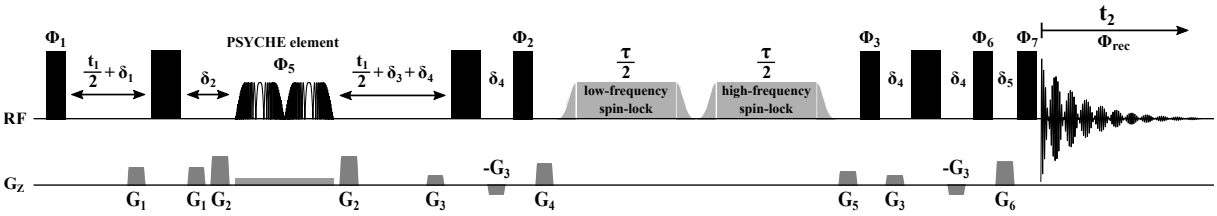

Figure 5.12: Pulse sequence scheme for the 2D *gradient-selected* $F1$-PSYCHE-EASY-ROESY experiment without Thrippleton-Keeler-filter. Narrow and wide rectangles represent hard 90° and 180° pulses, respectively. The double trapezoid corresponds to low-power chirp pulses of small flip angle, which sweep frequency in opposite directions simultaneously (PSYCHE element). Broad rectangles in grey are low- and high-frequency spinlocks of $\tau_m/2$ duration, half-Gaussian shaped pulses were used as adiabatic ramps. The gradients G_1 and G_2 are used for coherence selection, the gradients G_3 are for phase en- and decoding, G_4 to G_6 are purge gradients. The delays δ_1 through δ_5 are $\delta_1 = p_{17} + d_{16}$, $\delta_2 = 2p_{17} + 3d_{16}$, $\delta_3 = p_{17} + 2d_{16}$, $\delta_4 = p_{18} + d_{16}$ and $\delta_5 = p_{19} + d_{16}$, where p_{16} to p_{19} are the lengths of the gradients and d_{16} is a recovery delay. Scalar coupling refocusing is achieved before the ROESY mixing step, while chemical shifts have evolved for t_1. Phase cycling: All pulse phases are x unless denoted otherwise, $\Phi_1 = x\ -x$, $\Phi_2 = 8(x)\ 8(-x)$, $\Phi_3 = 4(x)\ 4(-x)$, $\Phi_5 = x\ x\ y\ y\ -x\ -x\ -y\ -y$, $\Phi_7 = 2(-x\ -x\ x\ x)$ and $\Phi_{rec} = -x\ x\ -x\ x\ x\ -x\ x\ -x\ x\ -x\ x\ -x\ -x\ x\ -x\ x$.

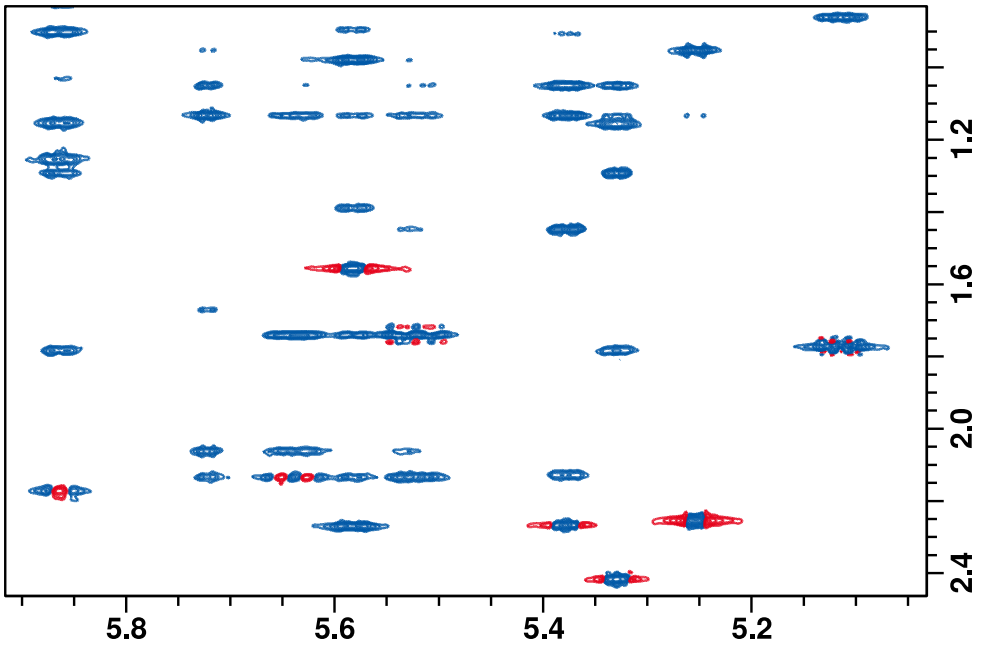

Figure 5.13: Part of a 2D *gradient-selected* $F1$-PSYCHE-EASY-ROESY spectrum acquired with the pulse sequence shown in Figure 5.12 of cyclosporine A in C_6D_6. Without the Thrippleton-Keeler element in the final z-filter zero-quantum coherences could not be dephased leading to line-shape distortions.

5.11 2D *gradient-selected* $F1$-PSYCHE-NOESY

All discussions provided in the main text concerning resolution enhancement in EASY-ROESY spectra by applying *pure shift* and cleaning up these spectra with gradient selection should apply for the NOESY experiment as well. Although the tetrapeptide - *R,R*-diol sample as well as the cyclosporine A sample show longitudinal cross-relaxation near the zero-crossing, leading to a reduced number of observable NOE cross-peaks, we developed an analoguous 2D *gradient-selected* $F1$-PSYCHE-NOESY experiment. The pulse sequence is quite similar to the 2D *gradient-selected* $F1$-PSYCHE-EASY-ROESY, whereby the spin-lock element for ROESY mixing was dropped. Although the *pure shift* element refocuses the evolution of scalar $J-$coupling and hence no *zero-quantum*-coherences should be generated, the pulse sequence is implemeted with a Thrippleton-Keeler filter element during the mixing-time. We have tested the pulse sequence with a strychnine sample in $CDCl_3$. The spectrum (see figure 5.15) was acquired with an insufficient amount of t_1-increments to benefit from the resolution gain caused by homonuclear decoupling.

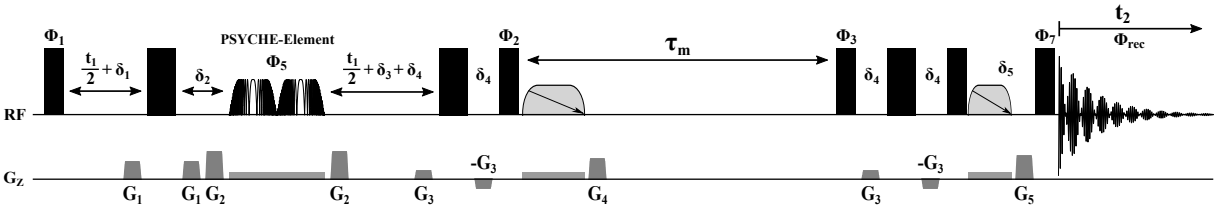

Figure 5.14: Pulse sequence scheme for the 2D *gradient-selected* $F1$-PSYCHE-NOESY experiment. Narrow and wide rectangles represent hard 90° and 180° pulses, respectively. The double trapezoid corresponds to low-power chirp pulses of small flip angle, which sweep frequency in opposite directions simultaneously (PSYCHE element). The Thrippleton-Keeler element during mixing time τ_m is indicated by a single trapezoid with diagonal arrow. The gradients G_1 and G_2 are used for coherence selection, the gradients G_3 are for phase en- and decoding, G_4 and G_5 are purge gradients. The delays δ_1 through δ_5 are $\delta_1 = p_{17} + d_{16}$, $\delta_2 = 2p_{17} + 3d_{16}$, $\delta_3 = p_{17} + 2d_{16}$, $\delta_4 = p_{18} + d_{16}$ and $\delta_5 = p_{42} + p_{19} + 2d_{16}$, where p_{16} to p_{19} are the lengths of the gradients, p_{42} the duration of the Thrippleton-Keeler element and d_{16} is a recovery delay. Scalar coupling refocusing is achieved before the NOESY mixing step, while chemical shifts have evolved for t_1. Phase cycling: All pulse phases are x unless denoted otherwise, $\Phi_1 = x\ -x$, $\Phi_2 = 8(x)\ 8(-x)$, $\Phi_3 = 4(x)\ 4(-x)$, $\Phi_5 = x\ x\ y\ y\ -x\ -x\ -y\ -y$, $\Phi_7 = 2(-x\ -x\ x\ x)$ and $\Phi_{rec} = -x\ x\ -x\ x\ x\ -x\ x\ -x\ x\ -x\ x\ -x\ -x\ x\ -x\ x$.

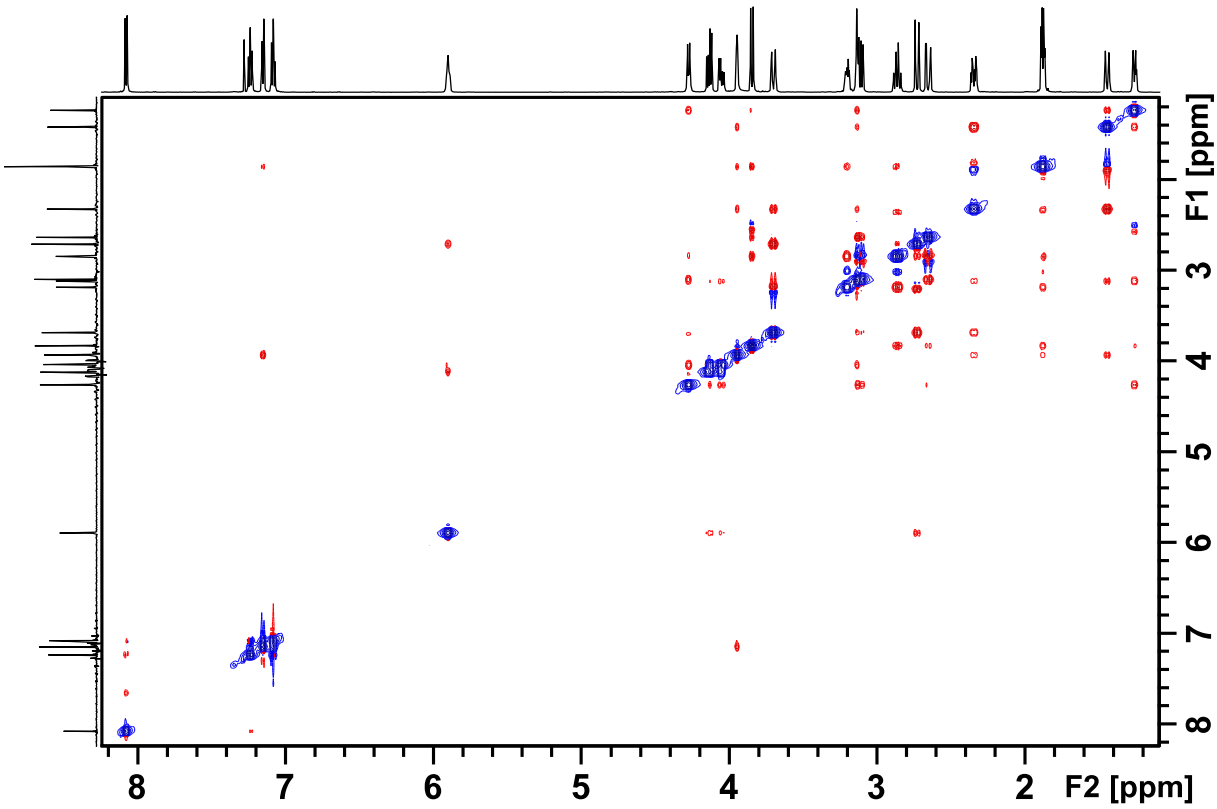

Figure 5.15: 2D *gradient-selected* $F1$-PSYCHE-NOESY spectrum acquired with a strychnine sample in $CDCl_3$. The spectrum was acquired with 7.1 ppm spectral width for both dimensions, 256 t_1-increments and a mixing-time of 500 ms.

6 Spectra

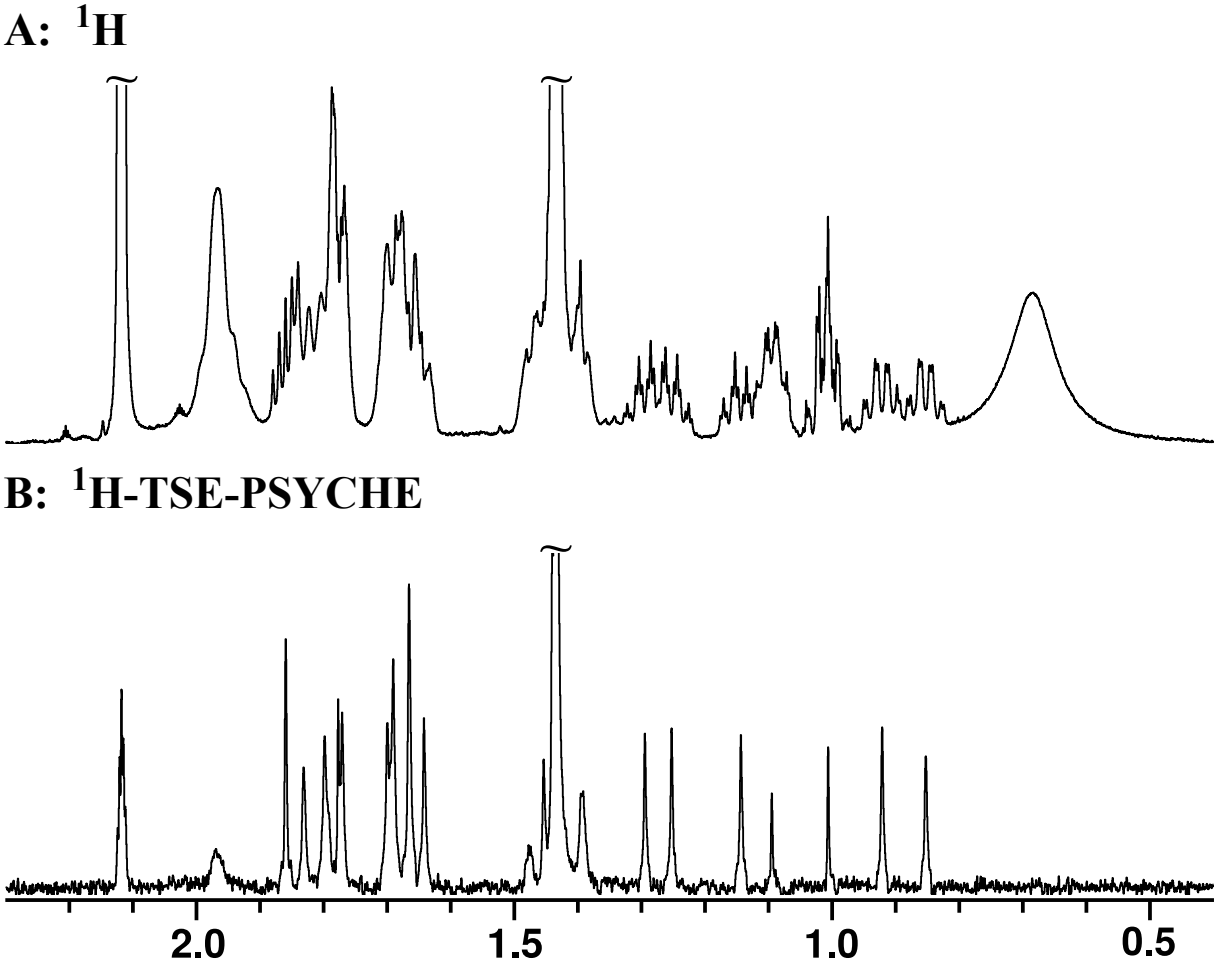

Figure 6.1: Aliphatic region of the tetrapeptide - *R,R*-cycohexane-1,2-diol sample acquired with conventional (A) 1D ^{1}H and (B) 1D ^{1}H-TSE-PSYCHE[43]. Both spectra were acquired at 700.17 MHz.

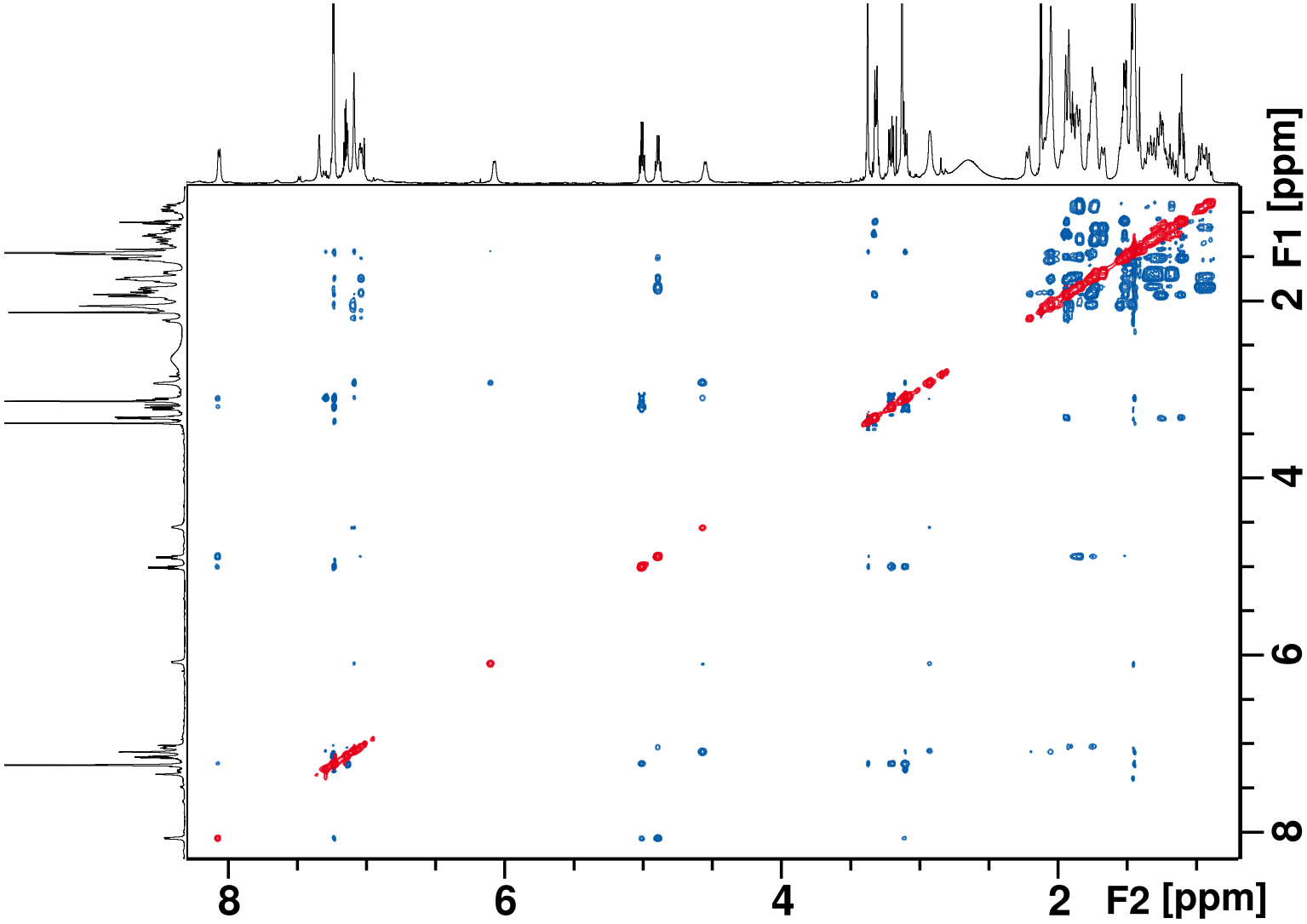

Figure 6.2: Full 2D-EASY-ROESY spectrum of the tetrapeptide - *R,R*-cyclohexane-1,2-diol sample acquired without homonuclear decoupling (*roesyadjsphpr* from the bruker pulse sequence library). The spectrum was acquired at 700.17 MHz with a mixing-time of 300 ms.

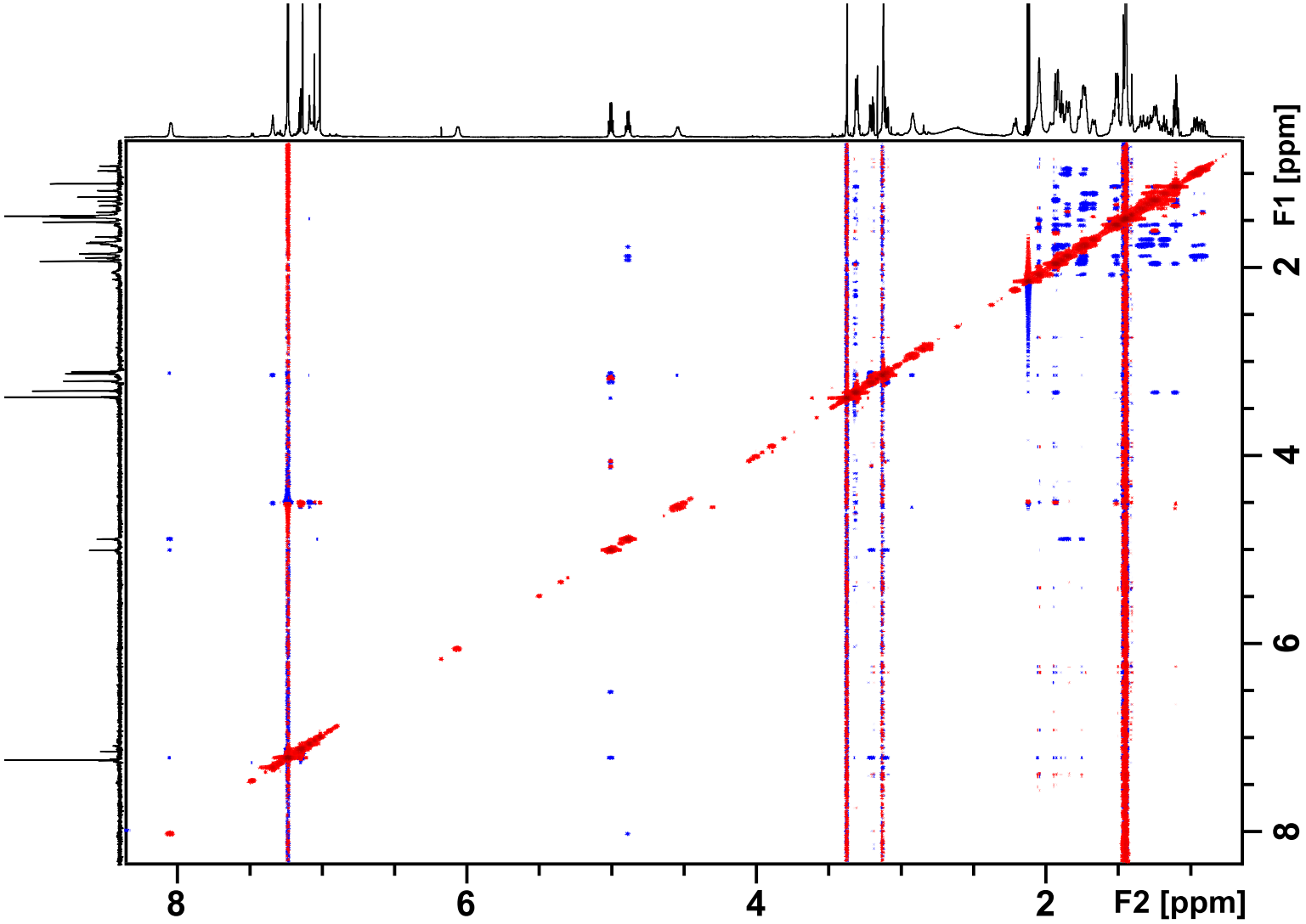

Figure 6.3: Full 2D $F1$-PSYCHE-EASY-ROESY spectrum of the tetrapeptide - R,R-cyclohexane-1,2-diol sample. The spectrum was acquired at 700.17 MHz with a mixing-time of 300 ms.

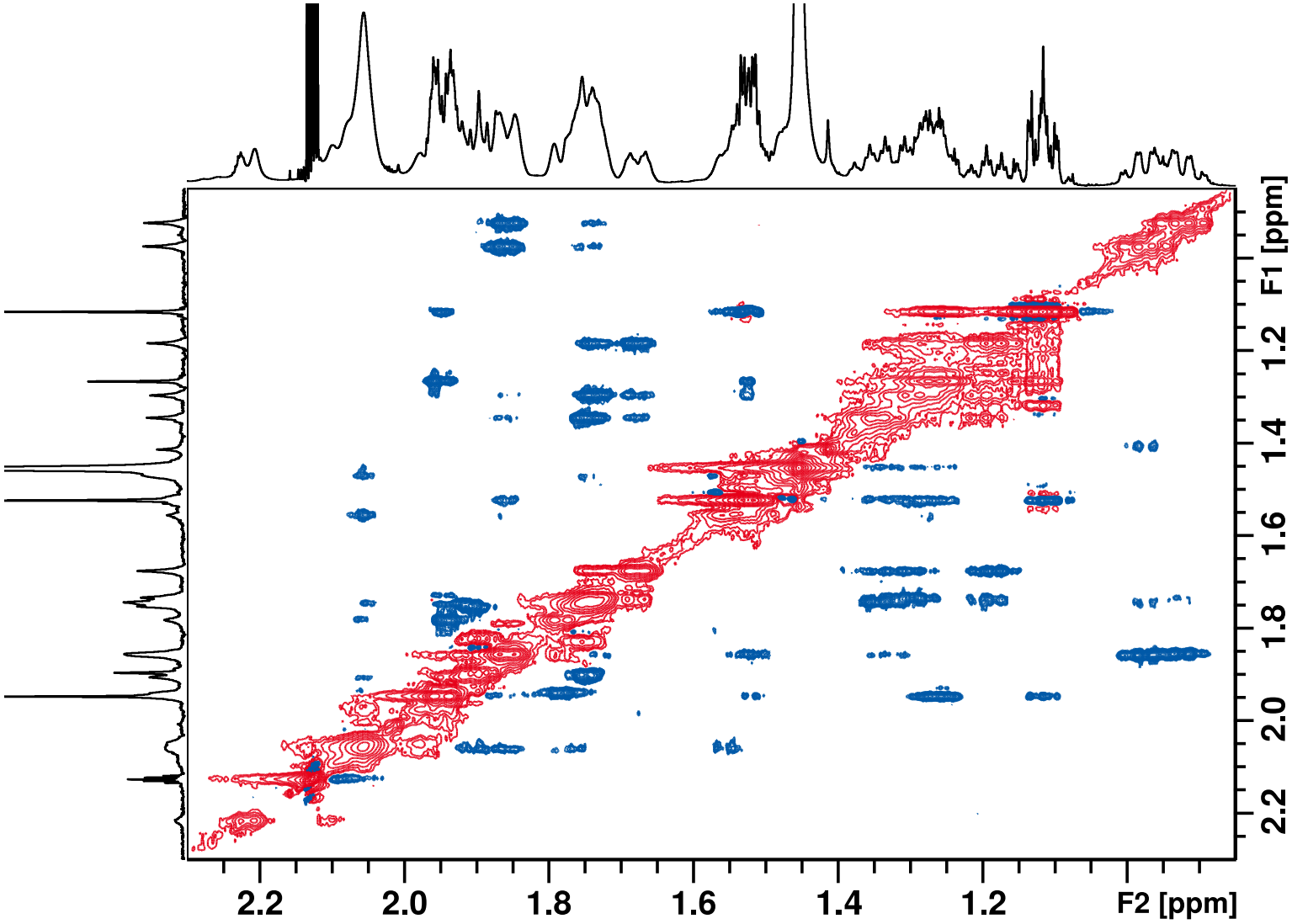

Figure 6.4: Aliphatic region of the tetrapeptide - *R,R*-cyclohexane-1,2-diol sample acquired at 700.17 MHz with the 2D *gradient-selected F*1-PSYCHE-EASY-ROESY. The spectrum was acquired with a mixing-time of 300 ms.

7 References

[1] E. Procházková, A. Kolmer, J. Ilgen, M. Schwab, L. Kaltschnee, M. Fredersdorf, V. Schmidts, R. C. Wende, P. R. Schreiner, C. M. Thiele, *Angewandte Chemie* **2016**, *128*, 15986–15991, DOI 10.1002/ange.201608559.

[2] E. Kupče, J. Boyd, I. D. Campbell, *Journal of Magnetic Resonance Series B* **1995**, *106*, 300–3, DOI http://dx.doi.org/10.1006/jmrb.1995.1049.

[3] J. Jeener, B. H. Meier, P. Bachmann, R. R. Ernst, *The Journal of Chemical Physics* **1979**, *71*, 4546–4553, DOI 10.1063/1.438208.

[4] K. Stott, J. Keeler, Q. N. Van, A. J. Shaka, *Journal of Magnetic Resonance* **1997**, *125*, 302–324, DOI DOI10.1006/jmre.1997.1110.

[5] D. Marion, M. Ikura, R. Tschudin, A. Bax, *Journal of Magnetic Resonance (1969)* **1989**, *85*, 393–399.

[6] M. Foroozandeh, R. W. Adams, N. J. Meharry, D. Jeannerat, M. Nilsson, G. A. Morris, *Angewandte Chemie International Edition in English* **2014**, *53*, 6990–6992, DOI 10.1002/anie.201404111.

[7] C. M. Thiele, K. Petzold, J. Schleucher, *Chemistry – A European Journal* **2009**, *15*, 585–8, DOI 10.1002/chem.200802027.

[8] D. G. Davis, *Journal of the American Chemical Society* **1987**, *109*, 3471–3472, DOI 10.1021/ja00245a054.

[9] C. Griesinger, R. R. Ernst, *Journal of Magnetic Resonance (1969)* **1987**, *75*, 261–271.

[10] S. Macura, R. R. Ernst, *Molecular Physics* **1980**, *41*, 95–117, DOI 10.1080/00268978000102601.

[11] A. A. Bothner-By, R. L. Stephens, J. Lee, C. D. Warren, R. W. Jeanloz, *Journal of the American Chemical Society* **1984**, *106*, 811–813, DOI 10.1021/ja00315a069.

[12] D. Sinnaeve, *Concepts in Magnetic Resonance Part A* **2012**, *40A*, 39–65, DOI 10.1002/cmr.a.21223.

[13] K. F. Sheberstov, E. Sistaré Guardiola, M. Pupier, D. Jeannerat, *Magnetic Resonance in Chemistry* **2020**, *58*, DOI 10.1002/mrc.4882.

[14] H. Hu, K. Krishnamurthy, *Journal of Magnetic Resonance* **2006**, *182*, 173–7, DOI 10.1016/j.jmr.2006.06.009.

[15] S. Macura, B. T. Farmer, L. R. Brown, *Journal of Magnetic Resonance (1969)* **1986**, *70*, 493–499, DOI 10.1016/0022-2364(86)90143-5.

[16] H. Kessler, H.-R. Loosli, H. Oschkinat, *Helvetica Chimica Acta* **1985**, *68*, 661–681, DOI 10.1002/hlca.19850680318.

[17] M. Foroozandeh, R. W. Adams, M. Nilsson, G. A. Morris, *Journal of the American Chemical Society* **2014**, *136*, 11867–11869, DOI 10.1021/ja507201t.

[18] H. Kessler, H.-R. Loosli, H. Oschkinat, *Helvetica Chimica Acta* **1985**, *68*, 661–681, DOI 10.1002/hlca.19850680318.

[19] H.-R. Loosli, H. Kessler, H. Oschkinat, H.-P. Weber, J. Petcher Trevor, A. Widmer, *Helvetica Chimica Acta* **1985**, *68*, 682–704, DOI 10.1002/hlca.19850680319.

[20] J. Lautz, H. Kessler, R. Kaptein, W. F. van Gunsteren, *Journal of Computer-Aided Molecular Design* **1987**, *1*, 219–241, DOI 10.1007/BF01677046.

[21] J. Lautz, H. Kessler, W. F. van Gunsteren, H. P. Weber, R. M. Wenger, *Biopolymers* **1990**, *29*, 1669–1687, DOI 10.1002/bip.360291214.

[22] H. Kessler, M. Köck, T. Wein, M. Gehrke, *Helvetica Chimica Acta* **1990**, *73*, 1818–1832, DOI 10.1002/hlca.19900730703.

[23] M. Koeck, H. Kessler, D. Seebach, A. Thaler, *Journal of the American Chemical Society* **1992**, *114*, 2676–2686, DOI 10.1021/ja00033a048.

[24] S. Y. Ko, C. Dalvit, *International Journal of Peptide and Protein Research* **1992**, *40*, 380–382, DOI 10.1111/j.1399-3011.1992.tb00314.x.

[25] P. Verheyden, H. Jaspers, E. D. Wolf, G. V. Binst, *International Journal of Peptide and Protein Research* **1994**, *44*, 364–371, DOI 10.1111/j.1399-3011.1994.tb01021.x.

[26] M. F. O'Donohue, A. W. Burgess, H. R. Treutlein, M. D. Walkinshaw, *Protein Science* **1995**, *4*, 2191–2202, DOI 10.1002/pro.5560041025.

[27] J. Klages, C. Neubauer, M. Coles, H. Kessler, B. Luy, *ChemBioChem* **2005**, *6*, 1672–1678, DOI 10.1002/cbic.200500146.

[28] S. V. Efimov, F. K. Karataeva, A. V. Aganov, S. Berger, V. V. Klochkov, *Journal of Molecular Structure* **2013**, *1036*, 298–304, DOI https://doi.org/10.1016/j.molstruc.2012.11.005.

[29] S. Efimov, Y. Zgadzay, V. Klochkov, *Applied Magnetic Resonance* **2014**, *45*, 1225–1235, DOI 10.1007/s00723-014-0602-y.

[30] J. Witek, B. G. Keller, M. Blatter, A. Meissner, T. Wagner, S. Riniker, *Journal of Chemical Information and Modeling* **2016**, *56*, 1547–1562, DOI 10.1021/acs.jcim.6b00251.

[31] J. Tropp, *The Journal of Chemical Physics* **1980**, *72*, 6035–6043, DOI 10.1063/1.439059.

[32] J. Ilgen, L. Kaltschnee, C. M. Thiele, *Magnetic Resonance in Chemistry* **2018**, *56*, 918–933, DOI 10.1002/mrc.4757.

[33] T. A. Halgren, *Journal of Computational Chemistry* **1996**, *17*, 616–641, DOI 10.1002/(SICI)1096-987X(199604)17:5/6<616::AID-JCC5>3.0.CO;2-X.

[34] J. Furrer, *Journal of Natural Products* **2009**, *72*, PMID: 19639988, 1437–1441, DOI 10.1021/np9003432.

[35] S. Boros, G. Batta, *Magnetic Resonance in Chemistry* **2016**, *54*, 947–952, DOI 10.1002/mrc.4474.

[36] J. Schleucher, J. Quant, S. J. Glaser, C. Griesinger, *Journal of Magnetic Resonance Series A* **1995**, *112*, 144–151, DOI DOI10.1006/jmra.1995.1025.

[37] K. Zangger, H. Sterk, *Journal of Magnetic Resonance* **1997**, *124*, 486–489, DOI DOI10.1006/jmre.1996.1063.

[38] L. Kaltschnee, K. Knoll, V. Schmidts, R. W. Adams, M. Nilsson, G. A. Morris, C. M. Thiele, *Journal of Magnetic Resonance* **2016**, *271*, 99–109, DOI 10.1016/j.jmr.2016.08.007.

[39] N. H. Meyer, K. Zangger, *Angewandte Chemie International Edition in English* **2013**, *52*, 7143–6, DOI 10.1002/anie.201300129.

[40] D. Sinnaeve, J. Ilgen, M. E. Di Pietro, J. J. Primozic, V. Schmidts, C. M. Thiele, B. Luy, *Angewandte Chemie International Edition* **2020**, *59*, 5316–5320, DOI 10.1002/anie.201915278.

[41] M. J. Thrippleton, J. Keeler, *Angewandte Chemie International Edition in English* **2003**, *42*, 3938–41, DOI 10.1002/anie.200351947.

[42] C. Dalvit, *Magnetic Resonance in Chemistry* **1995**, *33*, 570–576, DOI 10.1002/mrc.1260330713.

[43] M. Foroozandeh, R. W. Adams, P. Király, M. Nilsson, G. A. Morris, *Chemical Communications (Cambridge United Kingdom)* **2015**, *51*, 15410–3, DOI 10.1039/c5cc06293d.

9. Bruker pulse sequence codes

9.1 2D F1-PSYCHE-EASY-ROESY

```
; 2D EASY ROESY WITH F1-PSYCHE-HOMODECOUPLING
; based on F1-PSYCHE-EASY-ROESY taken from Eliska Procházková et al, Angew. Chem. Int. Ed. 2016, 55, 15754.
; This pulse sequence is part of the paper:
; Gradient Selected Pure-Shift EASY-ROESY techniques facilitate the quantitative measurement of 1H,1H-distance restraints in
; congested spectral regions
; Authors: Julian Ilgen, Jens Nowag, Lukas Kaltschnee, Volker Schmidts, Christina M. Thiele

; Julian Ilgen
; Technical University Darmstadt
; Avance III Version
; Topspin 3.2.6 or Topspin 3.5.7

; Description and Comments:
; The pulse sequence has been coded for test purposes only and may contain errors.
; It does contain arguments that can lead to hardware damages if acquisition parameters
; are set unfavorably. The functionality of the pulse sequence itself may differ
; depending on the hardware as well as the software used to execute it. Functionality
; on differing systems cannot be granted.
; Any use of this pulse sequence on a spectrometer is at your own risk!
; By using this pulse sequence or any modification of it in any published material
; you agree to acknowledge the above-mentioned publication.

; Jump-symmetrized spinlocks with adiabatic ramps for mixing
; Phase sensitive using States-TPPI or TPPI
; option for presaturation during relaxation delay, presaturation offset defined with cnst41 [ppm]
; Homonuclear broadband decoupling in indirect dimension F1 using PSYCHE
; J is refocused at the end of t1 evolution time
; Internal power and offset calibration of spinlock with 6500 Hz maximum RF-field strength
; Internal power and RF-amplitude calibration of PSYCHE element

; Further publications relevant to this pulse sequence:
; 1. M. Foroozandeh, R.W. Adams, N.J. Meharry, D. Jeannerat, M. Nilsson, G.A. Morris: Angew. Chem. Int. Ed. 2014, 53, 6990.
; 2. M. Foroozandeh, M. Nilsson, G. A. Morris: J. Am. Chem. Soc. 2014, 136, 11867.
; 3. M. Foroozandeh, R. W. Adams, P. Király, M. Nilsson, G. A. Morris, Chem. Commun. 2015, 51,15410–15413.
; 4. C.M. Thiele, K. Petzold, J. Schleucher: Chem. Eur. J. 2009, 15, 585–588.
; 5. J. Schleucher, J. Quant, S. Glaser, C. Griesinger: J. Magn. Reson A 1995, 112, 144–151.

;$CLASS=HighRes
;$DIM=2D
;$TYPE=
;$SUBTYPE=
;$COMMENT=

#include <Avance.incl>
#include <Grad.incl>
;;General statements;;
"d11=30m"
"d12=20u"
"p2=2*p1"
"d0=0u"
"in0=inf1/2"

;;Statements EASY-ROESY Spin-Lock;;
define pulse P_SL
"cnst24=1000000.0*tan((cnst28*2*PI)/360.0)/(dw*4)"
"if ( cnst24 > 6500 ) {cnst25 = 6400.0;} else {cnst25 = cnst24;}"
"if ( cnst24 > 6500 ) {cnst29 = atan(cnst25*4*dw/1000000.0)*360.0/(2*PI);} else {cnst29=cnst28;}"
"if (cnst26<cnst25) {cnst27=cnst25;} else {if (cnst26>6500) {cnst27=6400;} else {cnst27=cnst26;} }"
"cnst30=abs(cnst27/tan((cnst29*2*PI)/360.0))"
define list<frequency> roesylist={sfo hz, 0.0, -cnst30, cnst30, 0}
"p30=1000000.0/(cnst27*4)"
"cnst31= (p30/p1) * (p30/p1)"
"spw10=plw1/cnst31"
"spw12=plw1/cnst31"
"spw13=plw1/cnst31"
"spw16=plw1/cnst31"
"spw17=plw1/cnst31"
"cnst23=cnst30+cnst31+p30"
"p41=1m"
"P_SL=p15/2"
"spoff10=0"
"spoff12=0"
"spoff13=0"
"spoff16=0"
"spoff17=0"

;;Statements PSYCHE-decoupling;;
"cnst50=(cnst20/360)*sqrt((2*cnst21)/(p40/2000000))"       ; RF-amplitude PSYCHE element
"p35=1000000.0/(cnst50*4)"                                 ; equivalent 90 degree pulse
"cnst40= (p35/p1) * (p35/p1)"                              ; scaling factor for power level attenuation
"spw40=plw1/cnst40"                                        ; power level PSYCHE element
"p10=p40"                                                  ; duration of gradient during PSYCHE element

;;Statements solvent presaturation;;
#ifdef CWPR
"d18=d1-d19"
"cnst42=cnst41*bf1"                    ; changed to use ppm values for solvent offset, ji20170612
"cnst43=cnst42-o1"
#else

#endif /*CWPR*/

;;start pulsesequence;;
1 ze
2 d11
3 d12  roesylist:f1
  4u roesylist.inc
```

```
#ifdef CWPR                             ; begin of solvent presaturation
  d12 fq=0:f1
  d12 fq=cnst43:f1                      ; set frequency on f1-channel to solvent shift for presaturation [fq=SFO1+cnst42]
  d12
  d18 pl9:f1                            ; residual relaxation delay + set power level on f1-channel for presaturation
  d19 cw:f1 ph29                        ; solvent presaturation
  4u do:f1
  d12 fq=0:f1                           ; reset frequency on f1-channel [fq=SFO1]
  d12 pl1:f1                            ; reset power level on f1-channel
#else                                   ; no solvent presaturation
 d1
 d12 pl1:f1
#endif /*CWPR*/

  50u UNBLKGRAD
  p1 ph1                        ; 90 high power pulse for excitation
  d0                            ; incremented delay F1-dimension
  p17:gp1                       ; CTP gradient 1
  d16
  p2 ph4                        ; 180 high power pulse
  10u
  10u pl0:f1
  p17:gp1                       ; CTP gradient 1
  d16
  p17:gp2                       ; CTP gradient 2
  d16
  d16
  (center (p10:gp10) (p40:sp40 ph5):f1 )         ; PSYCHE element
  d16
  10u
  10u pl1:f1
  p17:gp2                       ; CTP gradient 2
  d16
  d0                            ; incremented delay F1-dimension
4 (p1 ph2):f1                   ; 90 high power pulse, start of ROESY mixing time
  4u
  p16:gp5                       ; 1st purge gradient
  d16 roesylist:f1
  4u roesylist.inc
#   ifdef AV2
  (p41:sp12 ph4):f1                     ; adiabatic ramp up (low frequency, negative offset)
  3u
  (P_SL:sp10 ph4):f1                            ; low frequency spinlock
  3u
  (p41:sp13 ph4):f1                     ; adiabatic ramp down (low frequency, negative offset)
#   else
  (p41:sp12 ph4):f1
  (P_SL:sp10 ph4):f1
  (p41:sp13 ph4):f1
#   endif /*AV2*/
  4u
  4u roesylist:f1
  4u roesylist.inc
#   ifdef AV2
  (p41:sp16 ph4):f1                     ; adiabatic ramp up (high frequency, positive offset)
  3u
  (P_SL:sp10 ph4):f1                            ; high frequency spinlock
  3u
  (p41:sp17 ph4):f1                     ; adiabatic ramp down (high frequency, positive offset)
#   else
  (p41:sp16 ph4):f1
  (P_SL:sp10 ph4):f1
  (p41:sp17 ph4):f1
#   endif /*AV2*/
  4u
  p16:gp6                       ; 2nd purge gradient
  d16 roesylist:f1
  4u roesylist.inc
  4u pl1:f1
  4u BLKGRAD
  (p1 ph3)                              ; 90 high power pulse, end of ROESY mixing time
  go=2 ph31
  d11 mc #0 to 2 F1PH(calph(ph1, +90), caldel(d0, +in0))
exit

; phase cycling
ph1= 0 2                                ; Hard 90 Excitation
ph2= 0 0 0 0 0 0 0 0 2 2 2 2 2 2 2 2    ; Hard 90 before mixing
ph3= 0 0 0 0 2 2 2 2                    ; Hard 90 after mixing
ph4= 0                                  ; Hard 180 and spin-lock
ph5= 0 0 1 1 2 2 3 3                    ; PSYCHE element
ph29=0                                  ; CW-presaturation
ph31=0 2 2 0 2 0 0 2 2 0 0 2 0 2 2 0    ; receiver

;p1 : f1 channel -  90 degree high power pulse
;p2 : high power 180 pulse width
;p10: duration of PSYCHE gradient
;p15: f1 channel - pulse for ROESY spinlock
;p16: homospoil/gradient pulse during ROESY mixing time             [1m]
;p17: homospoil/gradient pulse during F1-dimension                  [1m]
;p30: f1 channel -  90 degree pulse at sp10
;p35: f1 channel -  90 degree pulse at sp40
;p40: duration of PSYCHE element                [30m]
;p41: f1 channel - shaped pulse for adiabatic ramp     [1m]

;pl1 : f1 channel - power level for pulse (default)
;pl9 : f1 channel - power level for presaturation

;P_SL: f1 channel - pulse width for low and high frequency spinlock
;sp10: f1 channel - shaped pulse for ROESY-spinlock (= pl1 + cnst31)
;spnam10: Squa100.1000
;sp12: f1 channel - shaped pulse for adiabatic ramp down (low frequency, negative offset) (= pl1 + cnst31)
;spnam12: Gaussramp+down.1
;sp13: f1 channel - shaped pulse for adiabatic ramp up (low frequency, negative offset) (= pl1 + cnst31)
```

```
;spnam13: Gaussramp+up.1
;sp16: f1 channel - shaped pulse for adiabatic ramp down (high frequency, positive offset) (= pl1 + cnst31)
;spnam16: Gaussramp-down.1
;sp17: f1 channel - shaped pulse for adiabatic ramp up (high frequency, positive offset) (= pl1 + cnst31)
;spnam17: Gaussramp-up.1
;sp40: f1-channel - PSYCHE element
;spw40 : RF power of PSYCHE element
;spnam40: file name for PSYCHE element [Crp_psyche.20]

;gpz1: 1st CTP gradient: 77%
;gpz2: 2nd CTP gradient: 49%
;gpz5: 1st purge gradient: 31%
;gpz6: 2nd purge gradient: 11%
;gpz10: PSYCHE gradient: 1-3%
;gpnam1: SMSQ10.100
;gpnam2: SMSQ10.100
;gpnam3: SMSQ10.100
;gpnam4: SMSQ10.100
;gpnam10: RECT.1

;d0 : incremented delay (2D)
;d1 : relaxation delay; 1-5 * T1
;d11: delay for disk I/O                             [30 msec]
;d12: delay for power switching                      [20 usec]
;d16: delay for homospoil/gradient recovery
;d18: reduced relaxation delay
;d19: delay for solvent presaturation

;cnst20: PSYCHE flip-angle (degree) [10-25]
;cnst21: Sweepwidth of each chirp in PSYCHE element (Hz) [10000]
;cnst23; (for display purpose only)
;cnst24: min. RF field strength to make sure that the carrier is shifted
;           to the edge of the spectrum
;cnst25: reduced min. RF field strength in case an upper limit of 6.5kHz is exceeded
;           (set to 6.4kHz), this leads to a recalculation of the tilt angle (cnst29)
;cnst26: requested RF field strength (gammaB1) for ROESY spinlock [Hz]
;           reduced to 6.4kHz if an upper limit of 6.5kHz is exceeded
;cnst27: used RF field strength (gammaB1) for ROESY spinlock
;cnst28: requested tilt angle for ROESY spinlock (between axis of spinlock and z-axis) [45 degree]
;cnst29: used tilt angle for ROESY spinlock (between axis of spinlock and z-axis)
;cnst30: low and high frequency offset,
;          calculated from gammaB1 (cnst27) for tilt angle (cnst29)
;cnst31: difference in power level (dB) for spinlock relative to pl1
;cnst41: solvent offset [ppm]
;cnst50: RF amplitude for PSYCHE element

;inf1: 1/SW = 2 * DW
;in0: 1/(1 * SW) = 2 * DW
;nd0: 1
;NS : number of scans                  [8*n]
;DS : number of dummy scans            [16]
;td1 : number of t1 increments
;FnMODE: States-TPPI, TPPI, States or QSEQ

;Processing
;PHC0(F1): 90
;PHC1(F1): -180
;FCOR(F1): 1

;preprocessor-flags-start
;CWPR: presaturation of solvent at beginning of pulsesequence
; option -DCWPR (eda: ZGOPTNS)
;preprocessor-flags-end
```

9.2 2D *gradient-selected* F1-PSYCHE-EASY-ROESY

```
; GRADIENT SELECTED EASY ROESY WITH F1-PSYCHE-HOMODECOUPLING
; This pulse sequence is part of the paper:
; Gradient Selected Pure-Shift EASY-ROESY techniques facilitate the quantitative measurement of 1H,1H-distance restraints in
; congested spectral regions
; Authors: Julian Ilgen, Jens Nowag, Lukas Kaltschnee, Volker Schmidts, Christina M. Thiele

; Julian Ilgen
; Technical University Darmstadt
; Avance III Version
; Topspin 3.2.6 or Topspin 3.5.7

; Description and Comments:
; The pulse sequence has been coded for test purposes only and may contain errors.
; It does contain arguments that can lead to hardware damages if acquisition parameters
; are set unfavorably. The functionality of the pulse sequence itself may differ
; depending on the hardware as well as the software used to execute it. Functionality
; on differing systems cannot be granted.
; Any use of this pulse sequence on a spectrometer is at your own risk!
; By using this pulse sequence or any modification of it in any published material
; you agree to acknowledge the above-mentioned publication.

; Jump-symmetrized spinlocks with adiabatic ramps for mixing
; Phase sensitive
; option for presaturation during relaxation delay, presaturation offset defined with cnst41 [ppm]
; Homo broadband decoupling in indirect dimension F1 using PSYCHE
; J is refocused at the end of t1 evolution time
; Internal power and offset calibration of spinlock with 6500 Hz maximum RF-field strength
; Internal power and RF-amplitude calibration of PSYCHE element
; with gradient encoding before mixing and decoding after mixing
; with Thrippleton-Keeler z-filter element before acquisition
;
; Further publications relevant to this pulse sequence:
;(1) M. Foroozandeh, R.W. Adams, N.J. Meharry, D. Jeannerat, M. Nilsson, G.A. Morris: Angew. Chem. Int. Ed. 2014, 53, 6990.
;(2) M. Foroozandeh, M. Nilsson, G. A. Morris: J. Am. Chem. Soc. 2014, 136, 11867.
;(3) C.M. Thiele, K. Petzold, J. Schleucher: Chem. Eur. J. 2009, 15, 585-588.
```

```
;(4) J. Schleucher, J. Quant, S. Glaser, C. Griesinger: J. Magn. Reson A 1995, 112, 144-151.
;(5) J. Stonehouse, P. Adell, J. Keeler, A. J. Shaka: J. Am. Chem. Soc. 1994, 116 (13), 6037-6038.
;(6) V. Dötsch, G. Wider: J. Am. Chem. Soc. 1995, 117, 6064-6070.
;(7) V. Dötsch, G. Wider, K. Wüthrich: J. Magn. Reson. A 1994, 109, 263-264.
;(8) C. Dalvit: J. Magn. Reson. 1995, 33, 570-576.
;
;$CLASS=HighRes
;$DIM=2D
;$TYPE=
;$SUBTYPE=
;$COMMENT=
;
#include <Avance.incl>
#include <Grad.incl>
#include <Delay.incl>

;;General statements;;
"d11=30m"
"d12=20u"
"p2=2*p1"
"d0=0u"
"in0=inf1/2"

;;Statements EASY-ROESY Spin-Lock;;
define pulse P_SL
"cnst24=1000000.0*tan((cnst28*2*PI)/360.0)/(dw*4)"
"if ( cnst24 > 6500 ) {cnst25 = 6400.0;} else {cnst25 = cnst24;}"
"if ( cnst24 > 6500 ) {cnst29 = atan(cnst25*4*dw/1000000.0)*360.0/(2*PI);} else {cnst29=cnst28;}"
"if (cnst26<cnst25) {cnst27=cnst25;} else {if (cnst26>6500) {cnst27=6400;} else {cnst27=cnst26;} }"
"cnst30=abs(cnst27/tan((cnst29*2*PI)/360.0))"
define list<frequency> roesylist={sfo hz, 0.0, cnst30, -cnst30, 0}
"p30=1000000.0/(cnst27*4)"
"cnst31= (p30/p1) * (p30/p1)"
"spw10=plw1/cnst31"
"spw12=plw1/cnst31"
"spw13=plw1/cnst31"
"spw16=plw1/cnst31"
"spw17=plw1/cnst31"
"cnst23=cnst30+cnst31+p30"
"p41=1m"
"P_SL=p15/2"
"spoff10=0"
"spoff12=0"
"spoff13=0"
"spoff16=0"
"spoff17=0"

;;Statements PSYCHE-decoupling;;
"cnst50=(cnst20/360)*sqrt((2*cnst21)/(p40/2000000))"                ; PSYCHE RF-amplitude
"p35=1000000.0/(cnst50*4)"                                          ; equivalent 90 degree pulse
"cnst40= (p35/p1) * (p35/p1)"                                       ; scaling factor for power level attenuation
"spw40=plw1/cnst40"                                                 ; PSYCHE power level
"p10=p40"                                                           ; duration of PSYCHE gradient
"p11=p42"                                                           ; duration ZQC dephasing gradient

;;Statements solvent presaturation;;
#ifdef CWPR
"d17=d1-d18"
"cnst42=cnst41*bf1"                     ; changed to use ppm values for solvent offset, ji20170612
"cnst43=cnst42-o1"
#else

#endif /*CWPR*/

;;start pulsesequence;;
1 ze
2 d11
3 d12  roesylist:f1
  4u roesylist.inc
#ifdef CWPR                             ; begin of solvent presaturation
  d12 fq=0:f1
  d12 fq=cnst43:f1                      ; set frequency on f1-channel to solvent shift for presaturation [fq=SFO1+cnst42]
  d12
  d17 pl9:f1                            ; residual relaxation delay + set power level on f1-channel for presaturation
  d18 cw:f1 ph29                        ; solvent presaturation
  4u do:f1
  d12 fq=0:f1                           ; reset frequency on f1-channel [fq=SFO1]
  d12 pl1:f1                            ; reset power level on f1-channel
#else                                   ; no solvent presaturation
 d1
 d12 pl1:f1                             ; F1-channel power setting
#endif /*CWPR*/

  50u UNBLKGRAD
  p1 ph1                                ; 90 high power pulse for excitation
  d0                                    ; incremented delay F1-dimension
  p17:gp1                               ; CTP gradient 1
  d16

  p2 ph4                                ; 180 high power pulse
  10u
  p17:gp1                               ; CTP gradient 1
  d16 pl0:f1                            ; F1-channel power switching
  p17:gp2                               ; CTP gradient 2
  d16
  d16
  (center (p10:gp10) (p40:sp40 ph5):f1 )         ; PSYCHE-element
  d16
  p17:gp2                               ; CTP gradient 2
  d16 pl1:f1                            ; F1-channel power switching
  d0                                    ; incremented delay F1-dimension
  10u
  10u
  p18:gp4                               ; encoding gradient
  d16
```

```
  p2 ph4
  10u
  p18:gp4*-1                          ; encoding gradient
  d16
4 (p1 ph2):f1                         ; 90 high power pulse before ROESY mixing
  4u
  p16:gp5                             ; 1st purge gradient
  d16 roesylist:f1                    ; setting EASY-ROESY offset list
  4u roesylist.inc                    ; increment EASY-ROESY offset
#   ifdef AV2
  (p41:sp12 ph4):f1                   ; adiabatic ramp up (low frequency, negative offset)
  3u
  (P_SL:sp10 ph4):f1                  ; low frequency spinlock
  3u
  (p41:sp13 ph4):f1                   ; adiabatic ramp down (low frequency, negative offset)
#   else
  (p41:sp12 ph4):f1
  (P_SL:sp10 ph4):f1
  (p41:sp13 ph4):f1
#   endif /*AV2*/
  4u
  4u roesylist:f1
  4u roesylist.inc                    ; increment EASY-ROESY offset
#   ifdef AV2
  (p41:sp16 ph4):f1                   ; adiabatic ramp up (high frequency, positive offset)
  3u
  (P_SL:sp10 ph4):f1                  ; high frequency spinlock
  3u
  (p41:sp17 ph4):f1                   ; adiabatic ramp down (high frequency, positive offset)
#   else
  (p41:sp16 ph4):f1
  (P_SL:sp10 ph4):f1
  (p41:sp17 ph4):f1
#   endif /*AV2*/
  4u
  p16:gp6                             ; 2nd purge gradient
  d16 roesylist:f1
  4u roesylist.inc
  4u pl1:f1                           ; F1-channel power setting
  4u BLKGRAD
  (p1 ph3)                            ; 90 high power pulse after ROESY mixing
  10u
  p18:gp4                             ; decoding gradient
  d16
  p2 ph4
  10u
  p18:gp4*-1                          ; decoding gradient
  d16
  p1 ph6                              ; begin z-filter
  5u
  5u pl0:f1
  (center (p11:gp11)(p42:sp42 ph4):f1)          ; Thrippleton-Keeler z-filter element
  d16
  p19:gp7
  d16 pl1:f1
  10u BLKGRAD
  p1 ph7                              ; end z-filter
  go=2 ph31
  d11 mc #0 to 2 F1PH(calph(ph1, +90), caldel(d0, +in0))
exit

;;phase cycling;;
;ph1= Hard 90 Excitation
;ph2= Hard 90 before mixing
;ph3= Hard 90 after mixing
;ph4= Hard 180 & Thrippleton-Keeler
;ph5= PSYCHE element
;ph6= Hard 90 before z-filter
;ph7= Hard 90 after z-filter
;ph29= CW presaturation
;ph31= receiver

ph1= 0 2
ph2= 0 0 0 0 0 0 0 0 0 0 0 0 0 0 0 0 2 2 2 2 2 2 2 2 2 2 2 2 2 2 2 2
ph3= 0 0 0 0 0 0 0 0 2 2 2 2 2 2 2 2
ph4= 0
ph5= 0 0 1 1 2 2 3 3
ph6= 0
ph7= 0 0 0 0 2 2 2 2
ph29=0
ph31=0 2 2 0 2 0 0 2 2 0 0 2 0 2 2 0 2 0 0 2 0 2 2 0 0 2 2 0 2 0 0 2

;p1 : f1 channel -  90 degree high power pulse
;p2 : f1 channel - 180 degree high power pulse
;p10: duration of PSYCHE gradient
;p11: duration of ZQC dephasing gradient
;p15: f1 channel - pulse for ROESY spinlock
;p16: purge gradient          [1m]
;p17: CTP gradient  [1m]
;p18: en-/decoding gradient   [<1m]
;p19: purge gradient          [1.5-2.5m]
;p40: duration of PSYCHE element       [30m]
;p41: f1 channel - shaped pulse for adiabatic ramp         [1m]
;p42: duration of Thrippleton-Keeler z-filter element      [>10m]

;pl1 : f1 channel - power level for pulse (default)
;pl9 : f1 channel - power level for presaturation

;P_SL: f1 channel - pulse width for low and high frequency spinlock
;sp10: f1 channel - shaped pulse for ROESY-spinlock (= pl1 + cnst31)
;spnam10: Squa100.1000
;sp12: f1 channel - shaped pulse for adiabatic ramp down (low frequency, negative offset) (= pl1 + cnst31)
;spnam12: Gaussramp+down.1
;sp13: f1 channel - shaped pulse for adiabatic ramp up (low frequency, negative offset) (= pl1 + cnst31)
;spnam13: Gaussramp+up.1
```

```
;sp16: f1 channel - shaped pulse for adiabatic ramp down (high frequency, positive offset) (= pl1 + cnst31)
;spnam16: Gaussramp-down.1
;sp17: f1 channel - shaped pulse for adiabatic ramp up (high frequency, positive offset) (= pl1 + cnst31)
;spnam17: Gaussramp-up.1
;sp40: f1-channel - PSYCHE element
;spw40 : RF power of PSYCHE element
;spnam40: file name for PSYCHE element [Crp_psyche.20]
;sp42: f1-channel - adiabatic pulse for Thrippleton-Keeler
;spnam42: file name for Thrippleton-Keeler

;d0 : incremented delay (2D)
;d1 : relaxation delay; 1-5 * T1
;d11: delay for disk I/O     [30m]
;d12: delay for power switching        [20u]
;d16: gradient recovery delay [200-500u]
;d17: reduced relaxation delay
;d18: delay for solvent presaturation

;cnst20: PSYCHE flip angle (degree) [10-25]
;cnst21: PSYCHE sweepwidth (Hz) [10000]
;cnst24: min. RF field strength to make sure that the carrier is shifted to the edge of the spectrum
;cnst25: reduced min. RF field strength in case an upper limit of 6.5kHz is exceeded
;           (set to 6.4kHz), this leads to a recalculation of the tilt angle (cnst29)
;cnst26: requested RF field strength (gammaB1) for ROESY spinlock [Hz], reduced to 6.4kHz if an upper limit of 6.5kHz is
exceeded
;cnst27: used RF field strength (gammaB1) for ROESY spinlock
;cnst28: requested tilt angle for ROESY spinlock (between axis of spinlock and z-axis) [45 degree]
;cnst29: used tilt angle for ROESY spinlock (between axis of spinlock and z-axis)
;cnst30: low and high frequency offset, calculated from gammaB1 (cnst27) for tilt angle (cnst29)
;cnst41: solvent offset [ppm]
;cnst50: PSYCHE RF amplitude (Hz)

;gpz1: 1st CTP gradient: 77%
;gpz2: 2nd CTP gradient: 49%
;gpz4: en-/decoding gradient: 3-10%
;gpz5: 1st purge gradient: 31%
;gpz6: 2nd purge gradient: 11%
;gpz7: z-filter purge gradient: 61%
;gpz10: PSYCHE gradient: 1-3%
;gpz11: ZQC dephasing gradient: 2-12%
;gpnam1: SMSQ10.100
;gpnam2: SMSQ10.100
;gpnam3: SMSQ10.100
;gpnam4: SMSQ10.100
;gpnam5: SMSQ10.100
;gpnam6: SMSQ10.100
;gpnam7: SMSQ10.100
;gpnam10: RECT.1
;gpnam11: RECT.1

;inf1: 1/SW = 2 * DW
;in0: 1/(1 * SW) = 2 * DW
;nd0: 1
;ns: 8*n
;ds: 16
;FnMODE: States-TPPI, TPPI

;preprocessor-flags-start
;CWPR: presaturation of solvent at beginning of pulsesequence
; option -DCWPR (eda: ZGOPTNS)
;preprocessor-flags-end
```

9.3 2D *gradient-selected* F1-*perfect*BASH-EASY-ROESY

```
; 2D GRADIENT-SELECTED EASY-ROESY WITH F1-PERFECT-BASH HOMODECOUPLING
;
; This pulse sequence is part of the paper:
; Gradient Selected Pure-Shift EASY-ROESY techniques facilitate the quantitative measurement of 1H,1H-distance restraints in
; congested spectral regions
; Authors: Julian Ilgen, Jens Nowag, Lukas Kaltschnee, Volker Schmidts, Christina M. Thiele
;
; Julian Ilgen
; Technical University Darmstadt
; Avance III Version
; Topspin 3.2.6 or Topspin 3.5.7
;
; Description and Comments:
; The pulse sequence has been coded for test purposes only and may contain errors.
; It does contain arguments that can lead to hardware damages if acquisition parameters
; are set unfavorably. The functionality of the pulse sequence itself may differ
; depending on the hardware as well as the software used to execute it. Functionality
; on differing systems cannot be granted.
; Any use of this pulse sequence on a spectrometer is at your own risk!
; By using this pulse sequence or any modification of it in any published material
; you agree to acknowledge the above-mentioned publication.
;
; jump-symmetrized with adiabatic spinlocks for mixing
; correction to ensure symmetrically shifted offsets for spin-locking
; midpoint of symmetric offset shifting of spin-lock defined with cnst0 [ppm] and should be set center of 1H spectrum
; phase sensitive
; band selective homonuclear decoupling using frequency selective pulses incorporated in Perfect-Echo
; homodecoupling scheme based on perfectBASH and F1-PSYCHE-ROESY from Ref. (5) and (6)
; J is refocussed at the beginning of mixing
; option for solvent presaturation during relaxation delay, presaturation offset defined with cnst40 [ppm]
; avance-version (12/01/11)
;
; Relevant Papers:
;(1) J. Ilgen, L. Kaltschnee, C. M. Thiele, J. Magn. Reson. 2018, 286, 18-29
;(2) K. Zangger and H. Sterk, J. Magn. Reson., 1997, 124, 486-489.
;(3) C.M. Thiele, K. Petzold & J. Schleucher, Chem. Eur. J. 15, 585-588 (2009)
;(4) J. Schleucher, J. Quant, S. Glaser & C. Griesinger, J. Magn. Reson A 112, 144-151 (1995)
;(3) J.A. Aguilar, M. Nilsson, G. Bodenhausen and G.A. Morris, Chem. Commun.; 2012, 48, 811-813.
;(4) L. Kaltschnee, A. Kolmer, I. Timari, V. Schmidts, R. W. Adams, M. Nilsson, K. E. Köver, G. A. Morris and C. M. Thiele,
```

```
; Chem. Commun.; 2014, 50, 15702 – 15705
;(5) J. Ilgen, L. Kaltschnee, C. M. Thiele, Magn. Reson. Chem. 2018, 56, 918-933
;(6) Procházková, E., Kolmer, A., Ilgen, J., Schwab, M., Kaltschnee, L., Fredersdorf, M., Schmidts, V., Wende, R. C.,
; Schreiner, P. R., Thiele, C. M., Angew. Chem. Int. Ed. 2016, 55, 15754-15759
;
;$CLASS=HighRes
;$DIM=2D
;$TYPE=
;$SUBTYPE=
;$COMMENT=
#include <Avance.incl>
#include <Grad.incl>

;;General statements;;
"d11=30m"
"d12=20u"
"p2=2*p1"
"d0=0u"
"in0=inf1/2"

;;Statements for EASY-ROESY Spin-Lock;;
define pulse P_SL
"cnst24=1000000.0*tan((cnst28*2*PI)/360.0)/(dw*4)"
"if ( cnst24 > 6500 ) {cnst25 = 6400.0;} else {cnst25 = cnst24;}"
"if ( cnst24 > 6500 ) {cnst29 = atan(cnst25*4*dw/1000000.0)*360.0/(2*PI);} else {cnst29=cnst28;}"
"if (cnst26<cnst25) {cnst27=cnst25;} else {if (cnst26>6500) {cnst27=6400;} else {cnst27=cnst26;} }"
"cnst30=abs(cnst27/tan((cnst29*2*PI)/360.0))"
; difference between PerfectBASH offset and 1H-spectrum center, to allow symmetrical spin-locking, cnst0 defines the
; midpoint of symmetrical offset shifting!
"cnst33=o1-(cnst0*bf1)"
"cnst34=cnst30+cnst33"                          ; correction for low frequency SL offset
"cnst35=cnst30-cnst33"                          ; correction for high frequency SL offset
define list<frequency> roesylist={sfo hz, 0.0, -cnst34, cnst35, 0}
"p30=1000000.0/(cnst27*4)"
"cnst31= (p30/p1) * (p30/p1)"
"spw10=plw1/cnst31"
"spw12=plw1/cnst31"
"spw13=plw1/cnst31"
"spw16=plw1/cnst31"
"spw17=plw1/cnst31"
"cnst23=cnst30+cnst31+p30"
"p41=1m"
"P_SL=p15/2"
"spoff10=0"
"spoff12=0"
"spoff13=0"
"spoff16=0"
"spoff17=0"

;;Statements for perfectBASH;;
define delay tauA
"tauA=p17+d16"
"spoff40=bf1*(cnst1/1000000)-o1"
"p11=p42"

;;Statements solvent presaturation;;
#ifdef CWPR
"d18=d1-d19"
"cnst41=cnst40*bf1"                      ; changed to use ppm values for solvent offset
"cnst42=cnst41-o1"
#else
#endif /*CWPR*/

;; start pulsesequence ;;
1 ze
2 d11
3 d12 roesylist:f1
4u roesylist.inc
#ifdef CWPR                              ; begin of solvent presaturation
d12 fq=0:f1
d12 fq=cnst42:f1                         ; set frequency on f1-channel to solvent shift for presaturation [fq=SFO1+cnst42]
d12
d18 pl9:f1                               ; residual relaxation delay + set power level on f1-channel for presaturation
d19 cw:f1 ph29                           ; solvent presaturation
4u do:f1
d12 fq=0:f1                              ; reset frequency on f1-channel [fq=SFO1]
d12 pl1:f1                               ; reset power level on f1-channel
#else                                    ; no solvent presaturation
d1
d12 pl1:f1
#endif /*CWPR*/
50u UNBLKGRAD
4 p1 ph1                                  ; 90 high power excitation pulse
  5u
  5u pl0:f1                             ; power switching f1-channel
  d0                                    ; incremented delay
  tauA
  p17:gp1                               ; CTP gradient 1
  d16
  (p40:sp40 ph2:r):f1                   ; 1st selective refocusing pulse
  10u
  p17:gp1                               ; CTP gradient 1
  d16
  tauA pl1:f1                           ; power switching f1-channel
  d0                                    ; incremented delay
5 (p1 ph3):f1                           ; 90 high power pulse for perfect echo J-removal
  d0                                    ; incremented delay
  p17:gp2                               ; CTP gradient 2
  d16
  (p2 ph4):f1                           ; 180 high power pulse
  10u
  p17:gp2                               ; CTP gradient 2
  d16
  p17:gp3                               ; CTP gradient 3
  d16 pl0:f1                            ; power switching f1-channel
```

```
  (p40:sp40 ph5:r):f1                  ; 2nd selective refocusing pulse
  5u
  p17:gp3                              ; CTP gradient 3
  d16
  d0                                    ; incremented delay
  5u pl1:f1                             ; power switching f1-channel
  p18:gp4                               ; encoding gradient
  d16
  p2 ph4
  10u
  p18:gp4*-1                           ; encoding gradient
  d16
6 (p1 ph6):f1                          ; 90 high power pulse start ROESY mixing
  4u
  p16:gp5                              ; 1st purge gradient
  d16 roesylist:f1
  4u roesylist.inc
# ifdef AV2
  (p41:sp12 ph6):f1                    ; adiabatic ramp up (low frequency, negative offset)
  3u
  (P_SL:sp10 ph6):f1                   ; low frequency spinlock
  3u
  (p41:sp13 ph6):f1                    ; adiabatic ramp down (low frequency, negative offset)
# else
  (p41:sp12 ph6):f1
  (P_SL:sp10 ph6):f1
  (p41:sp13 ph6):f1
# endif /*AV2*/
  4u
  4u roesylist:f1
  4u roesylist.inc
# ifdef AV2
  (p41:sp16 ph6):f1                    ; adiabatic ramp up (high frequency, positive offset)
  3u
  (P_SL:sp10 ph6):f1                   ; high frequency spinlock
  3u
  (p41:sp17 ph6):f1                    ; adiabatic ramp down (high frequency, positive offset)
# else
  (p41:sp16 ph6):f1
  (P_SL:sp10 ph6):f1
  (p41:sp17 ph6):f1
# endif /*AV2*/
  4u
  p16:gp6                              ; 2nd purge gradient
  d16 roesylist:f1
  4u roesylist.inc
  4u pl1:f1
7 (p1 ph7)                             ; 90 high power pulse end ROESY mixing
  10u
  p18:gp4                              ; decoding gradient
  d16
  p2 ph5
  10u
  p18:gp4*-1                           ; decoding gradient
  d16
  p1 ph8                               ; begin z-filter
  5u
  5u pl0:f1
  (center (p11:gp11)(p42:sp42 ph4):f1) ; Thrippleton-Keeler z-filter element
  d16
  p19:gp7
  d16 pl1:f1
  10u BLKGRAD
  p1 ph9                               ; end z-filter
  go=2 ph31
  d11 mc #0 to 2 F1PH(calph(ph1, +90) & calph(ph2, +90) & calph(ph3, +90) & calph(ph4, +90) & calph(ph5, +90),
caldel(d0,+in0))
  exit

ph1= 0 2                                  ; Hard 90 excitation
ph2= 0 0 1 1                              ; First selective 180
ph3= 1 3 1 3                              ; Hard 90 Perfect Echo
ph4= 0                                    ; Hard 180
ph5= 0                                    ; Second selective 180
ph6= 0                                    ; Hard 90 ROESY mixing begin
ph7= 0 0 0 0 0 0 0 0 2 2 2 2 2 2 2 2      ; Hard 90 ROESY mixing end
ph8= 0
ph9= 0 0 0 0 2 2 2 2
ph29=0                                    ; CW presaturation
ph31=0 2 2 0 2 0 0 2 2 0 0 2 0 2 2 0      ; Receiver

;p1 : f1 channel - 90 degree high power pulse
;p2: high power 180 pulse width
;p11: duration of ZQC dephasing gradient
;p15: f1 channel - pulse for ROESY spinlock
;p16: purge gradient pulse during ROESY mixing time [1m]
;p17: homospoil/gradient pulse during F1-homodecoupling [1m]
;p18: en-/decoding gradient   [<1m]
;p19: purge gradient [1.5-2.5m]
;p30: f1 channel - 90 degree pulse at sp10
;p35: f1 channel - 90 degree pulse at sp40
;p40: duration of selective 180 pulse
;p41: f1 channel - shaped pulse for adiabatic ramp [1m]
;p42: duration of Thrippleton-Keeler z-filter element      [>10m]

;pl1 : f1 channel - power level for pulse (default)
;pl9 : f1 channel - power level for presaturation

;P_SL: f1 channel - pulse width for low and high frequency spinlock
;sp10: f1 channel - shaped pulse for ROESY-spinlock (= pl1 + cnst31)
;spnam10: Squa100.1000
;sp12: f1 channel - shaped pulse for adiabatic ramp down (low frequency, negative offset) (= pl1 + cnst31)
;spnam12: Gaussramp+down.1
;sp13: f1 channel - shaped pulse for adiabatic ramp up (low frequency, negative offset) (= pl1 + cnst31)
;spnam13: Gaussramp+up.1
```

```
;sp16: f1 channel - shaped pulse for adiabatic ramp down (high frequency, positive offset) (= pl1 + cnst31)
;spnam16: Gaussramp-down.1
;sp17: f1 channel - shaped pulse for adiabatic ramp up (high frequency, positive offset) (= pl1 + cnst31)
;spnam17: Gaussramp-up.1
;sp40: f1-channel - selective 180 pulse
;spw40 : RF power of selective 180 pulse
;spnam40: RSnob1000 or ReBurp1000
;sp42: f1-channel - adiabatic pulse for Thrippleton-Keeler
;spnam42: file name for Thrippleton-Keeler

;gpz1: 1st CTP gradient: 20-50%
;gpz2: 2nd CTP gradient: 20-50%
;gpz3: 3rd CTP gradient: 20-50%
;gpz4: en-/decoding gradient: 3-10%
;gpz5: 1st purge gradient: 31%
;gpz6: 2nd purge gradient: 11%
;gpz7: z-filter purge gradient: 61%
;gpz11: ZQC dephasing gradient: 2-12%
;gpnam1: SMSQ10.100
;gpnam2: SMSQ10.100
;gpnam3: SMSQ10.100
;gpnam4: SMSQ10.100
;gpnam5: SMSQ10.100
;gpnam6: SMSQ10.100
;gpnam7: SMSQ10.100
;gpnam10: RECT.1
;gpnam11: RECT.1

;d0 : incremented delay (2D)
;d1 : relaxation delay; 1-5 * T1
;d11: delay for disk I/O [30 msec]
;d12: delay for power switching [20 usec]
;d16: delay for homospoil/gradient recovery
;d18: reduced relaxation delay
;d19: delay for solvent presaturation

;cnst0: midpoint of symmetrical offset shifting, center of proton spectrum [ppm]
;cnst1: offset for selective refocusing [ppm]
;cnst23; (for display purpose only)
;cnst24: min. RF field strength to make sure that the carrier is shifted
; to the edge of the spectrum
;cnst25: reduced min. RF field strength in case an upper limit of 6.5kHz is exceeded
; (set to 6.4kHz), this leads to a recalculation of the tilt angle (cnst29)
;cnst26: requested RF field strength (gammaB1) for ROESY spinlock [Hz]
; reduced to 6.4kHz if an upper limit of 6.5kHz is exceeded
;cnst27: used RF field strength (gammaB1) for ROESY spinlock
;cnst28: requested tilt angle for ROESY spinlock (between axis of spinlock and z-axis) [45 degree]
;cnst29: used tilt angle for ROESY spinlock (between axis of spinlock and z-axis)
;cnst30: low and high frequency offset,
; calculated from gammaB1 (cnst27) for tilt angle (cnst29)
;cnst31: difference in power level (dB) for spinlock relative to pl1
;cnst40: solvent offset [ppm]

;inf1: 1/SW = 2 * DW
;in0: 1/(1 * SW) = 2 * DW
;nd0: 1
;NS : 8*n
;DS : 16
;td1 : number of t1 increments
;FnMODE: States-TPPI, TPPI, States or QSEQ

;preprocessor-flags-start
;CWPR: presaturation of solvent at beginning of pulsesequence
; option -DCWPR (eda: ZGOPTNS)
;preprocessor-flags-end
```

9.4 1D *selective, gradient-selected continuous-wave* ROESY (GS-CW-ROESY)

```
;1D SELECTIVE AND GRADIENT SELECTED CW-ROESY

; This pulse sequence is part of the paper:
; Gradient Selected Pure-Shift EASY-ROESY techniques facilitate the quantitative measurement of 1H,1H-distance restraints in
; congested spectral regions
; Authors: Julian Ilgen, Jens Nowag, Lukas Kaltschnee, Volker Schmidts, Christina M. Thiele

; Julian Ilgen
; Technical University Darmstadt
; Avance III Version
; Topspin 3.5

; Description and Comments:
; The pulse sequence has been coded for test purposes only and may contain errors.
; It does contain arguments that can lead to hardware damages if acquisition parameters
; are set unfavorably. The functionality of the pulse sequence itself may differ
; depending on the hardware as well as the software used to execute it. Functionality
; on differing systems cannot be granted.
; Any use of this pulse sequence on a spectrometer is at your own risk!
; By using this pulse sequence or any modification of it in any published material
; you agree to acknowledge the above-mentioned publication.

; cw spinlock for mixing
; based on Tr-ROESY implementation with gradient-selection: J. Furrer, J. Nat. Prod. (2009)
; using selective refocussing with a shaped pulse
; internal power calibration of selective refocusing pulse (only TopSpin 3.5 or higher!)

#include <Avance.incl>
#include <Grad.incl>

;;General statements;;
"d30=p16+d16"
"p2=2*p1"

;;Statements for selective pulse calibration – only TopSpin 3.5 or higher;;
```

```
"spoff2=bf1*(cnst1/1000000)-o1"
"if ( p12 == 0u ) {p13 = 40m;} else {p13 = p12;}"          ; compilation is executing even if p12 is zero
"cnst35=(1/(2*(p13/1000000)*integfac2))"          ; gamma*B1,max for shaped pulse, calculation with shape specific parameter
"p32=(1000000/(cnst35*4))"                        ; equivalent 90 degree soft pulse
"cnst36=(p32/p1)*(p32/p1)"                        ; power scaling factor
"spw2=plw1/cnst36"

;;start pulsesequence;;
1 ze
2 30m
  20u pl1:f1 BLKGRAD
  d1
  50u UNBLKGRAD
3 (p1 ph1):f1
  10u
  p16:gp1                                         ;1st defocusing gradient
  d16 pl0:f1
  p12:sp2:f1 ph2:r                                ;selective refocusing pulse
  10u
  p16:gp1*-1                                      ;2nd defocusing gradient
  d16 pl11:f1
  (p15 ph3):f1                                    ; CW spinlock for mixing
  20u pl1:f1
  d30
  p2 ph5
  p16:gp2                                         ;refocusing gradient
  d16
  20u BLKGRAD
go=2 ph31
30m mc #0 to 2 F0(zd)
20u
exit

;;phase cycling;;
ph1=0 2
ph2=0 0 1 1 2 2 3 3
ph3=1
ph5=0 0 0 0 2 2 2 2
ph31=0 2 2 0

;pl0 : zero power
;pl1 : f1 channel - power level for pulse (default)
;pl11: f1 channel - power level for CW ROESY-spinlock (5 - 8 kHz)

;p1 : f1 channel - 90 degree high power pulse
;p2 : f1 channel - 180 degree high power pulse
;p12: f1 channel - 180 degree shaped pulse
;p15: f1 channel - pulse for ROESY spinlock
;p16: gradient pulse [800u - 1m]

;sp2: f1 channel - shaped pulse
;spnam2: RSnob1000 or ReBurp1000

;d1 : relaxation delay; 1-5 * T1
;d16: delay for homospoil/gradient recovery

;cnst1: offset of selective refocusing pulse [ppm]
;gpz1: defocusing gradient 6-10%
;gpz2: refocusing gradient 12-20%
;gpnam1: SMSQ10.100
;gpnam2: SMSQ10.100

;NS: 2 * n, total number of scans: NS * TD0
;DS: 8
;choose p12 according to desired selectivity
;the flip-angle is determined by the amplitude
```

9.5 1D *selective, gradient-selected* EASY-ROESY

```
; 1D SELECTIVE GRADIENT-SELECTED EASY-ROESY
; This pulse sequence is part of the paper:
; Gradient Selected Pure-Shift EASY-ROESY techniques facilitate the quantitative measurement of 1H,1H-distance restraints in
; congested spectral regions
; Authors: Julian Ilgen, Jens Nowag, Lukas Kaltschnee, Volker Schmidts, Christina M. Thiele

; Julian Ilgen
; Technical University Darmstadt
; Avance III Version
; Topspin 3.5

; Description and Comments:
; The pulse sequence has been coded for test purposes only and may contain errors.
; It does contain arguments that can lead to hardware damages if acquisition parameters
; are set unfavorably. The functionality of the pulse sequence itself may differ
; depending on the hardware as well as the software used to execute it. Functionality
; on differing systems cannot be granted.
; Any use of this pulse sequence on a spectrometer is at your own risk!
; By using this pulse sequence or any modification of it in any published material
; you agree to acknowledge the above-mentioned publication.

; based on 1D EASY-ROESY from Ref. (5)
; jump-symmetrized with adiabatic spinlocks for mixing
; selective refocussing with a shaped pulse
; internal power and offset calibration of spinlock with 6500 Hz maximum RF-field strength
; internal power calibration for selective refocusing pulse (only TopSpin 3.5 or higher!)
; with gradient encoding before mixing and decoding after mixing
; O1 should be set to the center of the whole proton spectrum [ppm] to ensure symmetrical offset shifting of spin-lock
; offset of selective refocusing pulse is defined with cnst1 and should be set to desired proton shift

; literature
;(1) J. Stonehouse, P. Adell, J, Keeler and A. J. Shaka: J. Am. Chem. Soc., 116, 6037-6038 (1994)
;(2) J. Schleucher, J. Quant, S. Glaser, C. Griesinger: J. Magn. Reson A, 112, 144-151, 1995.
;(3) C. M. Thiele, K. Petzold, J. Schleucher: Chem. Eur. J. 15, 585-588, 2009.
```

```
;(5) S. Boros, Gy Batta: Magn. Reson. Chem., 54(12), 947-952, 2016
;
;$CLASS=HighRes
;$DIM=1D
;$TYPE=
;$SUBTYPE=
;$COMMENT=

#include <Avance.incl>
#include <Grad.incl>
#include <Delay.incl>


;;general statements;;
"d11=30m"
"d12=20u"
"DELTA=p17+d16+40u"
"p2=2*p1"

;;EASY-ROESY statements;;
define pulse P_SL
"cnst24=1000000.0*tan((cnst28*2*PI)/360.0)/(dw*4)"
"if ( cnst24 > 6500 ) {cnst25 = 6400.0;} else {cnst25 = cnst24;}"
"if ( cnst24 > 6500 ) {cnst29 = atan(cnst25*4*dw/1000000.0)*360.0/(2*PI);} else {cnst29=cnst28;}"
"if (cnst26<cnst25) {cnst27=cnst25;} else {if (cnst26>6500) {cnst27=6400;} else {cnst27=cnst26;} }"
"cnst30=abs(cnst27/tan((cnst29*2*PI)/360.0))"
define list<frequency> roesylist={sfo hz, 0.0, -cnst30, cnst30, 0}
"p30=1000000.0/(cnst27*4)"
"cnst31= (p30/p1) * (p30/p1)"
"spw10=plw1/cnst31"
"spw12=plw1/cnst31"
"spw13=plw1/cnst31"
"spw16=plw1/cnst31"
"spw17=plw1/cnst31"
"cnst23=cnst30+cnst31+p30"
"p41=1m"
"P_SL=p15/2"
"spoff10=0"
"spoff12=0"
"spoff13=0"
"spoff16=0"
"spoff17=0"

;;statements selective refocusing pulse calibration – only TopSpin 3.5 or higher!;;
"spoff2=bf1*(cnst1/1000000)-o1"
"if ( p12 == 0u ) {p13 = 40m;} else {p13 = p12;}"          ; compilation is executing even if p12 is zero
"cnst35=(1/(2*(p13/1000000)*integfac2))"         ; gamma*B1,max for shaped pulse, calculation with shape specific parameter
"p32=(1000000/(cnst35*4))"                                ; equivalent 90 degree soft pulse
"cnst36=(p32/p1)*(p32/p1)"                                ; power scaling factor
"spw2=plw1/cnst36"

;;start pulsesequence;;
1 ze
2 d11
3 d12  roesylist:f1
  4u roesylist.inc
  d1
  d12 pl1:f1
  50u UNBLKGRAD
  (p1 ph1):f1                           ; excitation
  5u
  p17:gp3                               ; 1st defocusing gradient
  d16 pl0:f1
  p12:sp2:f1 ph4:r                      ; selective refocusing
  5u
  p17:gp3*-1                            ; 2nd defocusing gradient
  d16 pl1:f1
4 (p1 ph3):f1                           ; start EASY-ROESY mixing
  10u pl0:f1
  p16:gp1                               ; 1st purge gradient
  d16 roesylist:f1                      ; setting EASY-ROESY offset list
  4u roesylist.inc                      ; increment EASY-ROESY offset
#   ifdef AV2
  (p41:sp12 ph0):f1                     ; adiabatic ramp up (low frequency, negative offset)
  3u
  (P_SL:sp10 ph0):f1                    ; low frequency spinlock
  3u
  (p41:sp13 ph0):f1                     ; adiabatic ramp down (low frequency, negative offset)
#   else
  (p41:sp12 ph0):f1
  (P_SL:sp10 ph0):f1
  (p41:sp13 ph0):f1
#   endif /*AV2*/
  4u
  4u roesylist:f1
  4u roesylist.inc                      ; increment EASY-ROESY offset
#   ifdef AV2
  (p41:sp16 ph0):f1                     ; adiabatic ramp up (high frequency, positive offset)
  3u
  (P_SL:sp10 ph0):f1                    ; high frequency spinlock
  3u
  (p41:sp17 ph0):f1                     ; adiabatic ramp down (high frequency, positive offset)
#   else
  (p41:sp16 ph0):f1
  (P_SL:sp10 ph0):f1
  (p41:sp17 ph0):f1
#   endif /*AV2*/
  4u
  p16:gp2                               ; 2nd purge gradient
  d16 roesylist:f1
  5u roesylist.inc
  5u pl0:f1                             ; F1-channel power setting
5 (p1 ph2):f1                           ; end EASY-ROESY mixing
  DELTA
  p2 ph0
```

```
  20u
  p17:gp4                              ;refocusing gradient
  d16
  20u BLKGRAD
  go=2 ph31
  30m mc #0 to 2 F0(zd)
  20u
exit

;;phase cycling;;
ph0=0
ph1=0 2
ph2=0 0 0 0 0 0 0 0 0 0 0 0 0 0 0 0 2 2 2 2 2 2 2 2 2 2 2 2 2 2 2 2
ph3=0 0 0 0 0 0 0 0 2 2 2 2 2 2 2 2
ph4=0 0 1 1 2 2 3 3
ph31=0 2 2 0 0 2 2 0 2 0 0 2 2 0 0 2 2 0 0 2 2 0 0 2 0 2 2 0 0 2 2 0

;pl1 : f1 channel - power level for pulse (default)
;pl0 : f1 channel - zero power
;p1 : f1 channel -  90 degree high power pulse
;p12: 180 degree shaped pulse for refocusing
;p15: pulse for ROESY spinlock [50m - 500m]
;p16: purge gradient          [1m]
;p17: gradient pulse [800u - 1m]
;p41: f1 channel - shaped pulse for adiabatic ramp         [1m]

;sp2: f1 channel - shaped pulse for refocusing
;spnam2: RSnob1000 or ReBurp1000
;P_SL: f1 channel - pulse width for low and high frequency spinlock
;sp10: f1 channel - shaped pulse for ROESY-spinlock (= pl1 + cnst31)
;spnam10: Squa100.1000
;sp12: f1 channel - shaped pulse for adiabatic ramp down (low frequency, negative offset) (= pl1 + cnst31)
;spnam12: Gaussramp+down.1
;sp13: f1 channel - shaped pulse for adiabatic ramp up (low frequency, negative offset) (= pl1 + cnst31)
;spnam13: Gaussramp+up.1
;sp16: f1 channel - shaped pulse for adiabatic ramp down (high frequency, positive offset) (= pl1 + cnst31)
;spnam16: Gaussramp-down.1
;sp17: f1 channel - shaped pulse for adiabatic ramp up (high frequency, positive offset) (= pl1 + cnst31)
;spnam17: Gaussramp-up.1

;d1 : relaxation delay; 1-5 * T1
;d11: delay for disk I/O     [30m]
;d12: delay for power switching        [20u]
;d16: gradient recovery delay[200-500u]

;cnst1: chemical shift of selected proton (ppm)
;cnst24: min. RF field strength to make sure that the carrier is shifted to the edge of the spectrum
;cnst25: reduced min. RF field strength in case an upper limit of 6.5kHz is exceeded
;          (set to 6.4kHz), this leads to a recalculation of the tilt angle (cnst29)
;cnst26: requested RF field strength (gammaB1) for ROESY spinlock [Hz], reduced to 6.4kHz if an upper limit of 6.5kHz is
;exceeded
;cnst27: used RF field strength (gammaB1) for ROESY spinlock
;cnst28: requested tilt angle for ROESY spinlock (between axis of spinlock and z-axis) [45 degree]
;cnst29: used tilt angle for ROESY spinlock (between axis of spinlock and z-axis)
;cnst30: low and high frequency offset, calculated from gammaB1 (cnst27) for tilt angle (cnst29)

;gpz1: purge gradient 31%
;gpz2: purge gradient 11%
;gpz3: defocusing gradient 6-10%
;gpz4: refocusing gradient 12-20% [gp4=2*gp3]
;gpnam1: SMSQ10.100
;gpnam2: SMSQ10.100
;gpnam3: SMSQ10.100
;gpnam4: SMSQ10.100

;NS: 8*n
;DS: 4
```

9.6 2D *gradient-selected* F1-PSYCHE-NOESY

```
; 2D GRADIENT SELECTED NOESY WITH F1-HOMODECOUPLING USING PSYCHE
; This pulse sequence is part of the paper:
; Gradient Selected Pure-Shift EASY-ROESY techniques facilitate the quantitative measurement of 1H,1H-distance restraints in
; congested spectral regions
; Authors: Julian Ilgen, Jens Nowag, Lukas Kaltschnee, Volker Schmidts, Christina M. Thiele

; Julian Ilgen
; Technical University Darmstadt
; Avance III Version
; Topspin 3.2.6 or Topspin 3.5.7

; Description and Comments:
; The pulse sequence has been coded for test purposes only and may contain errors.
; It does contain arguments that can lead to hardware damages if acquisition parameters
; are set unfavorably. The functionality of the pulse sequence itself may differ
; depending on the hardware as well as the software used to execute it. Functionality
; on differing systems cannot be granted.
; Any use of this pulse sequence on a spectrometer is at your own risk!
; By using this pulse sequence or any modification of it in any published material
; you agree to acknowledge the above-mentioned publication.

; 2D homonuclear correlation via dipolar coupling
; dipolar coupling may be due to noe or chemical exchange.
; broadband homodecoupling in the indirect dimension (F1) using PSYCHE
; J is refocused at the end of t1 evolution time
; Internal power and RF-amplitude calibration of PSYCHE element
; Thrippleton-Keeler z-filter element in mixing time
; phase sensitive
; option for presaturation during relaxation delay, presaturation offset defined with cnst41 [ppm]

; Further publications relevant to this pulse sequence:
;(1) M. Foroozandeh, R.W. Adams, N.J. Meharry, D. Jeannerat, M. Nilsson, G.A. Morris: Angew. Chem. Int. Ed. 2014, 53, 6990.
;(2) M. Foroozandeh, M. Nilsson, G. A. Morris: J. Am. Chem. Soc. 2014, 136, 11867.
```

```
;(3) M. Foroozandeh, R. W. Adams, P. KirÃ¡ly, M. Nilsson, G. A. Morris, Chem. Commun. 2015, 51,15410.

;$CLASS=HighRes
;$DIM=2D
;$TYPE=
;$SUBTYPE=
;$COMMENT=

#include <Avance.incl>
#include <Grad.incl>

;;general statements;;
"d11=30m"
"d12=20u"
"p2=2*p1"
"d0=0u"
"in0=inf1/2"
"p11=p42" ; adiabatic pulse as long as 2nd ZQC dephasing gradient

;;NOESY statements;;
define delay TAU
"TAU=d8-(p32+p16+d16*2+30u)"
"p12=p32" ; adiabatic pulse as long as 1st ZQC dephasing gradient

;;PSYCHE statements;;
"cnst50=(cnst20/360)*sqrt((2*cnst21)/(p40/2000000))"       ; RF-amplitude of PSYCHE pulse element
"p35=1000000.0/(cnst50*4)"                                 ; equivalent 90 degree low power pulse
"cnst40= (p35/p1)*(p35/p1)"                                ; scaling factor for power level attenuation
"spw40=plw1/cnst40"                                        ; power level PSYCHE pulse element
"p10=p40"                                                  ; duration of PSYCHE gradient (p40)

;;statements solvent presaturation;;
#ifdef CWPR
"d18=d1-d19"
"cnst42=cnst41*bf1"                    ; changed to use ppm values for solvent offset, ji20170612
"cnst43=cnst42-o1"
#else

#endif /*CWPR*/

;;start pulsesequence;;
1 ze
2 d11
3 d12
  4u
#ifdef CWPR                            ; begin of solvent presaturation
  d12 fq=0:f1
  d12 fq=cnst43:f1                     ; set frequency on f1-channel to solvent shift for presaturation [fq=SFO1+cnst43]
  d12
  d18 pl9:f1                           ; residual relaxation delay + set power level on f1-channel for presaturation
  d19 cw:f1 ph29                       ; solvent presaturation
  4u do:f1
  d12 fq=0:f1                          ; reset frequency on f1-channel [fq=SFO1]
  d12 pl1:f1                           ; reset power level on f1-channel
#else                                  ; no solvent presaturation
 d1
 d12 pl1:f1
#endif /*CWPR*/
  50u UNBLKGRAD
4 p1 ph1                       ; 90 high power excitation-pulse
  d0                           ; incremented delay F1-dimension
  p17:gp1                      ; CTP gradient 1
  d16
  p2 ph4                       ; 180 high power pulse
  10u
  10u pl0:f1
  p17:gp1                      ; CTP gradient 1
  d16
  p17:gp2                      ; CTP gradient 2
  d16
  d16
  (center (p10:gp10) (p40:sp40 ph5):f1 )         ; PSYCHE-element
  d16
  10u
  10u pl1:f1
  p17:gp2                      ; CTP gradient 2
  d16
  d0                           ; incremented delay F1-dimension
  10u
  p18:gp4                      ; encoding gradient
  d16
  p2 ph4
  10u
  p18:gp4*-1                   ; encoding gradient
  d16
  (p1 ph2)                             ; 90 high power pulse, start NOESY mixing time
  10u pl0:f1                           ; power switching f1-channel
  (center(p32:sp29 ph4:r):f1 (p12:gp12))         ; Thrippleton-Keeler z-filter element
  d16
  p16:gp5                      ; purge gradient
  d16 pl1:f1                   ; power switching f1-channel
  10u BLKGRAD
  TAU                          ; mixing time
  10u UNBLKGRAD
  (p1 ph3)                     ; 90 high power pulse at end of NOESY mixing time
  10u
  p18:gp4                      ; decoding gradient
  d16
  p2 ph4
  10u
  p18:gp4*-1                   ; decoding gradient
  d16
  p1 ph6                       ; begin z-filter
  5u
  5u pl0:f1
```

```
  (center (p11:gp11)(p42:sp42 ph4):f1)          ; Thrippleton-Keeler z-filter element
  d16
  p19:gp7
  d16 pl1:f1
  10u BLKGRAD
  p1 ph7                    ; end z-filter
  go=2 ph31
  d11 mc #0 to 2 F1PH(calph(ph1, +90), caldel(d0, +in0))
exit

; phase cycling
ph1=0 2                     ; Hard 90 Excitation
ph2=0 0 0 0 0 0 0 0 0 0 0 0 0 0 0 0 2 2 2 2 2 2 2 2 2 2 2 2 2 2 2 2 2 2          ; Hard 90 before mixing
ph3=0 0 0 0 0 0 0 0 2 2 2 2 2 2 2 2             ; Hard 90 after mixing
ph4=0                       ; Hard 180
ph5=0 0 1 1 2 2 3 3         ; PSYCHE element
ph6=0                       ; Hard 90 begin z-filter
ph7=0 0 0 0 2 2 2 2         ; Hard 90 end z-filter
ph29=0                      ; CW-presaturation
ph31=0 2 2 0 2 0 0 2 2 0 0 2 0 2 2 0 2 0 0 2 0 2 2 0 0 2 2 0 2 0 0 2          ; receiver

;p1 : f1 channel - 90 degree high power pulse
;p2: f1 channel - 180 degree pulse width
;p10 : duration of PSYCHE gradient
;p11: duration of 2nd ZQC dephasing gradient
;p12: duration of 1st ZQC dephasing gradient
;p16: purge gradient pulse during NOESY mixing time [5m]
;p17: gradient pulse for homodecoupling [1m]
;p18: en-/decoding gradient  [<1m]
;p19: purge gradient [1.5-2.5m]
;p32: duration of 1st Thrippleton-Keeler element [40m]
;p40: duration of PSYCHE pulse element [30m]
;p42: duration of 2nd Thrippleton-Keeler element [10m]

;pl1 : f1 channel - power level for pulse (default)
;pl9 : f1 channel - power level for presaturation

;sp29: f1 channel - shaped pulse (adiabatic)
;spw29: RF power of adiabatic 180 pulse
;spnam29: file name for adiabatic 180 pulse
;sp40: f1-channel - PSYCHE pulse element
;spw40 : RF power of PSYCHE pulse element
;spnam40: file name for PSYCHE pulse element
;sp42: f1 channel - shaped pulse (adiabatic)
;spw42: RF power of adiabatic 180 pulse
;spnam42: file name for adiabatic 180 pulse

;gpz1: 1st CTP gradient: 77%
;gpz2: 2nd CTP gradient: 49%
;gpz4: en-/decoding gradient: 2-10%
;gpz5: NOESY mixing time purge gradient: 40%
;gpz7: z-filter purge gradient: 61%
;gpz10: PSYCHE gradient: 1-3%
;gpz11: 2nd ZQC dephasing gradient: 2-12%
;gpz12: 1st ZQC dephasing gradient: 2-12%
;gpnam1: SMSQ10.100
;gpnam2: SMSQ10.100
;gpnam4: SMSQ10.100
;gpnam5: SMSQ10.100
;gpnam7: SMSQ10.100
;gpnam10: RECT.1
;gpnam11: RECT.1
;gpnam12: RECT.1


;d0: incremented delay (2D)
;d1: relaxation delay; 1-5 * T1
;d8: mixing time [50m-500m]
;d11: delay for disk I/O                             [30 msec]
;d12: delay for power switching                      [20 usec]
;d16: delay for homospoil/gradient recovery
;d18: reduced relaxation delay
;d19: delay for solvent presaturation

;cnst20: Flip Angle for PSYCHE pulse element (10-25 degree)
;cnst21: bandwidth of each chirp in PSYCHE pulse element (10000 Hz)
;cnst40: Scaling factor for power level attenuation of PSYCHE pulse element
;cnst41: solvent offset [ppm]
;cnst50: RF amplitude for PSYCHE pulse element (Hz)

;inf1: 1/SW = 2 * DW
;in0: 1/(1 * SW) = 2 * DW
;nd0: 1
;NS : number of scans                  [8*n]
;DS : number of dummy scans            [16]
;td1 : number of t1 increments
;FnMODE: States-TPPI, TPPI, States or QSEQ

;Processing
;PHC0(F1): 90
;PHC1(F1): -180
;FCOR(F1): 1

;preprocessor-flags-start
;LABEL_CWPR: presaturation of solvent at beginning of pulsesequence
; option -DLABEL_CWPR (eda: ZGOPTNS)
;preprocessor-flags-end

;for sweepwidth of adiabatic shape and adjusting gpz11:
;see supplementary material of M.J. Thrippleton & J. Keeler, Angew. Chem. Int. Ed. 42, 3938-3941 (2003)
```